Pontifícia Universidade Católica
do Rio de Janeiro

Alexandra Araujo Alicke

LAOS Rheological Characterization of an Elasto-Viscoplastic Material

Dissertação de Mestrado

Thesis presented to the Programa de Pós-graduação em Engenharia Mecânica of the Departamento de Engenharia Mecânica, PUC–Rio, as partial fulfillment of the requirements for the degree of Mestre em Engenharia Mecânica.

Advisor: Prof. Paulo Roberto de Souza Mendes

Rio de Janeiro
October 2013

PUC-Rio - Certificação Digital Nº 1121442/CA

Pontifícia Universidade Católica
do Rio de Janeiro

Alexandra Araujo Alicke

LAOS Rheological Characterization of an Elasto-Viscoplastic Material

Thesis presented to the Programa de Pós-graduação em Engenharia Mecânica of the Departamento de Engenharia Mecânica do Centro Técnico Científico da PUC–Rio, as partial fulfillment of the requirements for the degree of Mestre em Engenharia Mecânica. Approved by the following commission:

Prof. Paulo Roberto de Souza Mendes
Advisor
Departamento de Engenharia Mecânica — PUC–Rio

Prof. Mônica Feijó Naccache
Departamento de Engenharia Mecânica — PUC–Rio

Prof. Roney Leon Thompson
Departamento de Engenharia Mecânica — UFF

Prof. José Eugênio Leal
Coordinator of the Centro Técnico Científico da PUC–Rio

Rio de Janeiro, October 4th, 2013

PUC-Rio - Certificação Digital Nº 1121442/CA

All rights reserved.

Alexandra Araujo Alicke

Alexandra Alicke graduated in Petroleum Engineering from the Pontifical Catholic University of Rio de Janeiro (PUC-Rio) in 2011. Then, she started to work with rheology and non-Newtonian fluid mechanics in the Rheology Group (GReo) at PUC–Rio, where she already participated in research for three years as an undergraduate student.

PUC-Rio - Certificação Digital Nº 1121442/CA

Bibliographic data

Alicke, Alexandra Araujo

LAOS Rheological Characterization of an Elasto-Viscoplastic Material / Alexandra Araujo Alicke; advisor: Paulo Roberto de Souza Mendes — 2013.

88 f.: il. (color); 29,7 cm

Dissertação (Mestrado) — Pontifícia Universidade Católica do Rio de Janeiro, Departamento de Engenharia Mecânica, 2013.

Inclui Bibliografia.

1. Engenharia Mecânica – Teses. 2. Reologia. 3. Material Viscoplástico. 4. Reometria. I. de Souza Mendes, Paulo Roberto. II. Pontifícia Universidade Católica do Rio de Janeiro. Departamento de Engenharia Mecânica. III. Título.

CDD: 621

Acknowledgments

First, I would like to thank my advisor Paulo Roberto de Souza Mendes for the guidance, encouragement and support along the last couple of years. I deeply appreciate him trusting this exciting research topic on me, the patience to explain concepts that were not obvious to me and making sure I understand them, as well as for setting the bar high for me. I have learned a lot and I'm already looking forward to my doctorate research!

I would also like to thank the members of the Rheology Group at PUC-Rio for the assistance provided in many aspects, specially coworker Priscilla Varges, for lending me extra time at the rheometer when I needed and who has always been there to help and support, and Ricardo Leite, the undergraduate student who performed many of the tests contained in this thesis, for all dedication and enthusiasm expended on this research. In this sense, I also acknowledge Bruna Leopércio and Fernando Vasconcelos, my other two undergraduate students who were not involved in this particular research topic, but helped me a lot over the last two years. I have also learned a lot by advising these three students and I'm very proud to see their progress.

I'm thankful for my parents supporting and encouraging me in the pursuit of this masters degree. Moreover, I'm sorry for making them as nervous and concerned as me at the eve of every presentation, and I thank them for always cheering for my achievements. Furthermore, I thank my friends for understanding the lack of time to get together as a result of dedication to this thesis and simply for being there for me. I'm also indebted to CNPq for providing me a scholarship and for the financial support to this research.

Last, but definitely not least, I would like to thank Flávio Marchesini. First, as my supervisor during the three years as his undergraduate student, for teaching me great part of what I know about rheometry and for showing me how amazing it is to work with research. Second, as my beloved boyfriend, I thank him for all the support and great moments we have had along these almost five years we have been together. Also, for always making me believe

PUC-Rio - Certificação Digital Nº 1121442/CA

I was capable of presenting in conferences when I was hesitating, no matter how big the challenge was, for being truly happy for me, and for always being interested in my research. In addition, I thank him for the comprehension about the weekends spent at home working on this thesis, and for always calming me down and cheering me up during this process.

PUC-Rio - Certificação Digital Nº 1121442/CA

Abstract

Alicke, Alexandra Araujo; de Souza Mendes, Paulo Roberto (Advisor). **LAOS Rheological Characterization of an Elasto-Viscoplastic Material**. Rio de Janeiro, 2013. 88p. M.Sc. Thesis — Departamento de Engenharia Mecânica, Pontifícia Universidade Católica do Rio de Janeiro.

Large amplitude oscillatory shear flow (LAOS) is presently considered one of the most promising methodologies to investigate the behavior of complex materials. Since a wide range of industrial processes involves large deformations, understanding how complex materials behave under these conditions is fundamental for operation and design purposes. By performing a thorough rheological characterization of a commercially available hair gel, it was shown that a Jeffreys framework is suitable to interpret physically LAOS rheology data of complex materials. As the stress amplitude and frequency are independently varied, two classes of motion are observed, characterized by a non-sinusoidal and a sinusoidal response, respectively: structure-changing motions, when the stress amplitude is above the yield stress and the frequency is of the order of the reciprocal of the thixotropic characteristic time; and constant-structure motions, when either the stress amplitude is below the yield stress or the frequency is much larger than the reciprocal of the thixotropic characteristic time. Thus, a novel methodology, the quasi-linear LAOS (QL-LAOS) methodology, is suggested for rheological characterization and interpretation of LAOS results. Moreover, a remarkable agreement between the theoretical predictions and experimental results was obtained.

PUC-Rio - Certificação Digital Nº 1121442/CA

Keywords

Rheology; Viscoplastic Material; Rheometry; LAOS.

Resumo

Alicke, Alexandra Araujo; de Souza Mendes, Paulo Roberto. **Caracterização reológica em LAOS de um material elastoviscoplástico**. Rio de Janeiro, 2013. 88p. Dissertação de Mestrado — Departamento de Engenharia Mecânica, Pontifícia Universidade Católica do Rio de Janeiro.

O escoamento cisalhante oscilatório de grande amplitude ("large amplitude oscillatory shear - LAOS") é considerado atualmente uma das metodologias mais promissoras para caracterização de materiais complexos. Como uma grande faixa de processos industriais involve grandes deformações, é de extrema importância entender como esses materiais se comportam mecanicamente sob essas circunstâncias para o correto projeto e operação. Através de uma caracterização reológica completa de um material elastoviscoplástico mostramos que o modelo de Jeffreys é adequado para interpretar fisicamente os resultados em LAOS de materiais complexos. Conforme a amplitude de tensão e frequência são variados independentemente, dois tipos de movimento, caracterizados por respostas não senoidais e senoidais, foram observados respectivamente: i) "movimentos a estrutura variável", quando a amplitude de tensão é maior que a tensão limite de escoamento do material, e ii)"movimentos a estrutura constante", para casos onde a amplitude de tensão é menor que a tensão limite ou onde a frequência é muito maior que o inverso do tempo característico do material. Assim, uma nova metodologia, a "quasi-linear LAOS" (QL-LAOS) foi desenvolvida para a caracterização reológica e interpretação de resultados em LAOS. Ademais, foi obtida excelente concordância entre as previsões teóricas e os resultados experimentais.

Palavras–chave

Reologia; Material Viscoplástico; Reometria; LAOS.

PUC-Rio - Certificação Digital Nº 1121442/CA

Contents

PUC-Rio - Certificação Digital Nº 1121442/CA

List of Figures

PUC-Rio - Certificação Digital Nº 1121442/CA

PUC-Rio - Certificação Digital Nº 1121442/CA

PUC-Rio - Certificação Digital Nº 1121442/CA

List of Tables

PUC-Rio - Certificação Digital Nº 1121442/CA

PUC-Rio - Certificação Digital Nº 1121442/CA

"Be not diverted from your duty by any idle reflections the silly world may make upon you, for their censures are not in your power and should not be at all your concerns."

Epictetus

1
Introduction

1.1
Motivation

Oscillatory shear tests have been widely used to investigate the rheological behavior of many complex materials, which comprise a wide range of materials like polymer melts, suspensions, emulsions, biological macromolecules, among many others. Generally speaking, oscillatory tests consist of applying a sinusoidal deformation to the material and measuring its mechanical response. A typical strain sweep test at fixed frequency is presented in Fig. 1.1 in a plot of G' (storage modulus) and G" (loss modulus) as a function of the strain amplitude.

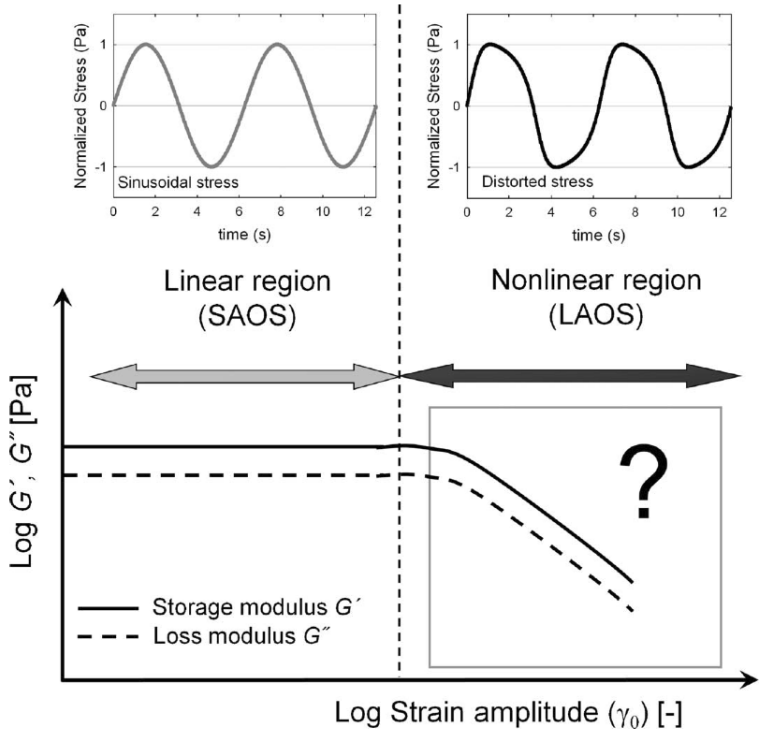

Figure 1.1: Schematic illustration of a strain sweep test, reproduced from [1].

PUC-Rio - Certificação Digital Nº 1121442/CA

At small amplitudes, the response of the material is also sinusoidal. This region of small amplitudes (SAOS) corresponds to the linear viscoelastic regime and is characterized by constant G' and G". As will be explained later (Sec. 2.1), G' is related to the elastic response of the material, whereas G" reflects the viscous behaviour. Both moduli are defined based on the assumption that the stress response is also sinusoidal.

However, at large enough amplitudes, the material response ceases to be sinusoidal, so that G' and G" can no longer be uniquely defined. This nonlinear behavior characterizes the large amplitude oscillatory shear, popularly known as LAOS.

LAOS is nowadays considered one of the most promising methodologies for assessing the mechanical behavior of complex materials. Since most industrial processes involve large stresses and deformations, understanding how complex materials behave under such conditions is fundamental for optimization and design purposes. Coating, spraying, lubrication, and injection molding can be cited as some processes that involve large deformations. Also, it is important to study complex materials under large amplitude oscillatory shear deformations once microstructural interactions, which greatly influence the rheology, may be greater under these circumstances.

Moreover, besides industrial applications, large deformations are also of great importance in more practical and everyday life situations. Recent studies attempted to correlate nonlinear viscoelastic properties of food products, such as cheese and dark chocolate, with composition [2] and with sensory and oral processing characteristics [3, 4]. In the cosmetics field, some skin and hair care gels' sensorial attributes, such as spreadability, slipperiness, and tackiness were found to be well predicted by LAOS rheology [5]. In addition, studies on soft biological tissues [6] and human skin [7] were performed under LAOS regime to investigate tissue injury and revealed strong nonlinearities in the mechanical behavior of these materials.

Hence, the growing interest in LAOS experiments is readily explained. As can be seen, large amplitude oscillatory shear experiments have a wide range of applicability, from industrial processes up to everyday life situations. Therefore, it is clear that there is a need for an appropriate methodology for characterization under LAOS, as well as for material functions in the nonlinear regime to predict mechanical behavior of complex materials under large deformations.

PUC-Rio - Certificação Digital Nº 1121442/CA

1.2 Research objectives

The present research aims at probing experimentally the predictions made by de Souza Mendes and Thompson [8] by fully investigating the rheological properties of an elasto-viscoplastic material, especially in the large amplitude oscillatory shear (LAOS) regime. According to the model predictions, it is expected that the LAOS results will show the existence of a quasi-linear viscoelastic regime at high enough frequencies, so that the appropriate material functions can be obtained.

1.3 Thesis overview

This thesis is divided into five chapters. As previously stated, the motivation and objectives of this research are briefly described in Chapter 1.

In the beginning of Chapter 2, the well-known linear viscoelasticity theory is summarized and its limitations are briefly discussed. Then, the literature on LAOS is revisited. Cited works include Lissajous-Bowditch curves' shapes analysis and attempts to mathematically describe the nonlinear regime using Fourier-Transform, Chebyshev polynomials, among other techniques. In the end of this chapter, the new proposed approach is presented.

Chapter 3 details the materials and methods used to characterize the elasto-viscoplastic material. The sample placement procedure, as well as the rheometric experiments, are described in detail. Also, the employed methodology - the quasi-linear LAOS methodology - is explained. This chapter also comprises the three appendixes, namely "Geometry selection" (App. A), "Parallel-plate correction" (App. B), and "Details on the LAOS experiments" (App. C).

The results of the rheological characterization are presented in Chapter 4. Data for constant shear rate (Sec. 4.1), steady state flow (Sec. 4.2), and constant stress tests (Sec. 4.3), as well as for different oscillatory experiments like time (Sec. 4.4), stress (Sec. 4.5) and strain (Sec. 4.6) sweeps are presented. Results of the LAOS experiments (Sec. 4.7) are shown in terms of the wave shapes, of Lissajous-Bowditch plots and of the LAOS viscosity. These results are compared with the theoretical predictions of the model proposed by de Souza Mendes and Thompson [8].

The main conclusions of the present research are highlighted in Chapter 5. At last, future steps are suggested.

PUC-Rio - Certificação Digital Nº 1121442/CA

2
Background and Literature

2.1
Linear viscoelasticity

Viscoelasticity, as its name implies, is the combination of viscous and elastic effects. One simple way of understanding this kind of behavior is by thinking of mechanical analogs, where springs and dashpots represent the elastic and viscous elements, respectively. A spring is an element in which the strain is proportional to the applied stress (Hooke's law), so that

$$\tau = G\gamma \tag{1}$$

The linear elastic response of a spring is immediate, as can be observed from Eq. 1, once time is not a variable. Also, if the applied stress is removed, the spring returns to its initial state. As for the dashpot, it represents the purely viscous behavior of liquids according to Newton's law, where the stress is proportional to the rate of deformation:

$$\tau = \mu\dot{\gamma} \tag{2}$$

When a stress is applied, the dashpot deforms at a constant rate, until the stress is removed.

The combination of these two elements can describe different kinds of materials, as exemplified in Fig. 2.1. By connecting a spring and a dashpot in series, the Maxwell model is obtained. It is a representation of a viscoelastic liquid. On the other side, to obtain a representation for a viscoelastic solid, a spring and a dashpot are placed in parallel (Kelvin-Voigt model).

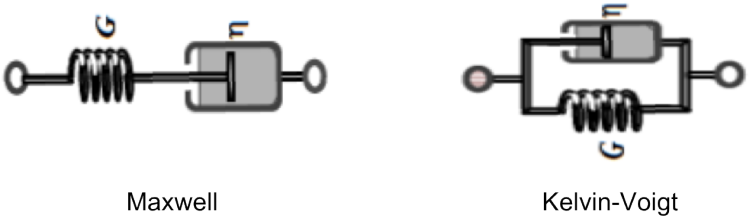

Figure 2.1: Representation of Maxwell and Kelvin-Voigt models.

PUC-Rio - Certificação Digital Nº 1121442/CA

These are the simplest possible combinations of the two elements, but many other are possible, such as the Burgers and the Jeffrey's models.

The general current understanding defines linear viscoelasticity for a particular material as a region of small amplitudes in which stress varies linearly with strain. The linear viscoelasticity has a well-developed framework, so that this Section is an attempt to summarize information found in many works [9, 10, 11, 12, 13], that seem to be most relevant to enable understanding the ideas and results presented later on this text.

There are a number of rheometric experiments to probe the linear viscoelasticity of a material, being the more common techniques the creep-recovery and oscillatory experiments. As the present work deals with oscillatory motions, this kind of experiment is detailed next.

Oscillatory testing consists of applying a sinusoidal motion to the sample with the possibility of controlling frequency and strain/stress amplitudes independently. When a sinusoidal deformation of amplitude γ_a, with γ_a pertaining to the linear viscoelastic regime (i.e. in the SAOS region), is applied to a sample at a fixed frequency ω , then

$$\gamma(t) = \gamma_a \sin(\omega t) \tag{3}$$

or, in terms of the shear rate

$$\dot{\gamma}(t) = \omega\gamma_a \cos(\omega t) = \dot{\gamma}_a \cos(\omega t) \tag{4}$$

In this case, the stress τ will also oscillate sinusoidally at the same frequency, but in general shifted by a phase angle δ with respect to the strain wave:

$$\tau(t) = \tau_a \sin(\omega t + \delta) \tag{5}$$

Fig. 2.2 illustrates the input and output waves for this rheometric flow. In Fig. 2.2a, the strain and shear rate waves are exhibited, while Fig. 2.2b displays three possible kinds of stress outputs: (i) purely elastic (Hookean), in phase with the strain wave, (ii) purely viscous (Newtonian), in phase with the shear rate wave, and (iii) linear viscoelastic, shifted by a phase angle δ from the input wave.

PUC-Rio - Certificação Digital Nº 1121442/CA

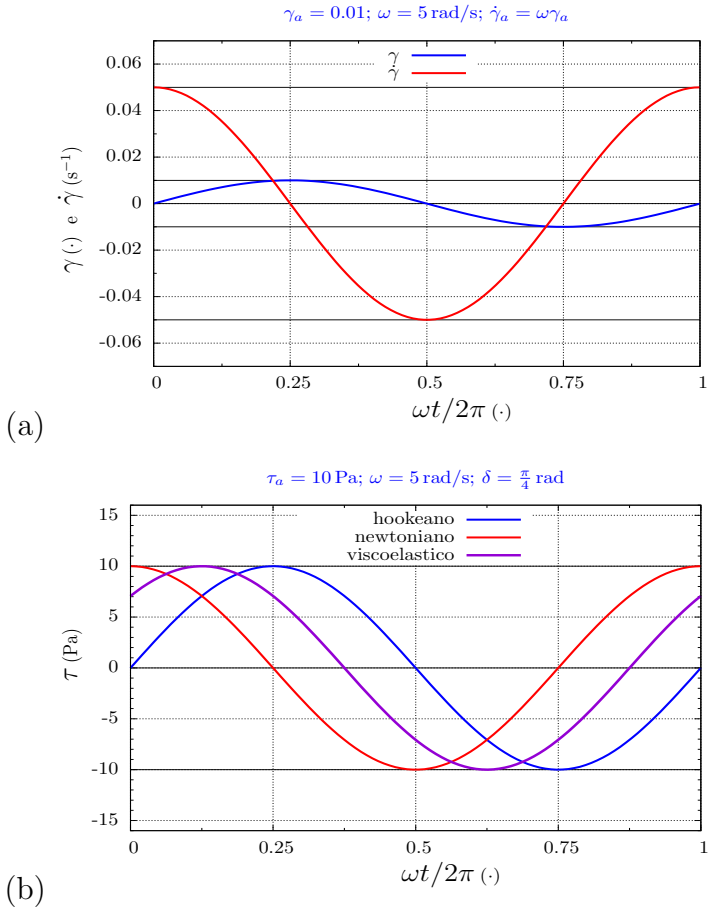

Figure 2.2: Illustration of the strain, shear rate and stress waves of a typical oscillatory test: (a) input waves; (b) possible output waves.

In general, the resulting stress wave can be decomposed into two waves of the same frequency: one in phase with the strain wave ($\sin\omega$t) and one 90° out of phase with the strain wave - or in phase with the strain rate wave - ($\cos$ ωt) :

$$\tau(t) = \tau_a' \sin\omega t + \tau_a'' \cos\omega t \tag{6}$$

Two material functions, the dynamic moduli G' and G", are defined as

$$G'(\omega) = \frac{\tau_a'}{\gamma_a} \quad , \quad G''(\omega) = \frac{\tau_a''}{\gamma_a} \tag{7}$$

where G' is the elastic or storage modulus, in phase with $\sin\omega t$, and G" the viscous or loss modulus, out of phase with $\sin\omega$t (in phase with $\cos\omega$t). Thus, we can rewrite the stress as

$$\tau(t) = G'\gamma_a \sin\omega t + G''\gamma_a \cos\omega t \tag{8}$$

PUC-Rio - Certificação Digital Nº 1121442/CA

to illustrate the elastic and viscous contributions. Also, it can be shown that

$$\tan\delta = \frac{\tau_a''}{\tau_a'} = \frac{G''}{G'} \tag{9}$$

The two particular cases belong to the Hookean solid (purely elastic response) and to the Newtonian liquid (purely viscous response). For a Hookean solid, $\delta = 0°$, $G' = G$ and $G'' = 0$. For a Newtonian liquid, $\delta = 90°$, $G' = 0$ and $G'' = \mu\omega$.

It is important to note that G' and G" are defined only in the case of a sinusoidal response. As previously commented in Sec. 1.1, this occurs in the small strain domain. Thus, attention must be paid to only rely on G' and G" when testing in the linear viscoelastic region. Moreover, although being popular and well-established material functions, they offer a rather qualitative idea of the behavior of a material, instead of a physical meaningful quantity, as for instance viscosity. Fig. 2.3 shows examples of a strain and a stress sweep tests to illustrate the threshold of linear viscoelasticity and consequent onset of non-linear behavior.

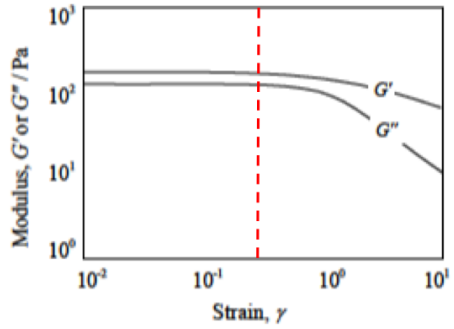

Figure 37: Non-linear oscillatory behaviour of Bonjela, a commercial oral preparation, at 1 Hz.

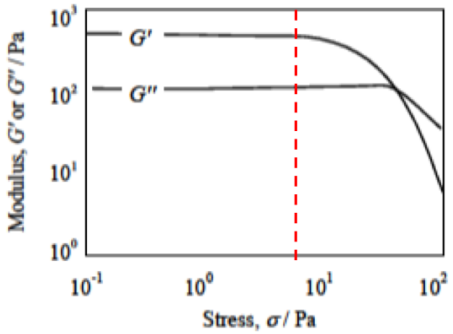

Figure 38: Non-linear oscillatory behaviour of a commercial sample of ketchup, see [40].

Figure 2.3: Strain sweeps reproduced from [13], with indication of the threshold of linear viscoelastic regime.

It is clear that in the linear viscoelastic region both moduli G' and G" are constant, i.e. independent on strain or stress amplitude. Identifying the linear viscoelastic region is important, once subsequent oscillatory testing, such as frequency and time sweeps, should be performed at a constant strain/stress amplitude pertaining to this region. Nevertheless, it is worth noting that G' and G" are frequency dependent, i.e. G'(ω) and G"(ω).

Indeed, the same analysis is valid for a sinusoidal stress input and resulting strain response, as is the case of a stress sweep test. In this case, the corresponding quantities are the storage compliance J'(ω) and the loss compliance J"(ω).

PUC-Rio - Certificação Digital Nº 1121442/CA

Another important parameter that influences the behavior of the material is the timescale of the flow, which in turn is directly linked to the frequency in oscillatory experiments. A silly putty toy is one of the best examples of this influence, because it shows a wide range of behaviors depending on time scale, once it acts as a viscous liquid over a long time period, but as an elastic solid over a short time period. Specifically, if it is let at rest over a long time, it will "spread" (flow), however it can bounce as an elastic solid at shorter times (See Fig. 2.4).

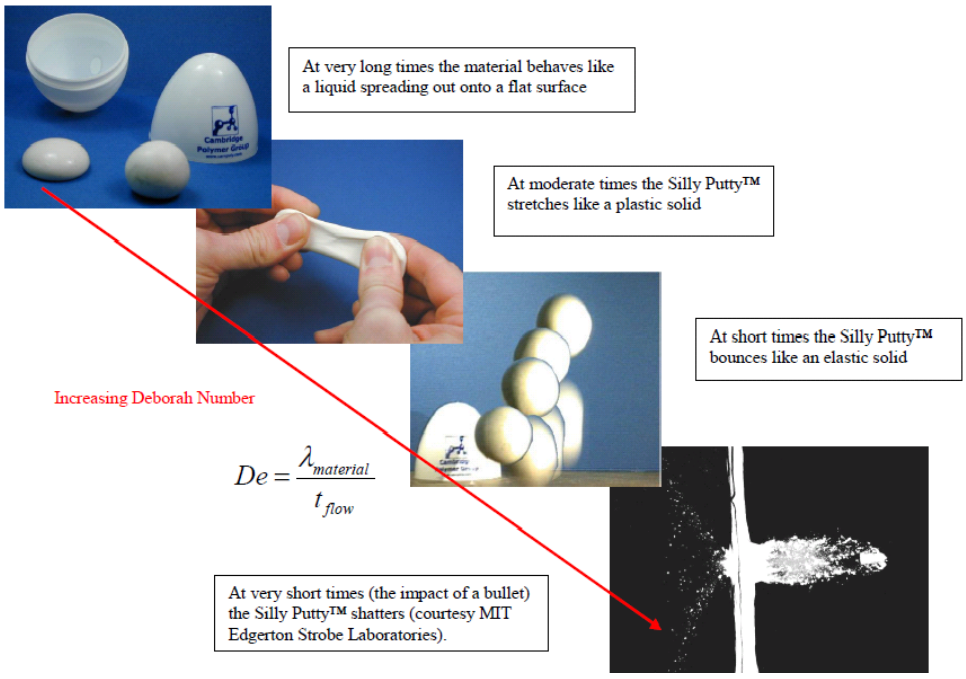

Figure 2.4: Behavior of a Silly Putty toy, reproduced from "Cambridge Polymer Group".

Indeed, it is the relation between the relaxation time of the material and the timescale of the experiment which will dictate the behavior of the material. This ratio is defined as the Deborah number (De)

$$De = \frac{\lambda}{t} = \lambda\omega \tag{10}$$

Low De indicate a liquid-like behavior, which occurs at long times and low frequencies, whereas high De indicates a solid-like behavior present at high frequencies and short time scales. Again, the limits reduce to a Newtonian liquid (De $\rightarrow$ 0) and to a Hookean solid (De $\rightarrow \infty$).

The Pipkin diagram [14] is a useful tool for visually displaying the material behavior under a wide range of conditions. It is a plot of strain (or shear rate) amplitude vs. frequency (or De number). An example is shown in Fig. 2.5.

PUC-Rio - Certificação Digital Nº 1121442/CA

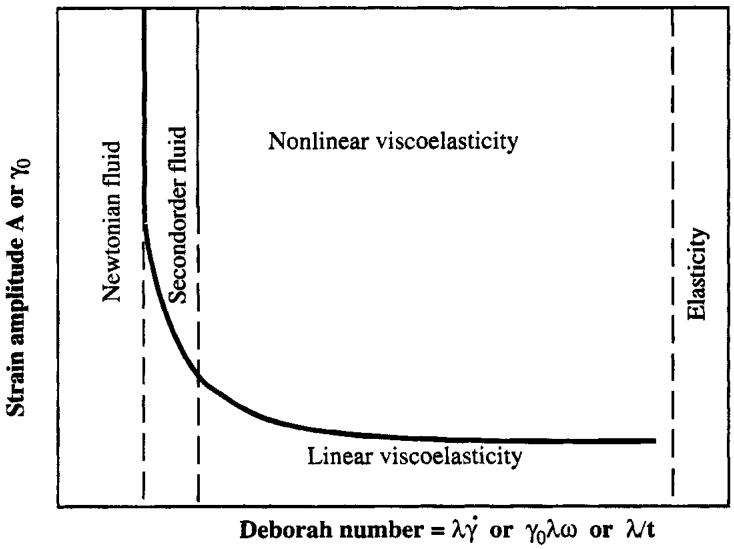

Figure 2.5: Pipkin diagram, reproduced from [12].

As previously discussed for the *De* number, at low frequencies (long timescales), the material behaves as a Newtonian fluid, while at high frequencies (short timescales), a purely elastic behavior is observed. In addition, for small amplitudes and a wide range of frequencies, the linear viscoelastic behavior is present. These "limits" of the Pipkin diagram are theoretically well defined.

It was discussed that the material functions G' and G" are valid only in the case of a sinusoidal response. However, for the big portion pertaining to the "nonlinear viscoelasticity", it is usually not well defined. This nonlinear behavior is the focus of the LAOS analysis encountered in the literature.

2.2 Literature on LAOS

The idea behind LAOS is to attempt to describe the mechanical behavior at large deformations, i.e. real processing conditions. Also, materials that exhibit similar linear viscoelastic properties may show different nonlinear viscoelastic properties. According to the review by Hyun et al. [1], the basic concept of LAOS was already introduced in the 1960, 1970s. In early publications, the nonlinear behavior was investigated for different viscoelastic materials under oscillatory shear, but technical problems, such as resolution of the torque transducer and hardware limitations, hindered the progress of the studies. Nevertheless, some analysis methods were already suggested, like the stress shape and Fourier transform analysis.

PUC-Rio - Certificação Digital Nº 1121442/CA

A qualitative indication of the behavior of the material under LAOS can be given by Lissajous-Bowditch curves [15, 16], which are plots of parametric equations of sinusoidal form:

$$x(t) = a\,sin(\omega t + \delta) \tag{11}$$

$$y(t) = b\,sin(t) \tag{12}$$

Many authors omit the Bowditch part of the name, though. Orbital trajectories bearing Lissajous' name were studied by Bowditch in 1815, predating Lissajous' treatment by more than 40 years. In this work, for the sake of simplicity, only the Lissajous name will be used to refer to Lissajous-Bowditch curves.

The construction of a Lissajous curve is illustrated in Fig. 2.6.

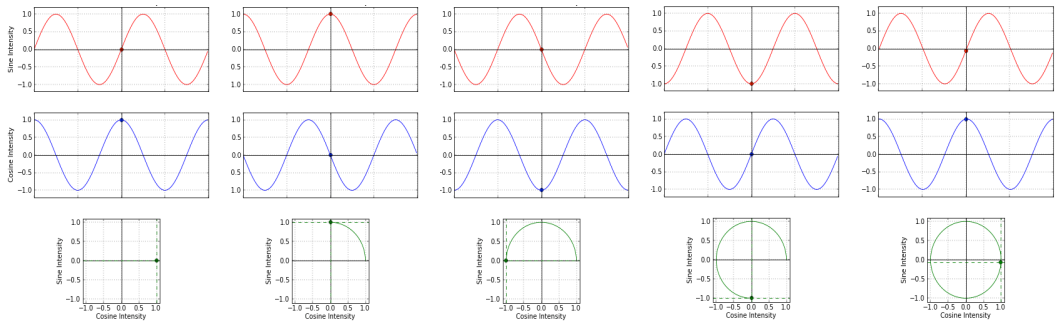

Figure 2.6: Illustration of the construction of a Lissajous curve. Images were obtained from an animated gif file found on Wikipedia.

Each column corresponds to an instant of time. The red waves (first row) correspond to the input signal as a function of time and the blue waves (middle row) correspond to the output signal, also as a function of time. The green curve (bottom row) is the resulting Lissajous curve, being drawn as time elapses from left to right. It can be seen that the input and output signals are 90-degrees phase shifted: this means that when the marked value on the red wave is equal to zero, the blue wave is at its maximum, and conversely, when the red wave is at its maximum, the marked value on blue wave is equal to zero, so that the resulting Lissajous is a circle.

In rheology, the Lissajous curves are plots of the instantaneous stress vs. strain (elastic form) or stress vs. shear rate (viscous form). Three examples of dimensionless Lissajous figures, corresponding to the waves in Fig. 2.2b, are shown next, in terms of elastic (first row) and viscous (second row) Lissajous curves:

PUC-Rio - Certificação Digital Nº 1121442/CA

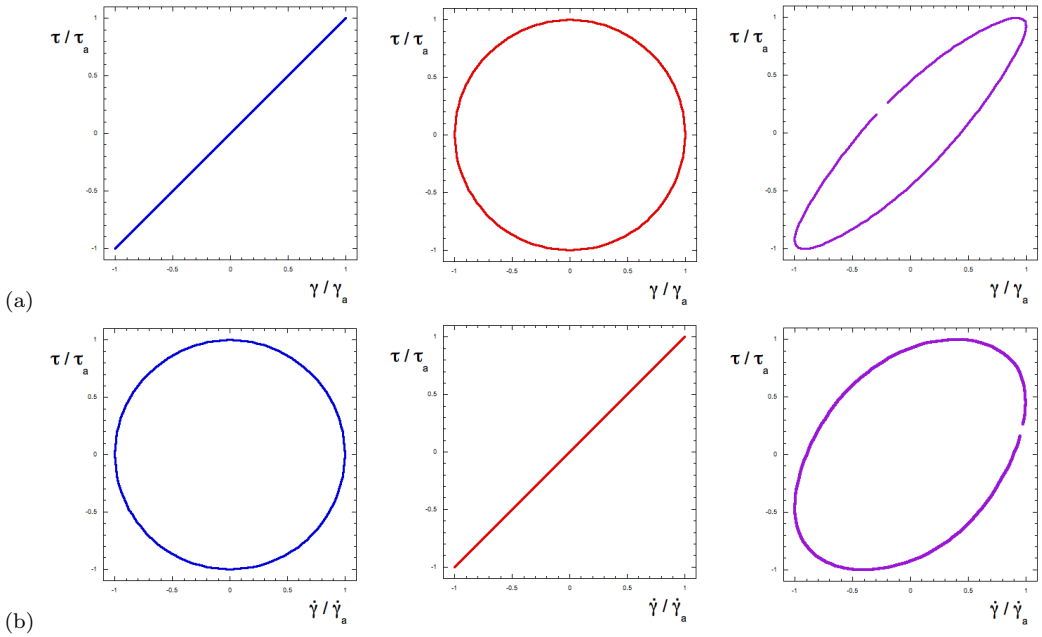

Figure 2.7: Lissajous curves in elastic (a) and viscous (b) forms. The blue curves belong to a Hookean solid, the red ones to a Newtonian liquid, and the purple to the linear viscoelastic behavior, according to Fig. 2.2.

As seen in Fig. 2.6, 90-degrees phase shifted signals generate circular orbits. Clearly, this occurs in the case of Newtonian liquids in the elastic form of the Lissajous and of Hookean solid in the viscous form. Conversely, when the input and output signals are in-phase, the resulting Lissajous curve is a straight line, as is the case of Hookean solid in the elastic form, once the shear stress is directly proportional to the strain, and the case of Newtonian liquid in the viscous form, as the stress is directly proportional to the shear rate.

Thus, it is intuitive that the shape of Lissajous curves of a linear viscoelastic response should be a combination of both. The resulting shapes are ellipses, which indicate that the output signal is shifted from the input signal by a phase angle δ, indicating the "tilting" of the ellipse.

However, for the LAOS regime, an infinity of Lissajous curve shapes are possible. Indeed, the degree of non-linearity of the response is indicated by the departure from the elliptical shape. The shape will also depend on the degree of elasticity, thixotropy, presence of yield stress, among other.

In addition, some recent works present Lissajous curves in a 3-D representation of stress, strain and shear rate. Ewoldt et. al [17] investigated the stress response of a pseudoplastic xanthan gum solution and an elasto-viscoplastic drilling fluid. Results are reproduced in Fig. 2.8, which include the 3D plot and Pipkin diagrams containing the elastic (left) and the viscous (right) forms of the Lissajous plots.

PUC-Rio - Certificação Digital Nº 1121442/CA

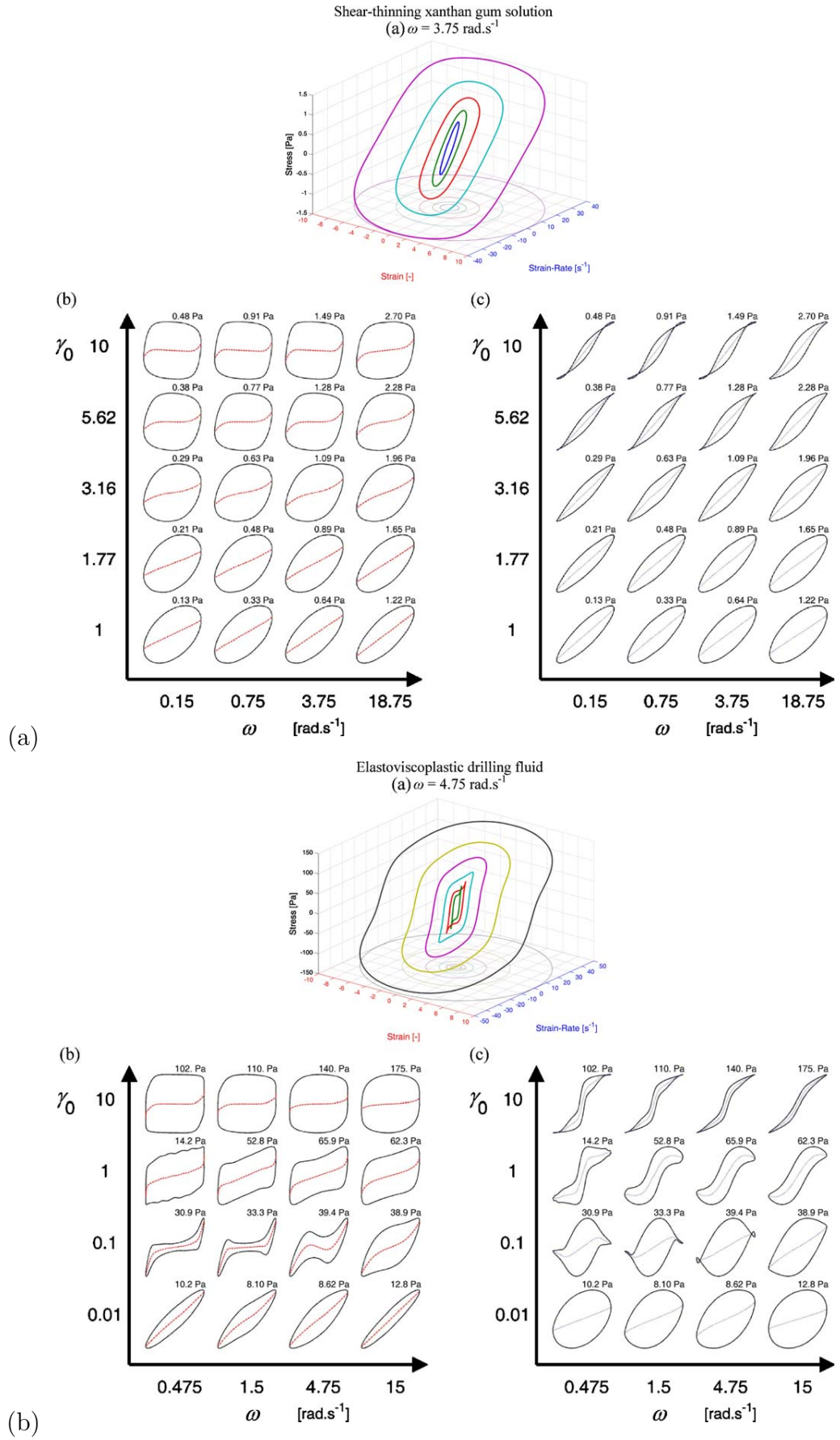

Figure 2.8: 3D representation of LAOS results for (a) shear-thinning xanthan gum solution and (b) elastoviscoplastic drilling fluid, reproduced from [17].

PUC-Rio - Certificação Digital Nº 1121442/CA

Although Lissajous curves may give a good insight into the material behavior, mathematically defined and physically meaningful quantities are necessary for proper description of the mechanical behavior of complex materials. To quantify the nonlinear oscillatory stress response, other material functions are needed, once G' and G" are not valid material functions in the LAOS regime. There are different approaches that can be found in the LAOS literature. It is worth noting that many of these existing approaches rely on heavy mathematics. Since our proposed methodology is quite different, based on rather physical arguments, it is beyond the scope of this text to discuss the other methodologies in detail. Thus, only the main idea of each approach will be discussed.

The Fourier transform rheology developed by M. Wilhelm [18, 19, 20] was the first well established method for analysing nonlinear viscoelastic oscillatory motions. The nonlinear response of the material is decomposed into a Fourier series, i.e. in the case of a strain input of a certain frequency, the stress signal is changed to display the amplitudes and phases as a function of the input frequency ω. According to the authors, the frequency dependent spectrum can detect even very weak nonlinearities in the stress response, in comparison to data in the time domain. The stress can be represented as [11, 19]

$$\sigma(t) = \sum_{n=1,odd} \sigma_n sin(n\omega t + \delta_n) \tag{13}$$

where the amplitude $\sigma_n(\omega,\gamma_0)$ and the phase angle $\delta_n(\omega,\gamma_0)$ of the harmonics depend on both frequency ω and strain amplitude γ_0. Eq. 13 is the starting point of the FT-rheology. It is also possible to rewrite each Fourier component from Eq. 13 in components which are in-phase and out-of-phase with the strain input as follows

$$\sigma(t) = \gamma_0 \sum_{n,odd} [G'_n(\omega,\gamma_0)sin(n\omega t) + G''_n(\omega,\gamma_0)cos(n\omega t)] \tag{14}$$

where G'_n and G''_n are the Fourier coefficients. In the linear viscoelastic regime, all moduli in Eq. 14 vanish, except the first harmonic moduli G'_1 and G''_1, reducing to the elastic modulus G' and loss modulus G". The intensity of the higher harmonics is the measure of nonlinearity, since they are not detectable in the small amplitude regime. Also, because of the odd symmetry between strain and stress signals, only odd harmonics are expected.

The FT is a complex transformation, so that even for a real time-domain data set s(t) the transformation results in a complex s(ω) with real and imaginary parts of the spectrum. Also according to the review by Hyun and coworkers [1], the complex mathematics is one of the reasons why there are

PUC-Rio - Certificação Digital Nº 1121442/CA

many ways to interpret the complex nonlinear response.

Experimentally, the time dependent deformation and the torque of the rheometric experiment are externally digitalized, Fourier transformed and further evaluated with a self-developed software, as illustrated in Fig. 2.9. A detailed description of the experimental methodology is given in the work by Wilhelm [19].

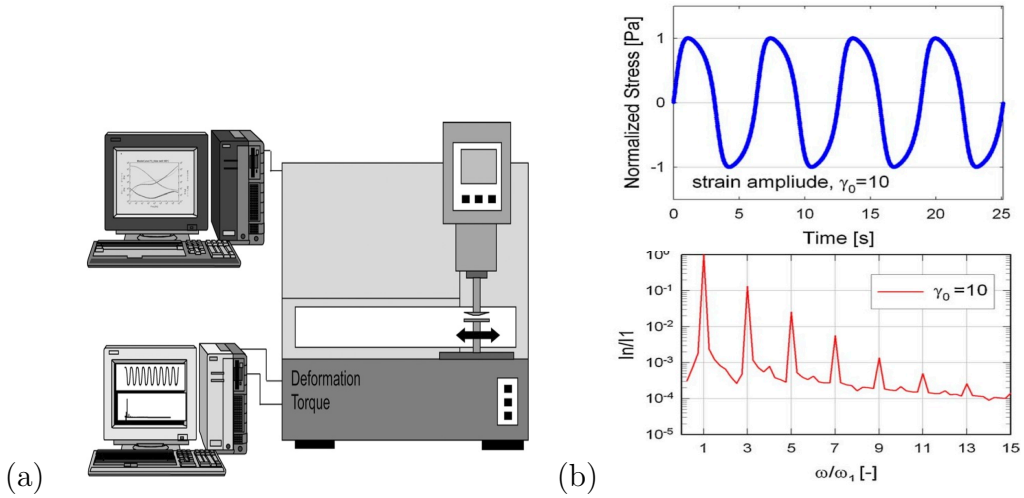

Figure 2.9: (a) FT-rheology experiment set-up, reproduced from [18], (b) Example of a nonlinear normalized stress wave together with its FT-spectrum.

Moreover, an example of a FT spectrum is shown in Fig. 2.9 b, where the magnitude of the odd harmonics represents the level of nonlinearity. Usually, the relative intensity of the third harmonic ($I_{3/1} \equiv I(3\omega)/\ I(\omega)$) is the most important when quantifying nonlinearity among the higher harmonics. The number of higher harmonics that can be measured depends mostly on precision of the measuring set-up, as well as on the signal-to-noise ratio of data. A lot of care needs to be taken when acquiring the time signal so as to obtain "highly resolved, artifact-free spectra with low noise level" [18]. Mechanical and electrical shielding, as well as data oversampling, are some techniques used to improve the raw data quality.

Despite being a complicated technique, the FT-rheology enabled the acquisition of high resolution torque signals from commercial rheometers and has been widely used in the literature for the LAOS characterization of various complex fluids.

An alternative technique to quantify the nonlinear behavior was developed by Cho et. al [21]. The "Stress Decomposition" (SD) method decomposes the nonlinear stress wave into "physically meaningful" elastic and viscous components. This was possible using geometrical arguments and considering the stress to be a function of the independent inputs of strain and strain-rate

PUC-Rio - Certificação Digital Nº 1121442/CA

$\sigma = \sigma(\gamma, \dot{\gamma})$, instead of the initial time domain representation $\sigma = \sigma(t)$. Thus, the stress σ can be decomposed into elastic stress σ' (single-valued function of strain) and viscous stress σ" (single-valued function of strain-rate) components as

$$\sigma' = \Gamma'(x, \gamma_0)\, x \;\;,\;\; \sigma'' = \Gamma''(y, \gamma_0)\, y \tag{15}$$

where Γ' and Γ'' are the generalized dynamic moduli, $x = \gamma$ and $y = \dot{\gamma} / \omega$. According to the authors, "although the SD decomposition analysis is equivalent to the FT analysis, it is superior to FT because it is based on a physical axyom, (...) rather than on a pure mathematical analysis of nonlinear signals.".

Figure 2.10 shows results by Ewoldt et. al [22] as an example of the geometrical interpretation (SD) by Cho et. al on LAOS data of a biological soft material.

PUC-Rio - Certificação Digital Nº 1121442/CA

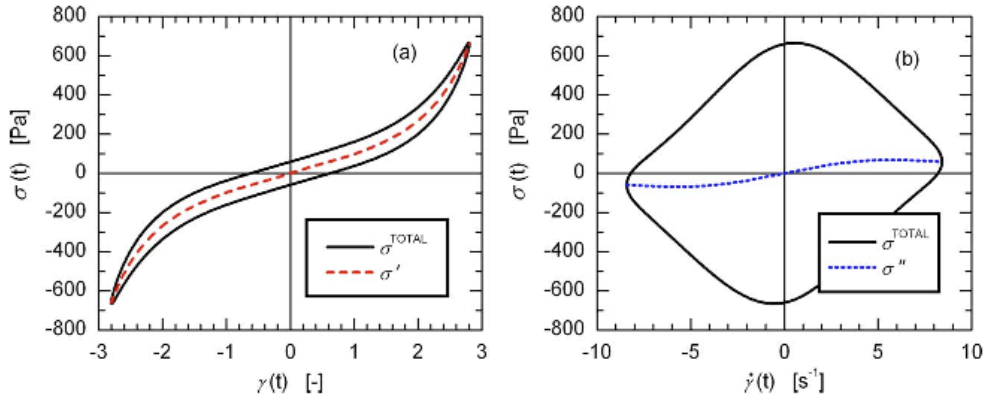

Figure 2.10: Example of SD on LAOS results, reproduced from [22].

Both elastic and viscous forms of the Lissajous curve are presented in Fig. 2.10. The plot on the left corresponds to the total stress (black line) and elastic stress σ' (red dotted line) as a function of the strain, while the plot on the right exhibits the total stress (black line) and viscous stress σ" (blue dotted line) as a function of the shear rate. As can be seen, the plots of σ' and σ" yield single-valued functions, instead of the closed loops formed by the total stress plots. Then, Cho et. al [21] suggest a polynomial regression of the form

$$\begin{aligned} \sigma'(x, \gamma_0) &= G'(\omega)x + G'_3(\omega, \gamma_0)x^3 + G'_5(\omega, \gamma_0)x^5 + ... \\ \sigma''(y, \gamma_0) &= G''(\omega)y + G''_3(\omega, \gamma_0)y^3 + G''_5(\omega, \gamma_0)y^5 + ... \end{aligned} \tag{16}$$

to fit the σ' and σ" curves. However, the material properties obtained from the polynomial coefficients may depend on the order of the polynomial chosen.

Thus, in the same work by Ewoldt and coworkers, the authors extend the concept of SD using the Chebyshev polynomials of the first kind to describe $\sigma'(x)$ and $\sigma''(y)$. They claim the Chebyshev polynomials is the most appropriate set of basis functions since it can describe the measured stress in the orthogonal space formed by the strain and strain-rate. It also has the advantage of considering the stress dependence only on frequency and strain amplitude.The stress is decomposed as

$$\begin{aligned} \sigma'(x) &= \gamma_0 \sum_{n:odd} e_n(\omega, \gamma_0) T_n(x) \\ \sigma''(y) &= \dot{\gamma}_0 \sum_{n:odd} v_n(\omega, \gamma_0) T_n(y) \end{aligned} \tag{17}$$

where $T_n(x)$ is the n-th order Chebyshev polynomial of the first kind, $x = \gamma/\gamma_0$, $y = \dot{\gamma}/\dot{\gamma}_0$, $e_n(\omega,\gamma_0)$ the elastic Chebyshev coefficients, and v_n (ω,γ_0) the viscous Chebyshev coefficients. When the stress components σ' and σ" are related to the Fourier decomposition (Eq. 14), Chebyshev coefficients can be calculated from the Fourier coefficients. In this sense, this framework is said to give physical meaning to Fourier coefficients.

In addition, Ewoldt et al. [22] proposed viscoelastic moduli for the nonlinear regime, e.g. minimum-strain and large-strain elastic modulus, and minimum-rate and large-rate dynamic viscosity, which are identified in Lissajous plots as shown in Fig. 2.11.

The minimum-strain modulus G'_M is the tangent modulus at zero instantaneous strain (maximum $\dot{\gamma}$)

$$G'_M \equiv \left.\frac{d\sigma}{d\gamma}\right|_{\gamma=0} = \sum_{n=odd} nG'_n \tag{18}$$

and G_L, the large-strain modulus, is the secant at maximum strain ($\dot{\gamma} = 0\ s^{-1}$) and is given as

$$G'_L \equiv \left.\frac{d\sigma}{d\gamma}\right|_{\gamma=\gamma_0} = \sum_{n=odd} nG'_n(-1)^{\frac{n-1}{2}} \tag{19}$$

The minimum-rate dynamic viscosity η'_M is the instantaneous viscosity at the smallest shear-rate, defined as

$$\eta'_M \equiv \left.\frac{d\sigma}{d\dot{\gamma}}\right|_{\dot{\gamma}=0} = \frac{1}{\omega} \sum_{n:odd} nG''_n(-1)^{\frac{n-1}{2}} \tag{20}$$

PUC-Rio - Certificação Digital Nº 1121442/CA

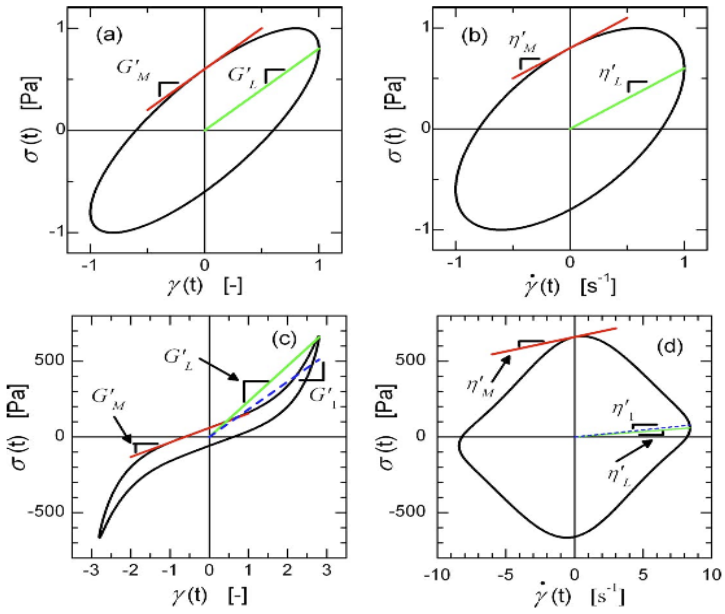

Figure 2.11: Illustration of viscoelastic moduli proposed by Ewoldt et al., reproduced from [22].

PUC-Rio - Certificação Digital Nº 1121442/CA

and the large-rate dynamic viscosity, the instantaneous viscosity at the largest $\dot{\gamma}$, as

$$\eta'_M \equiv \left.\frac{d\sigma}{d\dot{\gamma}}\right|_{\dot{\gamma}=\dot{\gamma}_0} = \frac{1}{\omega}\sum_{n:odd} nG''_n \tag{21}$$

A parameter called strain stiffening ratio, defined as

$$S = \frac{G_L - G_M}{G_L} \tag{22}$$

indicates the behavior of the sample: (i) S = 0 indicates a linear response; (ii) S > 0 indicates intra-cycle strain stiffening, and (iii) S < 0 indicated intra-cycle strain softening. Conversely, the parameter T (shear thickening ratio) was defined as

$$T = \frac{\eta'_L - \eta'_M}{\eta'_L} \tag{23}$$

where (i) T = 0 indicates a single harmonic linear viscous response; (ii) T > 0 indicates intra-cycle shear thickening, and (iii) T < 0 indicated intra-cycle shear thinning.

This framework was used to study the behavior of pseudoplastic and elasto-viscoplastic materials [17], as well as model power-Law gluten dough [23], to study self-intersection and seconday loops on LAOS results [24], in-

vestigate differences when performing LAOStress (i.e. stress-controlled experiments) [25], among other. McKinley's group at MIT also provides a free software for analyzing raw data within their framework.

Rogers and Lettinga [26] reviewed and discussed the previous mentioned approaches. Rogers et al. [27, 28] developed a technique which is not based on the assumptions of linear algebra to analyze LAOS responses. Instead, nonlinear oscillatory responses are described as a result of periodic sequences of physical processes (SPP) when observing the response wave in a 3D space formed by stress, strain and shear rate. In the author's words, "we are able to discern elastic and viscous processes in the waveforms by analyzing the wave shapes in a manner that is based not on whole-waveform approach but rather on a sequence of physical processes.". Moreover, the authors claim this approach might be more straightforward, since it does not rely on infinite series as in the Fourier and Chebyshev analysis techniques.

Quantitatively, the SPP approach [29] relies on three vectors in the 3D space defined by strain, strain rate and stress: the binomial vector B (normal to the space curve), and two reference vectors s_1 and s_2 with

$$\begin{aligned} s_1 &= [-1,\, 0,\, 0] \\ s_2 &= [0,\, 0,\, 1] \\ B^{mod} &= [B_\gamma,\, \omega B_{\dot{\gamma}},\, B_\sigma] \end{aligned} \tag{24}$$

A typical linear viscoelastic response is shown in Fig. 2.12.

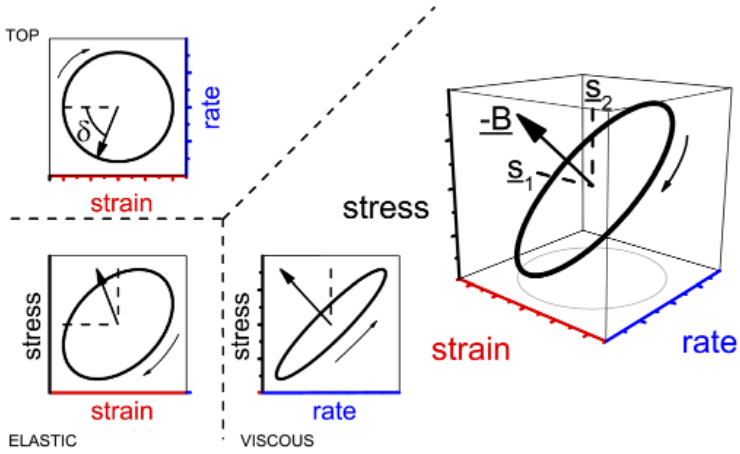

Figure 2.12: Linear viscoelastic response plotted in a 3D plane, together with projections of the periodic orbit on 2D planes. The binomial vector B and reference vectors s_1 and s_2 are indicated (reproduced from [29]).

PUC-Rio - Certificação Digital Nº 1121442/CA

From the vectors above, the phase angle δ and complex modulus G^* can be obtained. Also, dynamic moduli R' and R" are defined as the projections of the binomial vector into the strain and shear rate directions and can be obtained with

$$R'(\gamma_0, \omega, t) = |G^*(\gamma_0, \omega, t)| cos\, \delta(t)$$
$$R''(\gamma_0, \omega, t) = |G^*(\gamma_0, \omega, t)| sin\, \delta(t) \tag{25}$$

Again, in the linear viscoelastic regime, R' and R" reduce to G' and G", respectively.

The SPP methodology attempts to analyze the nonlinear material response by considering two material functions in a similar way as the SD approach. However, by reducing the number of material functions to two, these functions depend on frequency, amplitude, and time, while in the Fourier and Chebyshev approaches strain and frequency are decoupled from time.

On the other side, both Fourier and Chebyshev techniques rely on the idea of generalizing the linear viscoelastic material functions G' and G" by a series of infinite coefficients (G'_n and G''_n in the former, and e_n and v_n in the latter), so as to obtain the elastic and viscous contributions. Moreover, it is difficult to attribute physical meaning to the different higher harmonics.

The authors from the previous cited review [1] suggest that the best method to analyze the nonlinear viscoelastic response of a complex material may depend on the material at hand, once each approach has its own merits and disadvantages. Thus, there is still the need in the literature for a more general, capable of accommodating all kinds of behaviors, and physically meaningful model to analyze LAOS results.

To this end, a novel methodology for LAOS data analysis was developed during this research [30]. Thompson and de Souza Mendes [31] proposed a model-based framework (MBFR) to analyze LAOS results. In the MBFR, the parameters of any model become the material functions describing the mechanical behavior of a complex material. The constitutive model developed by de Souza Mendes [32] and de Souza Mendes and Thompson [8] is based on the Jeffrey's model, whose mechanical analog is displayed in Fig. 2.13. The authors emphasize the importance of choosing the appropriate model framework, which should be capable of predicting all types of mechanical behavior [31].

PUC-Rio - Certificação Digital Nº 1121442/CA

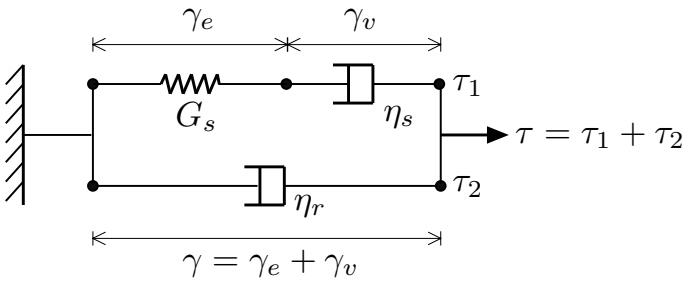

Figure 2.13: The mechanical analog corresponding to the Jeffrey's model.

In this figure, G_s is the structuring-level-dependent elastic modulus, η_s the structuring-level-dependent relaxation viscosity, and η_r the structuring-level-dependent retardation viscosity. Also, the total structuring-level-dependent viscosity is defined as $\eta_v \equiv \eta_s + \eta_r$. The difference from the classical Jeffrey's model is that here G_s, η_s, and η_r are functions of the structuring level λ, which describes the state of the microstructure. λ can vary from 0 (completely unstructured state) to λ_0 (fully structured state). Different kinds of behavior corresponding to different structuring levels can be predicted, from a purely elastic solid up to a purely viscous liquid, including viscoelastic solid and viscoelastic liquid behaviors.

The following equations originate from the Jeffrey's analog:

$$\begin{aligned} \tau &= \tau_1 + \tau_2 \\ \tau_1 + \tfrac{\eta_s}{G_s}\dot{\tau}_1 &= \eta_s\dot{\gamma} \\ \tau_2 &= \eta_r\dot{\gamma} \end{aligned} \tag{26}$$

These equations have an analytical solution for oscillatory flows as long as the Jeffreys material functions remain fixed throughout a cycle, i.e, when the stress response is sinusoidal. Therefore, the following analysis is expected to be valid only in the cases that an elliptical viscous Lissajous curve is obtained.

The results obtained by numerical integration of the model equations for the case of oscillatory flows already showed the existence of sinusoidal stress responses at high enough frequencies, i.e. "whenever the characteristic time of change of the microstructure is much larger than the reciprocal frequency of the LAOS test" [8]. An example is shown in Fig. 2.14.

PUC-Rio - Certificação Digital Nº 1121442/CA

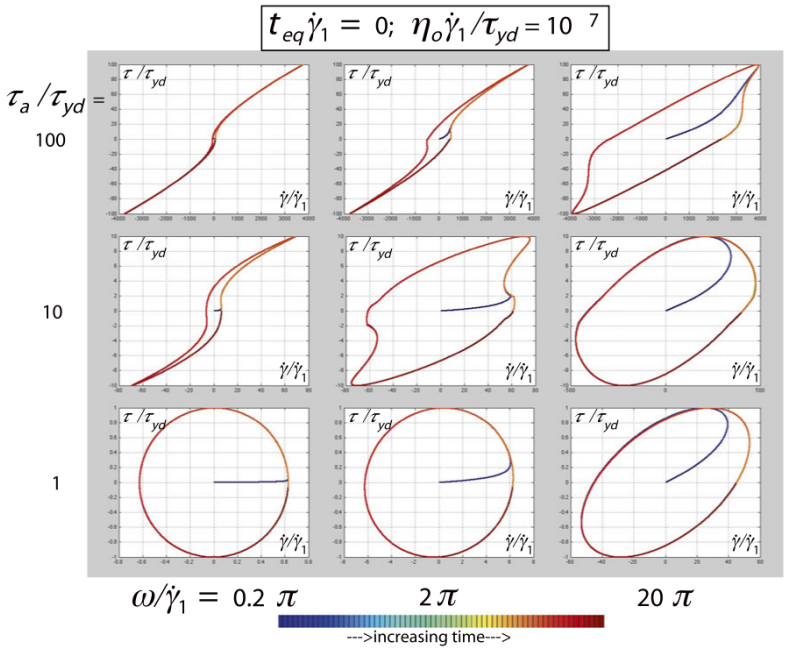

Figure 2.14: Model predictions of de Souza Mendes and Thompson [8].

The existence of two classes of motion were shown: i) structure-changing motions, characterized by a non-sinusoidal response; and ii) constant-structure motions, characterized by a sinusoidal response. In the first type of motion, the state of the material microstructure is periodically changing along the experiment. Since these changes can be dramatic dependent upon the type of the material, they can greatly disturb the interpretation of the results and the understanding of the mechanical behavior of the material.

Thus, while all present LAOS analysis focus on non-sinusoidal stress responses, which imply major microstructural changes along the cycles, the proposed methodology relies on data obtained from sinusoidal responses, or the "constant-structure motions", which dramatically simplifies the analysis. We call this approach the quasi-linear LAOS (QL-LAOS), once it is similar to the linear viscoelastic regime in the sense that the output wave is also sinusoidal. The main advantage of the MBFR methodology combined with the QL-LAOS experiments is to provide material functions whose physical meanings are evident, as opposed to what is usually employed in the literature, as well as being capable of predicting the material behavior under different flow conditions. Details of the employed methodology are discussed in Sec. 3.2.

PUC-Rio - Certificação Digital Nº 1121442/CA

3
Materials and Methods

A commercial hair gel ("Gel Bozzano 4 - mega fixação extra forte"), which is basically a concentrated Carbopol dispersion, was chosen as our elasto-viscoplastic material. It is worth noting that an elasto-viscoplastic material behaves as a linear viscoelastic solid at stresses below the yield stress τ_y, but irreversibly deform and flow as a fluid for stresses above τ_y. To assure that the same material was tested throughout the research, which spanned for several months, approximately 3 Kg of gel were used to perform the almost 500 tests contained in this work.

Two rheometers were employed, namely a stress controlled AR-G2 and a strain-controlled ARES-G2, both by *TA Instruments* (Fig. 3.1).

(a)  (b) 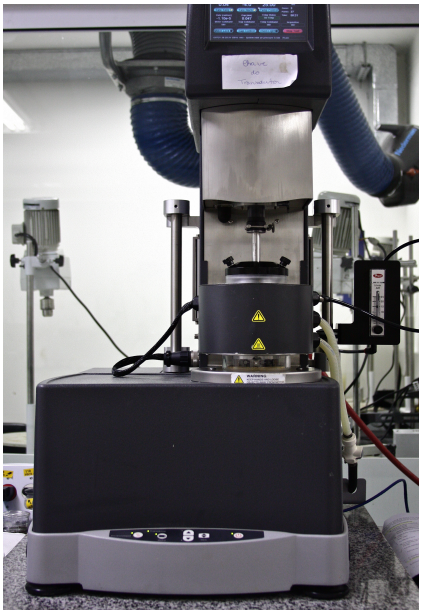

Figure 3.1: Rheometers (a) AR-G2; (b) ARES-G2.

The AR-G2 has a combined motor and transducer, which means that both applied stress and measured strain derive from the upper fixture. This is possible due to an accurate PID control. On the other hand, the ARES-G2 has separate motor and transducer, which permits inertia-free torque measurements. The motor controls the lower geometry by imposing a displacement/angular velocity, which is related to the strain/shear rate, and the res-

PUC-Rio - Certificação Digital Nº 1121442/CA

ulting torque is measured by the transducer located in the upper part of the rheometer.

Since apparent wall slip is known to occur at low shear rates for most dispersions, cross-hatched parallel plates (Fig. 3.2) were used in the rheological characterization of this gel. More details on geometry selection are given in Appendix A.

(a)

(b)

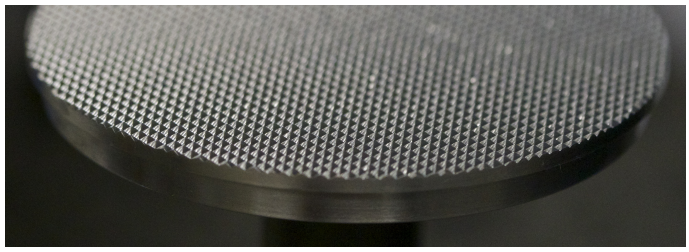

Figure 3.2: Cross hatched parallel plate geometry: (a) lower and upper plates; (b) detail.

However, the shear rate is not constant across the radius in the parallel plate geometry [12]. Thus, the flow is inhomogeneous and the calculated stress needs to be corrected for this geometry. The well-known Weissenberg-Rabinowitsch equation was employed for steady state flow data, and a novel correction for oscillatory flows was developed. This topic is better addressed in Appendix B.

The sample placement procedure is illustrated in Fig. 3.3. A lot of care is taken in order to obtain repeatable results.

PUC-Rio - Certificação Digital Nº 1121442/CA

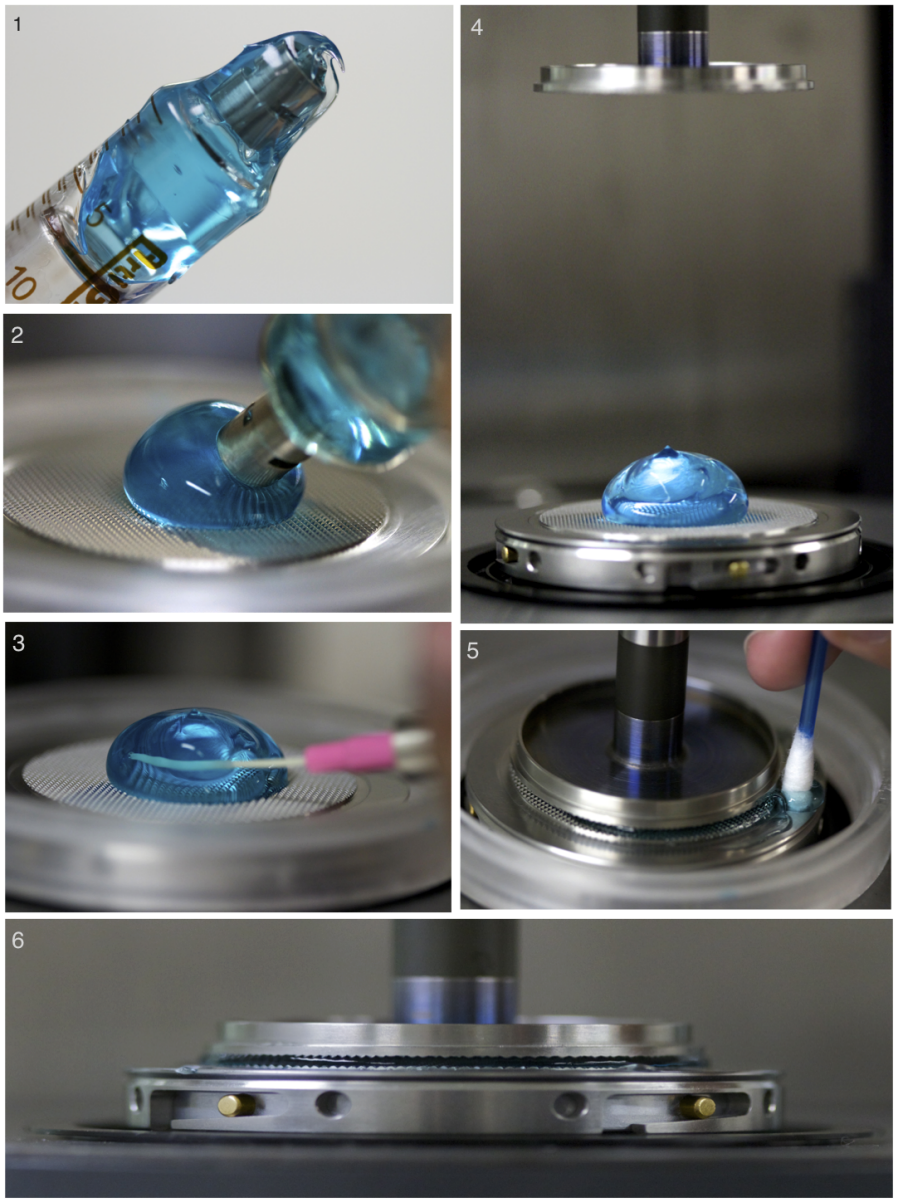

Figure 3.3: Steps for setting up the rheometric experiments.

For every run, a new gel sample is used. The gel is loaded on the center of the lower plate with a glass syringe (Figs. 3.3-1 and 2). Air bubbles need to be eliminated from the sample so as not to violate the continuum hypothesis, which states that the gap needs to be at least ten times bigger than the particle/droplet/bubble size. With the aid of an empty syringe, the bubbles are "sucked" from the sample, one bubble at a time (Fig. 3.3-3). Once all bubbles are removed, the upper fixture is slowly lowered (Fig. 3.3-4) to avoid air entrapment and the gel spreads across the gap. When a 1.05mm gap is reached, the sample is carefully trimmed with a cotton swab (Fig. 3.3-5). Finally, the gap is set to 1.00mm (Fig. 3.3-6). Then, a solvent trap cover is placed to minimize evaporation of the sample.

PUC-Rio - Certificação Digital Nº 1121442/CA

Before testing, the sample is kept at rest for stabilization of the temperature and relaxation of the material. It was observed that if the sample is not kept at rest for enough time, total relaxation will not occur and a residual stress can affect the results. If this happens, the output stress wave, and thus the Lissajous curve, will be vertically shifted, i.e., maximum and minimum values have not the same modulus, although the amplitude of the wave is correct. Hence, this step is particularly important for the experiments presented in Sec. 4.7, where we observe the response of the individual oscillation cycles, and not just the amplitude values. Residual torque might be generated from spreading of the material across the gap or from trimming the sample. Hence, after setting up the test, the torque acting on the sample is monitored. After about 15 minutes, the torque stops decreasing and reaches an approximate constant value, so that the rheometric experiment can be performed.

3.1 Rheometric experiments

A large set of rheometric experiments was carried out to fully characterize the material behavior. Every curve plotted in Chapter 4 is an average of at least three tests, except for the Lissajous plots. All strain-rate controlled experiments, i.e. constant shear rate, strain- and time sweeps, were performed in the ARES-G2 rheometer, whereas the stress controlled tests (creep and stress sweeps) were carried out in the AR-G2 rheometer. Flow curves and time sweeps were carried out in both rheometers for comparison purposes.

Indeed, the steady state flow curve is perhaps the most popular rheometric experiment. It shows the general behavior of the material, for example if shear thinnnig, shear thickening or viscoplastic. Moreover, the parameters of the appropriate constitutive equation for shear stress (or shear viscosity) can be obtained. In our case, the Herschel-Bulkley model, given by

$$\tau(\dot{\gamma}) = \tau_y + k\,\dot{\gamma}^{\,n} \tag{1}$$

was chosen to fit the data of the viscoplastic gel and consequently the yield stress (τ_y), the consistency index (k), and the power-law exponent (n) can be determined.

Constant shear rate tests are useful to obtain the time needed for the material to reach steady state at different shear rates, and thus the minimum point time input for the flow curve. Moreover, the steady state values of shear stress and viscosity can be compared with the ones obtained from the flow curve, for different shear rates.

PUC-Rio - Certificação Digital Nº 1121442/CA

Creep (constant stress) tests are commonly performed to assess the yield stress of a material. A constant stress is applied to the sample and the strain and/or strain rate responses are measured as a function of time. If the applied stress is below τ_y, the strain tends to a constant value and the shear rate goes to zero, indicating that no flow occurs. At each experiment, the applied stress is increased until it is sufficiently high to make the material flow. If the viscosity response over time is analyzed instead, viscosity bifurcation curves are obtained [33, 34].

In addition, different oscillatory experiments were performed, namely 1) stress amplitude sweep, and 2) strain amplitude sweep, and 3) time sweep. Oscillatory tests consist mainly of tuning frequency and strain or stress amplitudes by imposing a sinusoidal motion to the sample.

Stress and strain amplitude sweeps are similar tests. Both are carried out at a fixed frequency, sweeping either the strain or stress amplitude. From these tests, the linear viscoelastic region can be determined as the region where G' and G" are constant (and parallel to each other).

Time sweeps were performed to evaluate possible changes in the sample due to evaporation. A fixed frequency and a constant strain amplitude (belonging to the viscoelastic region) are applied to the sample, and the response of the G' and G" material functions are recorded over time. If the sample is stable, no changes occur in the moduli, i.e. G' and G" remain constant over the duration of the test. Hence, from this test we can obtain the maximum test time.

The LAOS results are achieved using individual time sweeps under the transient acquisition mode. This means that instead of obtaining the data in terms of the wave amplitudes, as in regular oscillatory experiments, the "raw data", i.e. data corresponding to the entire individual cycles, is saved. Since the focus of this work is on the large amplitude domain, these experiments are described next in detail.

3.2 Quasi-linear LAOS methodology

The idea of the employed LAOS methodology is to probe the material under a wide range of time scales and amplitudes. In this work, we chose to investigate the material's behavior under a broad range of frequencies, varying from 0.01 to 100 Hz, for four different stress amplitudes, namely 10 Pa, 95 Pa, 125 Pa, and 312Pa. Different stress levels correspond to different structuring levels (λ) of the material.

To obtain inertia-free torque measurements, the strain rate controlled

PUC-Rio - Certificação Digital Nº 1121442/CA

rheometer was employed. That means we actually control the strain amplitude instead of the stress amplitude. Nevertheless, it is possible to indirectly control the stress amplitude: for each frequency, a preliminary strain amplitude sweep test was performed, and the strain amplitude that corresponds to the sought-for stress amplitude was determined.

To guarantee that steady state data was always achieved, each LAOS result corresponds to an individual time sweep test with fixed frequency and amplitude, as previously mentioned. To obtain the raw data, i.e. data for each individual cycle performed, instead of the regular amplitude data recorded from oscillatory tests, the "correlation" mode of data acquisition must be changed to "transient" mode. Then, the number of points per cycle, the delay time and/or delay cycles, and the sampling cycles can be set. Obviously, the number of recorded cycles depends on the imposed frequency and on the duration of the test. More details on the set-up of these experiments is given in Appendix C.

It is also important to note that since the parallel-plate geometry was employed, the stress amplitude obtained from each test is corrected using the equation presented in Appendix B:

$$\tau_{R,a} = \frac{T_a}{2\pi R^3}\left[3 + \frac{d\ln\left(T_a/2\pi R^3\right)}{d\ln\dot{\gamma}_{R,a}}\right] \tag{2}$$

where the derivative $\frac{d\ln\left(T_a/2\pi R^3\right)}{d\ln\dot{\gamma}_{R,a}}$ is a function of the amplitude $\dot{\gamma}_{R,a}$ and needs to be evaluated at a constant frequency and varying $\dot{\gamma}_{R,a}$ around the value of interest. Unfortunately, this correction is applicable only to the stress amplitude, and not to the instantaneous stress along the cycle, so that the Lissajous curves cannot be corrected. Moreover, Equation 2 is valid only for sinusoidal responses.

To analyze the LAOS results, a model-based framework, the quasi-linear LAOS (QL-LAOS) methodology, is employed. As mentioned in the end of Sec. 2.2, the structuring-level-dependent Jeffreys model proposed by de Souza Mendes and Thompson [8] is applied to rheometric oscillatory flows to obtain physically meaningful material functions.

It is important to emphasize that this methodology differs significantly from the ones usually employed in the literature, since most works focus on analyzing the structure changing motions, i.e. the non-sinusoidal responses. During a cycle in a large-amplitude oscillatory experiment, the stress varies from zero to large values. Consequently, the state of the microstructure changes along each cycle, rendering the task of assessing the mechanical behavior of the material rather difficult. Contrariwise, when performing experiments in

PUC-Rio - Certificação Digital Nº 1121442/CA

the quasi-linear regime, for each λ the mechanical behavior of the material is measured at a fixed microstructural state.

As previously discussed and according to de Souza Mendes and Thompson [8], elliptical curves are obtained when: (i) $\tau_a < \tau_y$, for all frequencies, and (ii) $\tau_a \gtrsim \tau_y$ for $t_{eq} \gg 1/\omega$, as illustrated in Fig. 3.4.

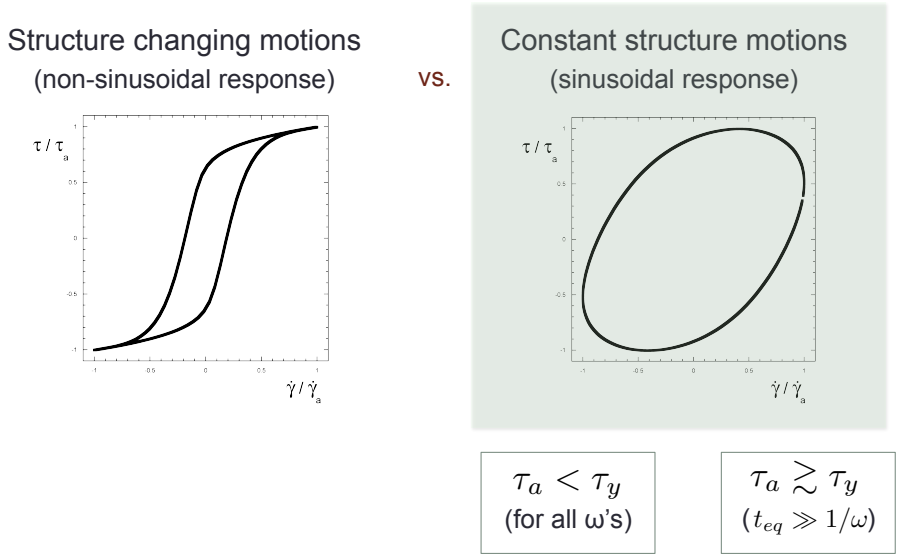

Figure 3.4: Focus of our quasi-linear LAOS methodology.

However, in general it is not guaranteed that a constant-structure motion is always attainable. There may exist materials whose time scale of microstructure buildup is so small that the structuring level will change significantly along the cycle even at the highest frequencies available. For these materials, QL-LAOS might not be useful. For the hair gel employed here, however, constant-structure motions were attained for a wide range of frequencies as will be seen in Chapter 4.

From each Lissajous curve it is possible to calculate the ratio $\tau_a/\dot{\gamma}_a$, referred to as QL-LAOS viscosity. Thus, for each stress amplitude τ_a (or structuring level λ) a plot of the LAOS viscosity vs. frequency can be obtained, and the experimental results can be fitted by the following expression [30]:

$$\frac{\tau_a}{\dot{\gamma}_a} = \sqrt{\frac{(\eta_v/\eta_r)^2 + [(\eta_v - \eta_r)(\omega/G_s)]^{2(1-\alpha)}}{1 + [(\eta_v - \eta_r)(\omega/G_s)]^{2(1-\alpha)}}} \tag{3}$$

PUC-Rio - Certificação Digital Nº 1121442/CA

Hence, the following parameters can be obtained from the curve fitting:

- η_v, the asymptotic value of the QL-LAOS viscosity as the frequency becomes very small;
- η_r, the asymptotic value of the QL-LAOS viscosity for high frequencies;
- G_s, a measure of the slope of the curve at intermediate frequencies;
- α, empirical constant which indicates the departure from the Jeffreys-like behaviour, since the value predicted by the analytical solution is zero;
- θ_1, the relaxation time, calculated with the previously obtained η_r, η_v, and G_s with:
$$\theta_1 = (1 - \frac{\eta_r}{\eta_v})\frac{\eta_v}{G_s} \tag{4}$$
- θ_2, the retardation time, also calculated with the previously obtained η_r, η_v, and G_s;
$$\theta_2 = (1 - \frac{\eta_r}{\eta_v})\frac{\eta_r}{G_s} \tag{5}$$

A numerical result for the QL-LAOS viscosity is illustrated in Fig. 3.5 together with the obtained parameters.

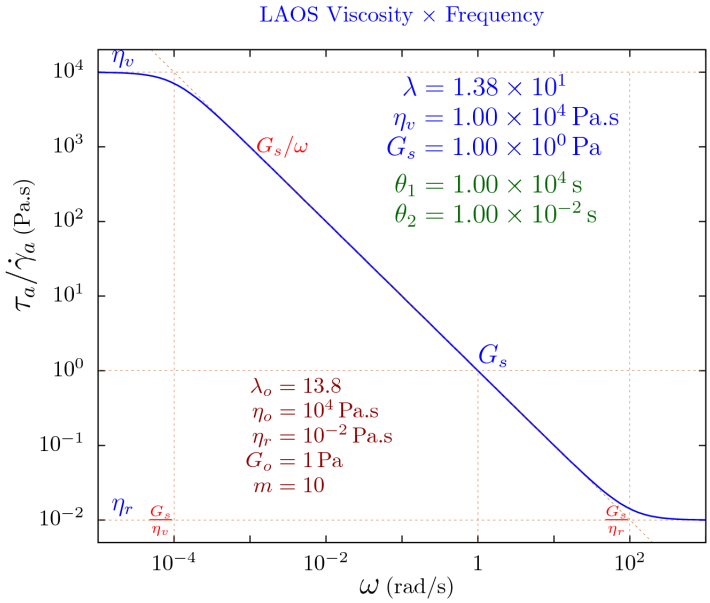

Figure 3.5: Focus of our quasi-linear LAOS methodology.

As will be shown in Chapter 4, the agreement between the theoretical predictions and experimental data is quite remarkable.

PUC-Rio - Certificação Digital Nº 1121442/CA

4
Results and Discussion

This chapter contains the results of the rheological characterization of the elasto-viscoplastic gel. First, constant shear rate results (Sec. 4.1) are presented. Steady state values of stress and viscosity are compared to the flow curve (Sec. 4.2). The yield stress of the material is inferred from constant stress tests (Sec. 4.3). Next, results pertaining to oscillatory experiments are exhibited in Secs. 4.4 (time sweeps), 4.5 (stress sweeps), and 4.6 (strain sweeps). Then, LAOS results are presented in Sec. 4.7 in terms of the wave shapes (4.7.1), of the Lissajous-Bowditch plots (4.7.2) and of the LAOS viscosity (4.7.3).

PUC-Rio - Certificação Digital Nº 1121442/CA

4.1
Constant shear rate tests

Constant shear rate tests were performed to evaluate the time needed for the material to reach steady state, which is an input of the flow curve. Moreover, the values of shear stress and viscosity at equilibrium can be compared to those obtained in the flow curve, as will be illustrated in Sec. 4.2. Results for five different shear rates are presented in Fig. 4.1.

As expected, samples submitted to high shear rates reach steady state almost instantly. As the shear rate is decreased, the time needed to reach equilibrium increases. For the lowest shear rate, $\dot{\gamma} = 0.001\ s^{-1}$, more than 1000 seconds are needed to reach a constant value of stress (and consequently of viscosity). As will be discussed later in Sec. 4.4, the duration of a test performed in the ARES rheometer is limited to 1000 seconds, so that the steady state was not obtainable for this shear rate.

From Fig. 4.1a, it is possible to note that the steady-state values of stress decrease as the applied shear rate decreases and approach the yield stress as the shear rate tends to zero. The same results are plotted in terms of viscosity in Fig. 4.1b. The steady-state viscosity values decrease progressively with increase of applied shear rate. Again, for the lowest shear rate, the equilibrium was not obtained in the experiment time.

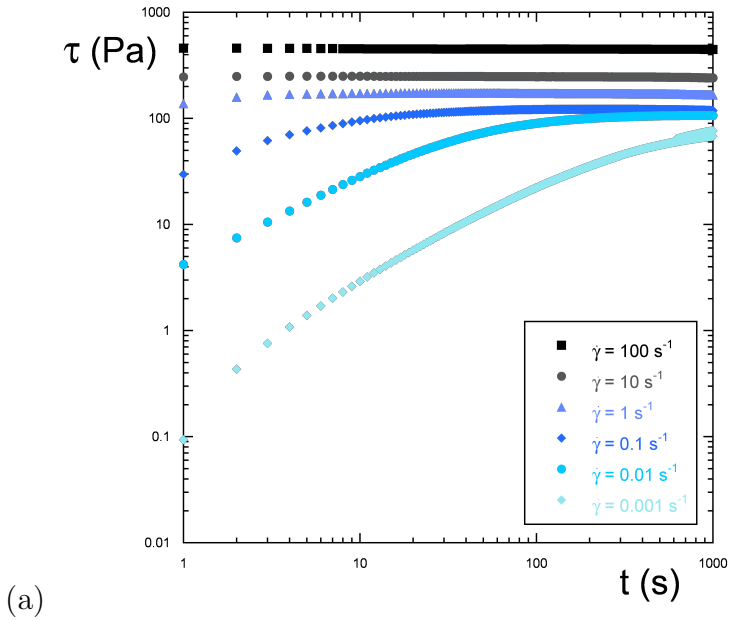

(a)

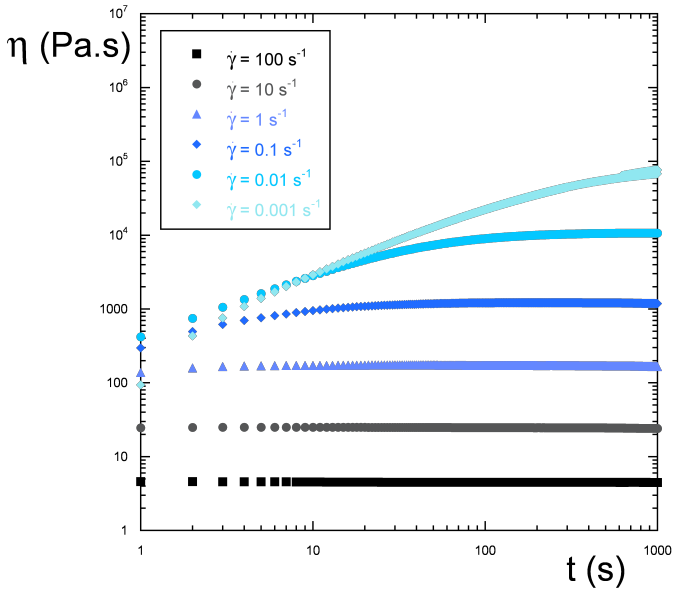

(b)

Figure 4.1: Constant shear rate tests: (a) Stress vs. time (b) viscosity vs. time.

Although the values of stress and viscosity should be corrected due to the non-homogeneous flow, the information obtained on the time needed to reach steady state still is valid. Moreover, the values of stress and viscosity at equilibrium can be compared to the non-corrected flow curve, and then the entire flow curve can be corrected using the Weissenberg-Rabinowitsch equation.

4.2 Steady state flow

A large number of steady state flow curves were carried out in both rheometers over a wide range of shear rates. The average of these tests is

PUC-Rio - Certificação Digital Nº 1121442/CA

plotted in Fig. 4.2 together with the values of equilibrium stress (Fig. 4.1a) and viscosity (Fig. 4.1b) obtained from the constant shear rates experiments presented in the previous section.

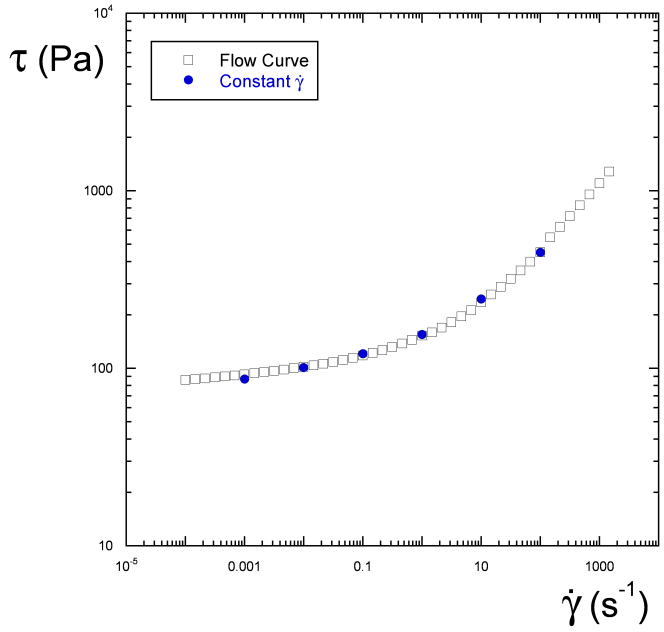

(a)

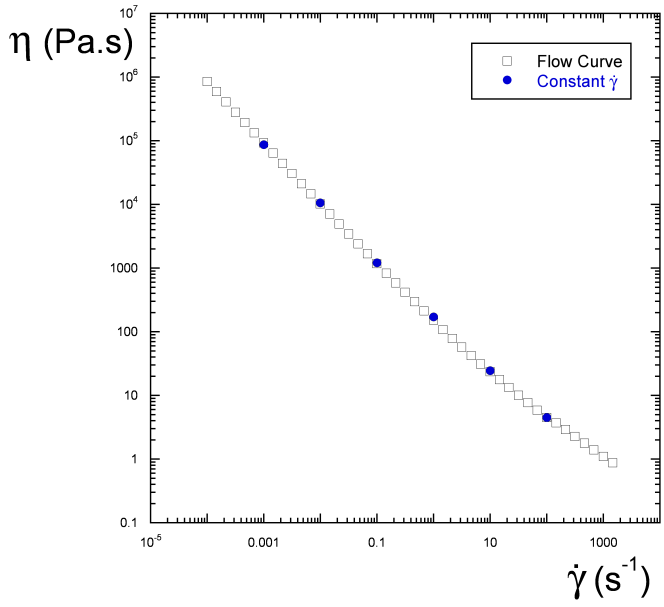

(b)

Figure 4.2: Steady state flow curve and constant shear rate tests plotted together: (a) Stress vs. shear rate (b) viscosity vs. shear rate.

The flow curve reveals a shear-thinning behavior of the gel and the existence of a yield stress. As can be seen, the agreement between the different rheometric experiments is good. In the low shear rate region, the stress values slightly decrease, instead of reaching a plateau corresponding to the yield stress, which indicates that maybe not enough time was waited for the sample to reach steady state or that the shear rate was not low enough.

PUC-Rio - Certificação Digital Nº 1121442/CA

Nevertheless, this flow curve needs to be corrected with the Weissenberg-Rabinowtisch equation (Eq. 1). Fig. 4.3 shows the comparison between the corrected and the non-corrected data.

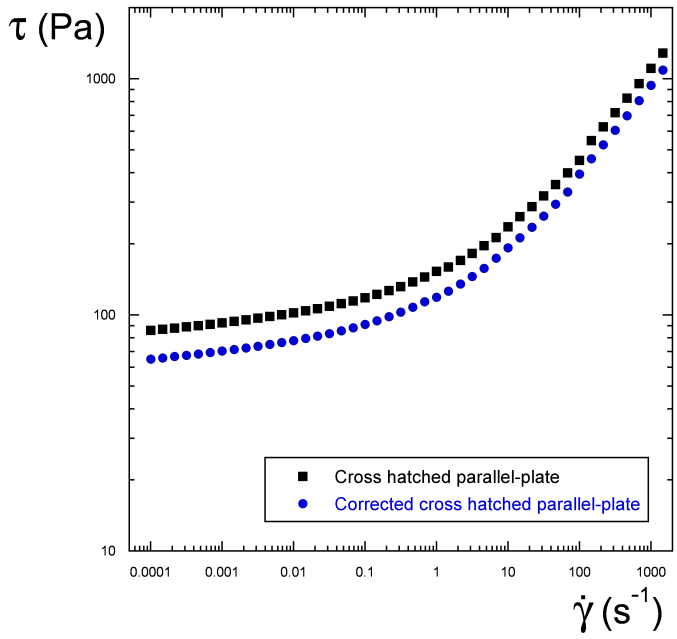

Figure 4.3: Steady state flow curve: comparison between corrected and non-corrected curves.

It is possible to note that the correction is not a constant, being of greater importance in the vicinity of the yield stress. At high shear rates (power-law region), the ratio between the corrected stress and the non-corrected is equal to 0.85, whereas at the low shear rate range this ratio equals to 0.75.

The corrected curve is presented in Fig. 4.4 along with a curve fitting with the Herschel-Bulkley equation.

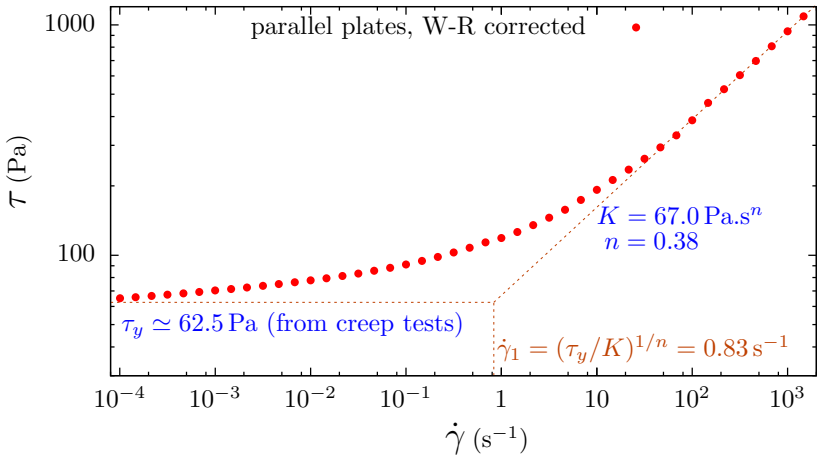

Figure 4.4: Steady state flow curve, Weissenberg-Rabinowitsch corrected.

PUC-Rio - Certificação Digital Nº 1121442/CA

As can be seen, the equation fits well the flow-curve data, with a yield stress of $\tau_y \approx 62.5$ Pa, a consistency index of K = 67 Pa.s^n, and a power-law index of n = 0.38.

4.3 Constant stress tests

Next, constant stress tests were carried out to assess the yield stress of the gel. A wide range of stresses, from 50 to 200Pa, was investigated as can be seen in Fig. 4.5. Results are presented in terms of strain (Fig. 4.5a) and shear rate (Fig. 4.5b) versus time.

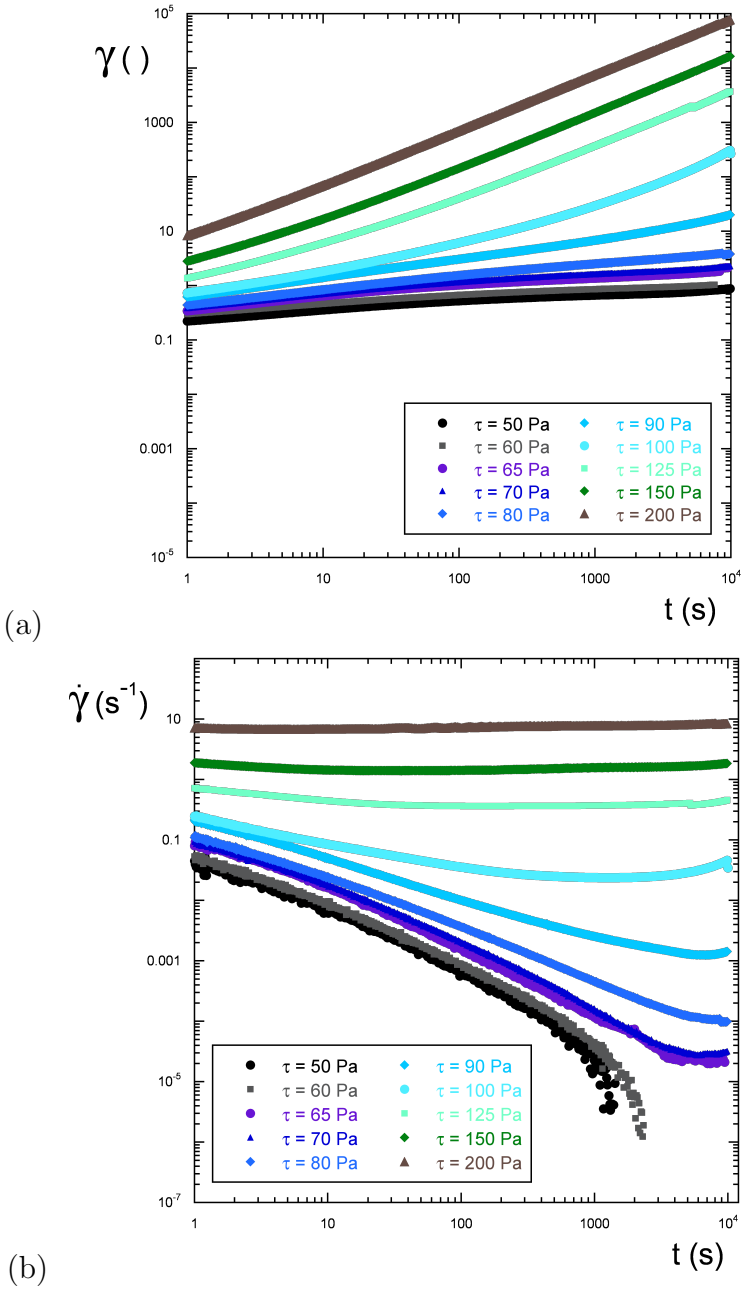

Figure 4.5: Creep tests: (a) Strain vs. time and (b) Shear rate vs. time.

PUC-Rio - Certificação Digital Nº 1121442/CA

There are two expected results in creep tests: if the applied stress is not sufficient to make the material flow, the strain is constant over time, and the shear rate goes to zero. On the other hand, if the stress is above the yield stress, an increasing strain and consequent constant shear rate are observed.

In this case, the strain response may be misleading, once all curves seem to have increasing strain with time, so that from this plot we may assume the yield stress is below 50 Pa.

However, if results are plotted in terms of the shear rate, it is evident that the shear rate goes to zero for 50 and 60 Pa, indicating that no flow occurs. For slightly higher stresses, an interesting response is observed: the shear rate initially decreases, tending to zero, but at some point around 2000 seconds, it stops diminishing and increases again. This delayed response may be explained due to the thixotropy of the material. Also, the higher the applied stress, the smaller the time needed to reach a steady state. For high enough shear stresses (125, 150 and 200 Pa), the shear rate tends to a constant value rather quickly. Therefore, from the results it is clear that the yield stress is between 60 and 65 Pa, which is in accordance with the steady state flow curve.

Although the yield stress is not a time-dependent material property, because of the delayed response of the material it is important to evaluate the sample response along a sufficient amount of time. For instance, if the duration of our creep experiments was of only 100 seconds (which is common to see in the literature), we would wrongly estimate the yield stress to $\approx$ 90 - 100 Pa.

Considering the strict definition of yield stress, it cannot really be measured over a finite time of observation. However, for practical purposes, when measuring the yield stress of a material it is important to always bear in mind its associated application's characteristic time. For example, in drilling operations, a maximum stoppage time of 6 hours is considered before restarting the flow in the well annulus, so that the yield stress of drilling mud or cement pastes needs to be estimated for this amount of time. Thus, it is important to tune duration of the test with the characteristic time of the application.

In the case of the present research, no specific application is considered, though. Nevertheless, due to experimental limitations, such as evaporation of the sample, the duration of each rheometric experiment is limited. As will be discussed in the next Section (4.4), a duration of 10.000 seconds was considered in the stress-controlled rheometer employed for the creep tests.

Furthermore, it is important to emphasize that the results displayed in Fig. 4.5 also need correction due to the non-homogeneous flow. However, the estimated yield stress is still correct, because the point below which no flow

PUC-Rio - Certificação Digital Nº 1121442/CA

occurs does not depend on the correction, once the correction accounts for the varying shear rate across the radius (and in this case the shear rate is zero).

4.4 Time sweep tests

As previously explained, time sweeps were performed to evaluate possible changes in the sample due to evaporation, once the hair gel has alcohol (which is highly volatile) in its composition. Experiments were performed in both rheometers with a frequency of 1 Hz and duration of 10.000s. The tests presented in Fig. 4.6 are essentially the same, except that in the stress controlled rheometer (AR-G2) a stress amplitude of 10 Pa was imposed (black curves), while a corresponding strain amplitude was maintained in the strain-controlled ARES-G2 (blue curves), with both amplitude values corresponding to the linear viscoelastic regime. The results are shown in terms of G' and G".

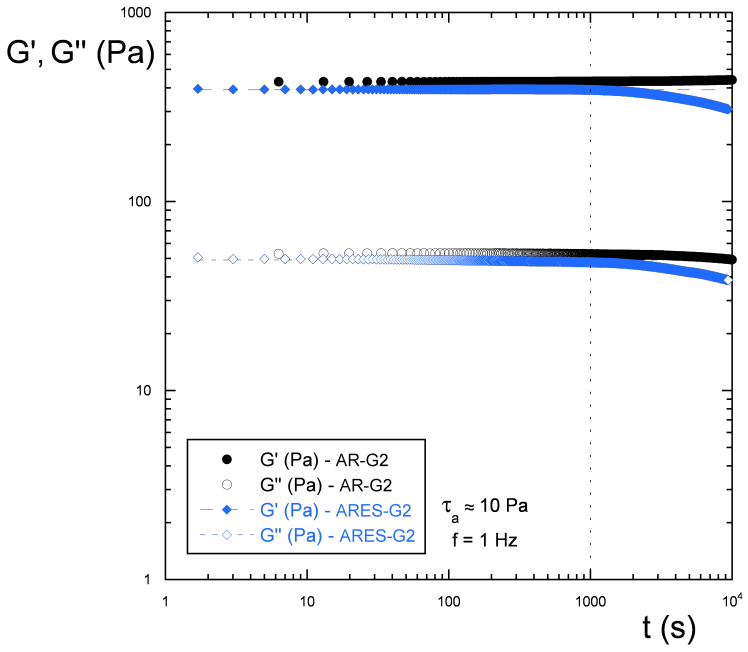

Figure 4.6: Time sweep performed with $\tau_a = 10$ Pa and f = 1 Hz.

A remarkable difference can be observed between the rheometers' results. The black curves show that in the AR-G2 rheometer the sample is very stable, with both moduli constant throughout the entire duration of the test.

However, in the ARES-G2 the sample is very stable until approximately 1000 seconds of test, when both moduli start to decrease. A dotted line, corresponding to constant values of G' and G", was plotted with the ARES-G2 data to clarify the deviation from the linear behavior. Indeed, if the test is stopped beyond this point, visual inspection of the sample shows that gel has evaporated. This effect can be significant, because a slight reduction of 1mm

PUC-Rio - Certificação Digital Nº 1121442/CA

in the radius of the sample leads to a 10% error in the stress calculated by the rheometer for this geometry. Thus, for all rheometric experiments performed in the ARES-G2 rheometer, a maximum duration of 1000 seconds is considered, whereas in the AR-G2 experiments may be carried out with a duration of up to 10.000 seconds. The difference in amount of sample evaporation between rheometers remains to be investigated.

4.5 Stress sweep tests

Stress sweeps were performed at four different frequencies to unveil the elastic behavior of the material along a broad range of imposed stress amplitudes. Results are presented in Fig. 4.7, in terms of the storage modulus (G', filled markers), and of loss modulus (G", empty markers).

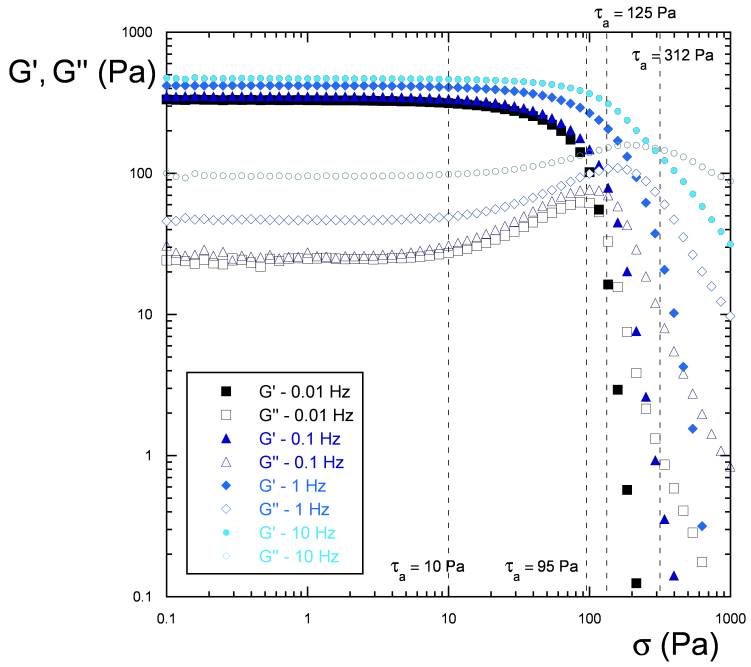

Figure 4.7: Stress sweeps performed at different frequencies. The four dotted lines indicate the aimed stress amplitudes in the LAOS tests.

For all frequencies, G' is higher than G" for a great range of stress amplitudes, indicating the solid-like/elastic behavior of the gel.

Also, the four vertical dotted lines indicate the stress amplitudes chosen for the LAOS experiments. It is possible to note that $\tau_a = 10$ Pa pertains to the linear viscoelastic region, once this value of stress is below the yield stress (τ_y). The other three stress amplitudes, 95 Pa, 125 Pa, and 312 Pa correspond to approximately 1.5 τ_y, 2 τ_y, and 5 τ_y, respectively.

PUC-Rio - Certificação Digital Nº 1121442/CA

4.6 Strain sweep tests

As previously said, stress and strain sweeps are analogous tests. From both it is possible to obtain the linear viscoelastic region, either in terms of stress or strain amplitude, respectively. To illustrate the agreement between these two tests, sweeps for two different frequencies of 0.1Hz (Fig. 4.8a) and 10Hz (Fig. 4.8b) are presented next. The results are plotted in terms of the strain amplitude. The black curves correspond to the stress sweeps and the colored curves to the strain sweeps. Again, the filled markers correspond to G' and the empty markers to G".

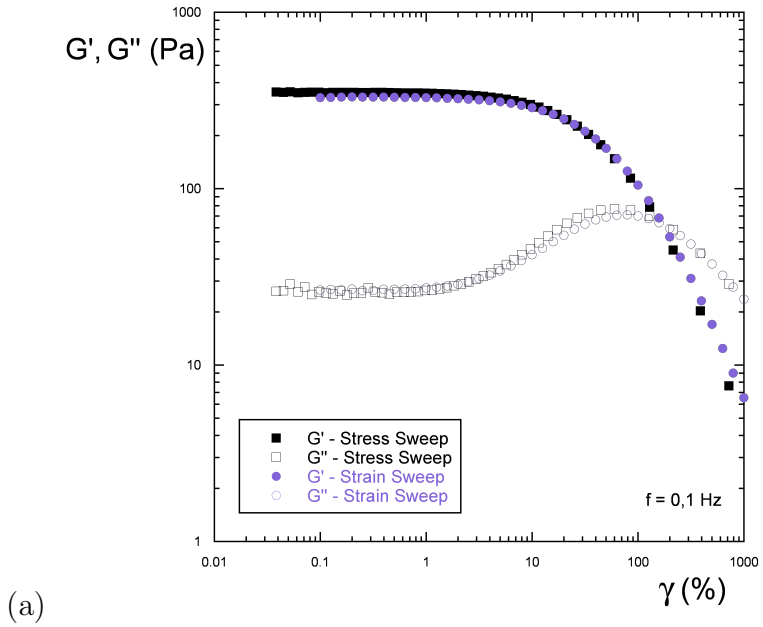

(a)

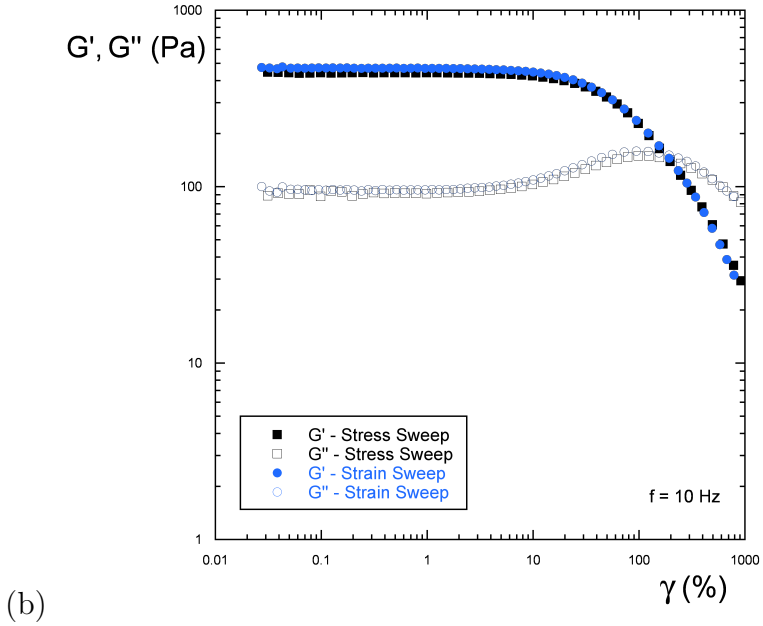

(b)

Figure 4.8: Comparison between strain and stress sweeps, plotted as G' / G" vs. strain (%).

PUC-Rio - Certificação Digital Nº 1121442/CA

It is clear that both tests give rise to the same result. This shows that, a priori, it is indifferent wether we perform stress- or strain-controlled experiments for oscillatory testing. For our research, this is particularly important, once we actually perform strain-controlled experiments to evaluate the results in terms of the stress amplitudes.

Next, we present the strain amplitude sweeps results for all frequencies investigated. To better accommodate the large amount of data, results were divided into four different plots, each for a range of frequencies, namely 0.01 - 0.1Hz (Fig. 4.9a), 0.1 - 1Hz (Fig. 4.9b), 1 - 10Hz (Fig. 4.9c), and 10 - 100Hz (Fig. 4.9d).

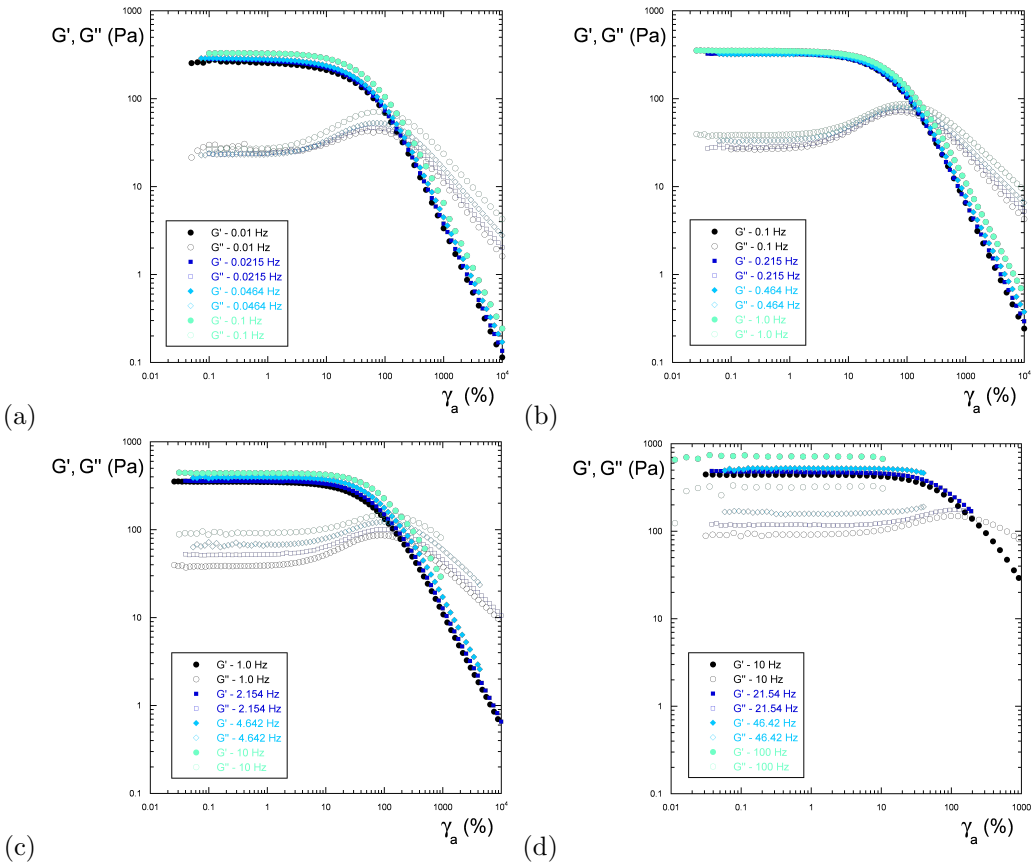

Figure 4.9: Strain sweeps at different frequency ranges: (a) 0.01 - 0.1 Hz; (b) 0.1 - 1 Hz; (c) 1 - 10 Hz; (d) 10 - 100 Hz.

It is clear that all strain sweeps present the same general behavior: presence of a linear viscoelastic region at low strain amplitudes, with constant G' and G", where G' > G". This linear viscoelastic region is followed by a decrease in G', which indicate the yielding of the material. In the case of G", the curve first increases and then drops. The crossover of G' and G" occurs approximately at the maximum of the G" curve.

Although G' and G" are no longer valid quantities in the large amplitude oscillatory shear regime, Hyun et. al [35] arguee that the behavior observed in

PUC-Rio - Certificação Digital Nº 1121442/CA

a strain sweep can be linked to microstructural changes. In their work, it was found that there exists at least four types of LAOS behavior, as presented in Fig. 4.10.

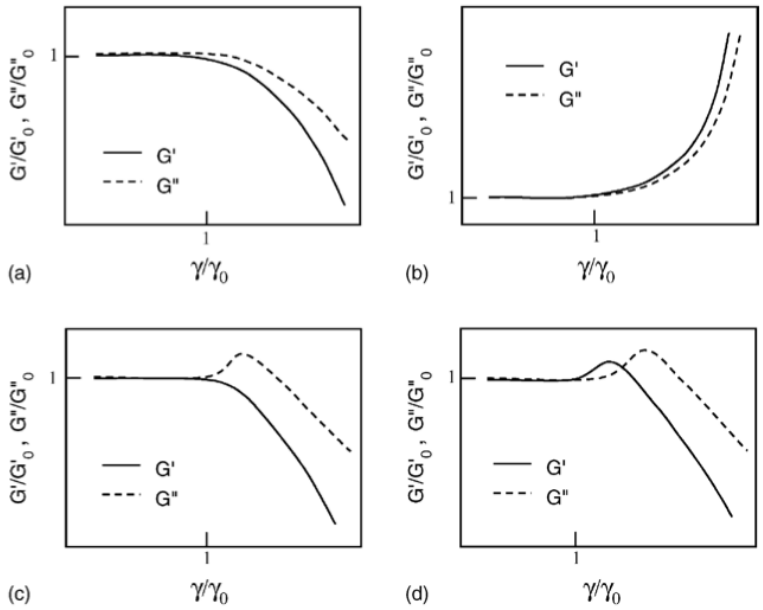

Figure 4.10: Types of LAOS behavior, presented in dimensionless strain sweeps: (a) strain thinning; (b) strain hardening; (c) weak strain overshoot; (d) strong strain overshoot. Reproduced from [35].

The four types of LAOS behavior are:

- Type I - strain thinning : G' and G" decreasing (Fig. 4.10a);
- Type II - strain hardening : G' and G" increasing (Fig. 4.10b);
- Type III - weak strain overshoot: G' decreasing, G" increasing followed by decreasing (Fig. 4.10c);
- Type IV - strong strain overshoot: G' and G" increasing followed by decreasing (Fig. 4.10d).

Clearly, the behavior of the hair gel pertains to the type III. According to Hyun et. al, when an external strain is imposed to the sample, the microstructure initially resists against this deformation, which increases G", up to a certain critical strain above which the polymer chains align with the flow field, leading to a decrease in G".

The difference between the imposed frequencies is not clear in Fig. 4.9. Therefore, the same results are plotted in a different way in Fig. 4.11. Each graph contains four frequencies pertaining to four different decades.

PUC-Rio - Certificação Digital Nº 1121442/CA

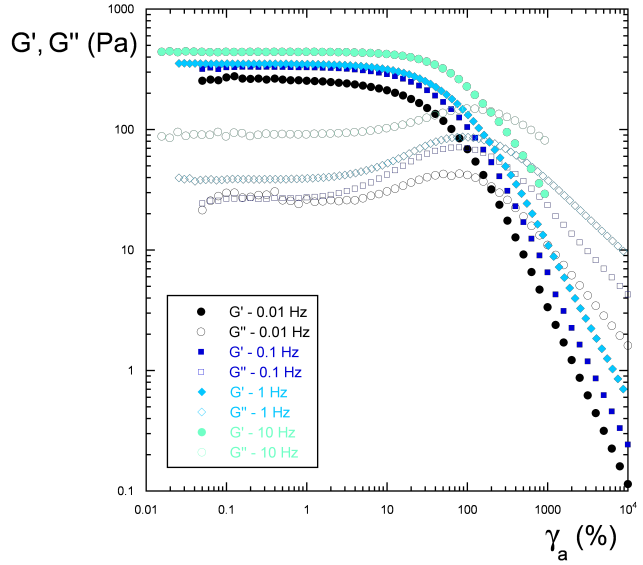

(a)

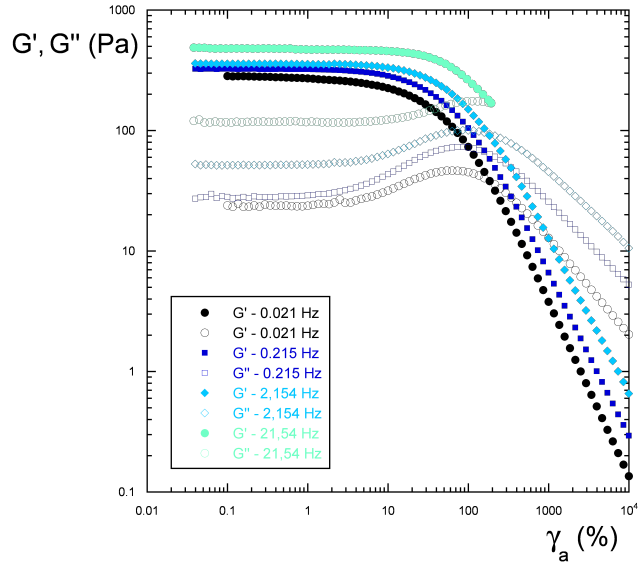

(b)

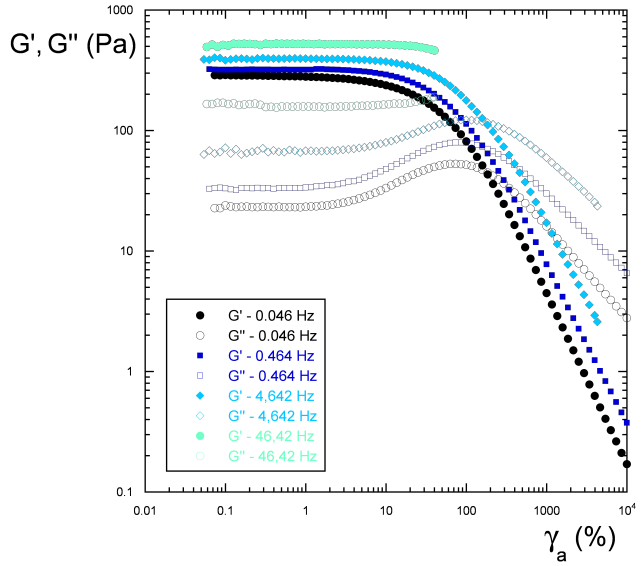

(c)

Figure 4.11: Strain sweeps performed at different frequencies: (a) multiples of 1.0Hz; (b) multiples of 2.15Hz; (c) multiples of 4.64Hz.

PUC-Rio - Certificação Digital Nº 1121442/CA

As can be seen in the three graphs, as the frequency is increased, both moduli G' and G" increase. At the highest frequencies, the curves are interrupted because the rheometer stops increasing the strain amplitude, possibly because of difficulty in controlling a large deformation at short times or in switching the transducer mode. In LAOS experiments, however, tests were conducted without any problems.

Also, these strain sweeps were carried out at different frequencies to obtain the strain amplitude values that should be imposed to the gel sample in LAOS experiments to achieve the sought-for stress amplitude, as previously explained (Sec. 3.2). The strain amplitude values [%] to be imposed in LAOS experiments, for each frequency (different columns) and stress amplitude (different rows), are displayed in Tables 4.1 and 4.2.

Table 4.1: Values of strain amplitudes [%] to be imposed in LAOS experiments, range ω = 0.01 - 0.464 Hz.

τ_a [Pa]	0.01 Hz	0.0215 Hz	0.0464 Hz	0.1 Hz	0.215 Hz	0.464 Hz
10	4.21	3.64	3.46	2.79	2.70	2.64
95	149.93	134.92	89.79	61.69	54.78	44.83
125	2499.61	449.78	299.32	164.57	139.42	109.56
312	75088.85	32020.20	16469.1	6780.9	3505.0	1741.9

Table 4.2: Values of strain amplitudes [%] to be imposed in LAOS experiments, range ω = 1 - 100 Hz.

τ_a [Pa]	1 Hz	2.15 Hz	4.64 Hz	10 Hz	21.54 Hz	46.42 Hz	100 Hz
10	2.37	2.27	2.49	2.18	1.96	1.57	1.12
95	37.53	30.85	26.81	21.70	18.13	13.32	7.95
125	74.66	54.74	45.69	33.85	27.06	19.49	10.46
312	835.79	509.56	248.35	147.74	95.583	-	-

It is important to note that these values already account for the parallel plate correction. This was done by correcting the stress amplitude from the strain sweeps, so that the displayed values of strain amplitude already belong to corrected values of stress. However, as previously explained, the instantaneous stress cannot be corrected, only the amplitude of the wave. Hence, in all figures presented in Secs. 4.7.1 and 4.7.2, no stress correction is present. Nevertheless, the results of LAOS viscosity presented in Sec. 4.7.3 account for the stress correction, once they only depend on stress amplitude τ_a and shear rate amplitude $\dot{\gamma}_a$.

PUC-Rio - Certificação Digital Nº 1121442/CA

4.7 LAOS tests

This section presents LAOS results corresponding to four different stress amplitudes τ_a, namely 10, 95, 125 and 312 Pa. Actually, $\tau_a = 10$ Pa does not belong to the large amplitude oscillatory shear regime, but tests were carried out at this amplitude for comparison purposes. The other stress amplitudes correspond approximately to 1.5 τ_y, 2 τ_y and 5 τ_y, respectively.

As previously explained (Sec. 3.2), the LAOS experiments consist of individual time sweep steps, performed under fixed frequency and strain amplitude. An example of a complete LAOS experiment is shown in Fig. 4.12 in terms of stress as a function of the shear rate.

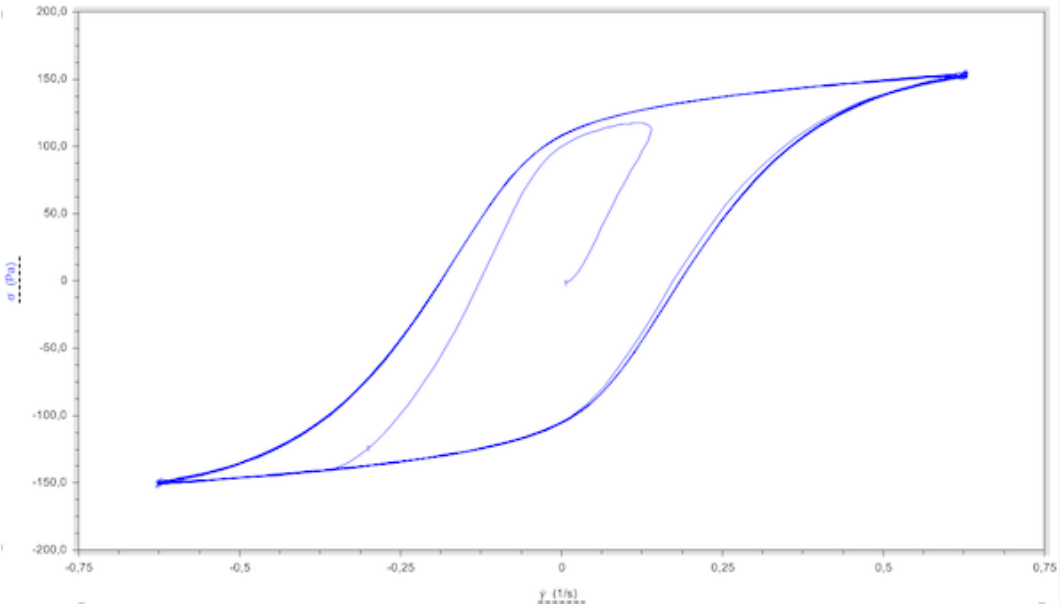

Figure 4.12: Viscous Lissajous plot as an example of a complete time sweep test.

From the figure it is possible to see the initial transient response of the material, beginning in the origin, and that the steady state regime (indicated by the superposed curves) is achieved within few cycles. Henceforward, in all figures presented in this section, a single cycle corresponding to the steady state was selected.

Hereafter, the differences between shapes of the input and output waves are analyzed. Then, viscous Lissajous plots are used to unveil characteristics of the mechanical behavior of the elasto-viscoplastic material under different circumstances. All results obtained are summarized in a Pipkin diagram (Fig. 4.22). Finally, quasi-linear LAOS viscosity plots are presented to compare the experimental results with the theoretical predictions of the Jeffrey's framework and with the numerical results by de Souza Mendes and Thompson [8].

PUC-Rio - Certificação Digital Nº 1121442/CA

4.7.1 Wave shapes

The shear rate and stress waves pertaining to the LAOS experiments are presented in Figs. 4.13, 4.14, 4.15, and 4.16, where each figure corresponds to a different stress amplitude. In each figure we present a set of plots of both shear rate and stress responses as a function of a dimensionless time ($\omega t \,/\, 2\,\pi$), for four different frequencies, namely 0.01, 0.1, 1 and 10 Hz. The blue curves correspond to the shear rate waves, which are the input of the test, and the red curves correspond to the stress response, which is the output of the test.

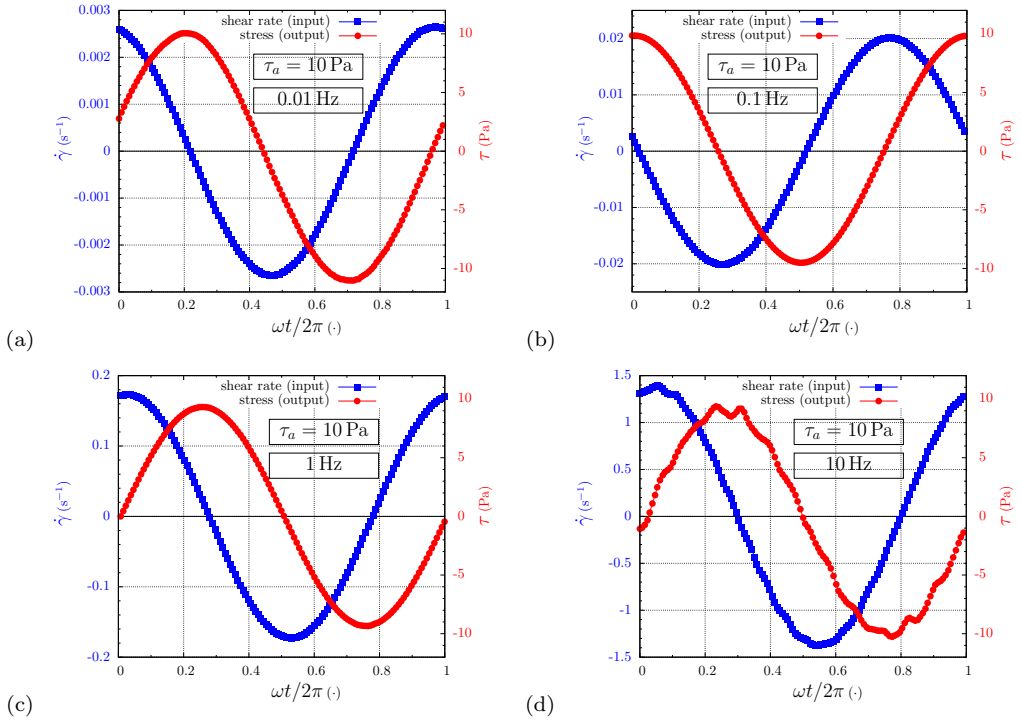

Figure 4.13: Input shear-rate wave and output raw-stress wave of $\tau_a = 10$Pa for different frequencies: (a) 0.01Hz; (b) 0.1Hz; (c) 1.0Hz and (d) 10Hz.

For $\tau_a = 10$ Pa (Fig. 4.13), it can be seen that for all frequencies the stress response is sinusoidal, even for the lowest frequency of 0.01Hz. It is also clear that the result for the highest frequency is not good, with "oscillations" within the waves. As will be shown later, this actually occurs for all frequencies higher than 4.64Hz, so that it seems to be some kind measurement artifact. Indeed, this is puzzling, once difficulty in controlling the oscillatory motion would be expected in the case of very low frequencies, or else for high frequencies in large amplitudes, and none of both presented such problem. *TA Instruments*, manufacturer of the rheometer, was contacted to clarify this issue, but no response was avaiable at the time this thesis was written.

PUC-Rio - Certificação Digital Nº 1121442/CA

The results for the other stress amplitudes indicate a different trend. In general, a clear non-sinusoidal stress wave is observed for lower frequencies, but the sinusoidal response is recovered at high enough frequencies.

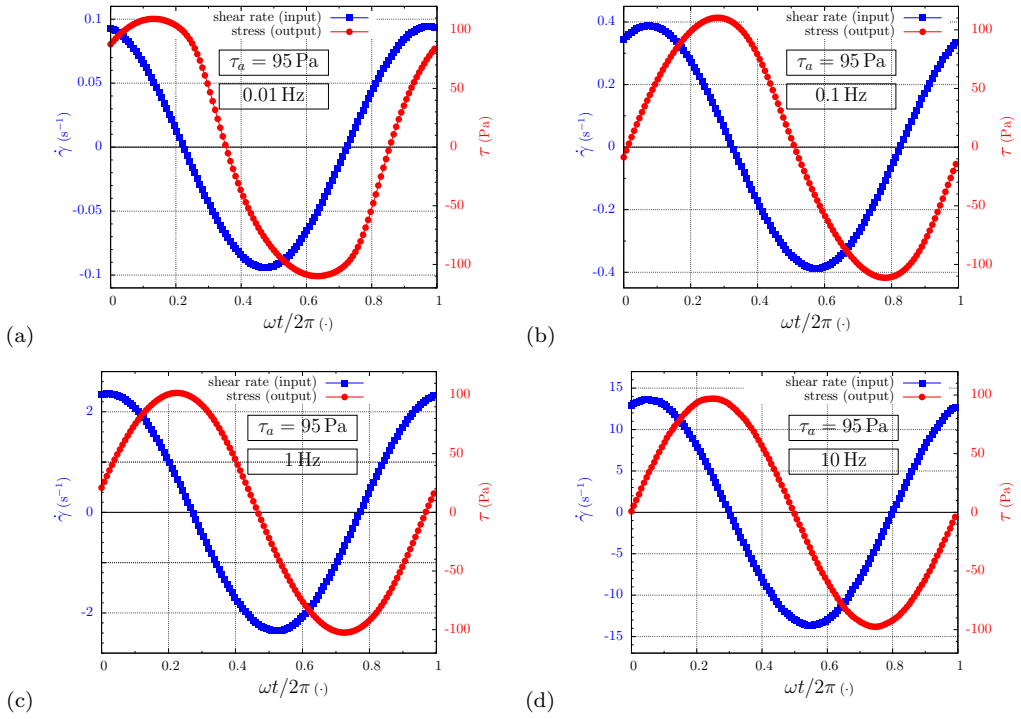

Figure 4.14: Input shear-rate wave and output raw-stress wave of $\tau_a = 95$Pa for different frequencies: (a) 0.01Hz; (b) 0.1Hz; (c) 1.0Hz and (d) 10Hz.

For $\tau_a = 95$ Pa, the two lowest frequencies (0.01 and 0.1Hz) exhibit a non-sinusoidal stress response, so that at a frequency of 1 Hz a sinusoidal stress response is again obtained. As for the stress amplitude of 125 Pa, clear non-sinusoidal responses are observed both for 0.01 and 0.1 Hz, and for 1 Hz the stress wave is almost sinusoidal, so that only at 10 Hz a sinusoidal response was obtained. In the case of $\tau_a = 312$ Pa, very non-sinusoidal stress waves are obtained for the low frequencies. Only the highest frequency shown (21.54 Hz) displays a sinusoidal stress response.

As can be seen, if high enough frequencies are applied a sinusoidal stress response seems to be always attainable. As the stress amplitude is increased, the frequency at which the sinusoidal response is restored also increases. This fact is also illustrated in the next subsection with the aid of Lissajous figures.

PUC-Rio - Certificação Digital Nº 1121442/CA

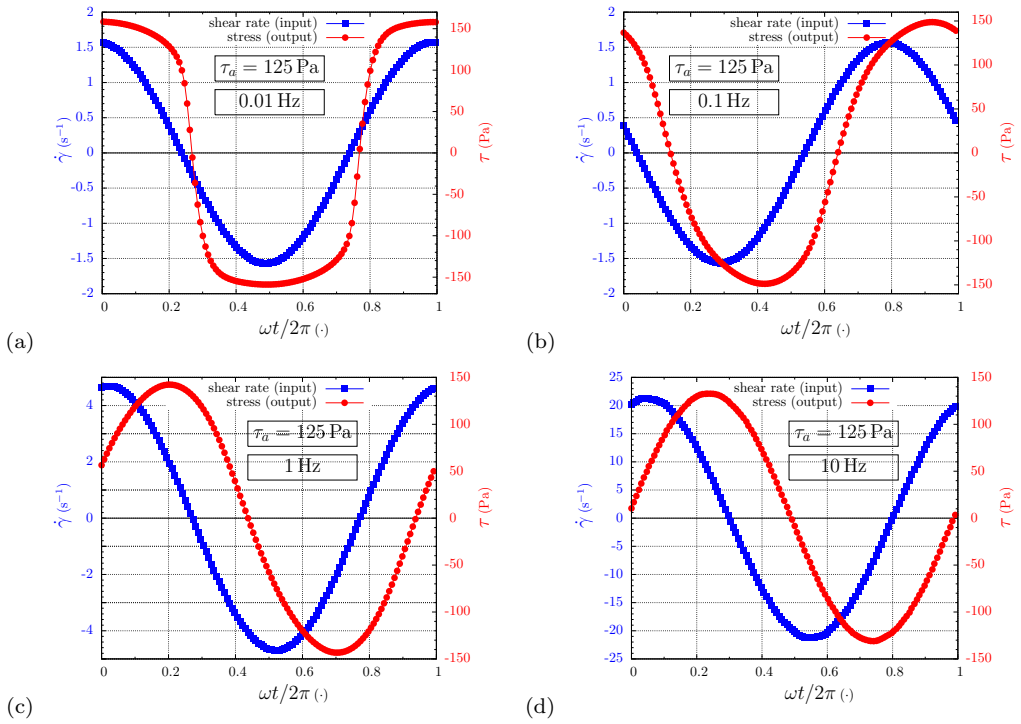

Figure 4.15: Input shear-rate wave and output raw-stress wave of $\tau_a = 125$Pa for different frequencies: (a) 0.01Hz; (b) 0.1Hz; (c) 1.0Hz and (d) 10Hz.

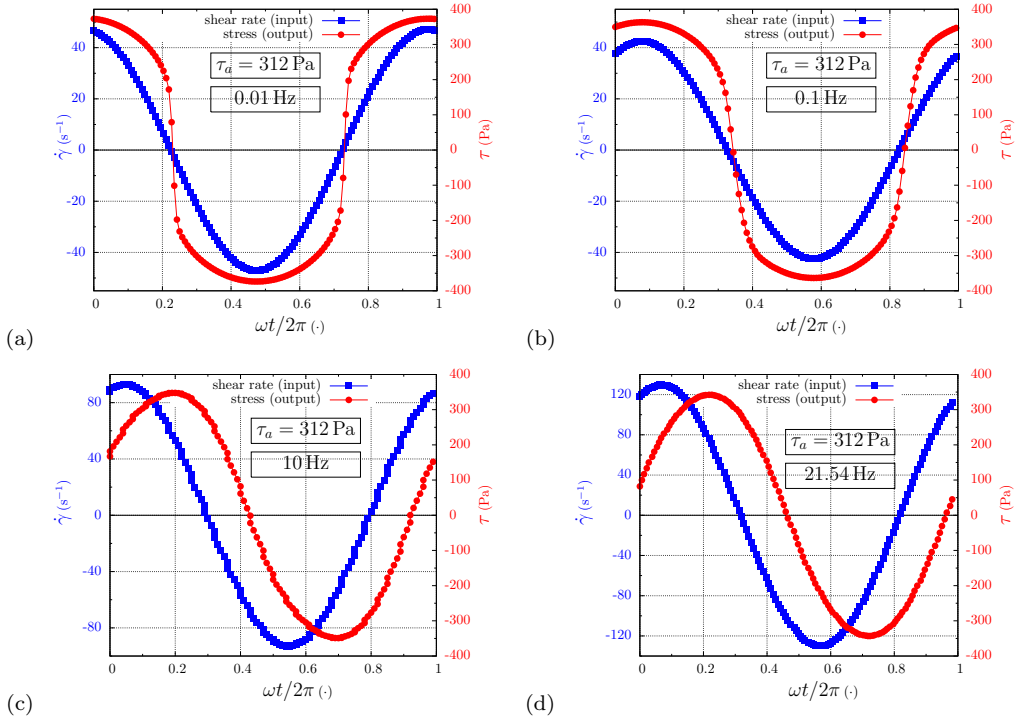

Figure 4.16: Input shear-rate wave and output raw-stress wave of $\tau_a = 312$Pa for different frequencies: (a) 0.01Hz; (b) 0.1Hz; (c) 10Hz and (d) 21.54Hz.

PUC-Rio - Certificação Digital Nº 1121442/CA

4.7.2 Lissajous-Bowditch figures

When the results of the LAOS experiments are plotted in terms of stress vs. shear rate, viscous Lissajous curves are obtained. In the present work, viscous Lissajous plots were chosen to display the results, once we find it is the obvious choice since we are dealing with materials that flow. Indeed, Dealy and coworkers [36] observed that departures from linear viscoelasticity were clearer on a stress vs. shear rate plot, as opposed to a stress vs. strain plot.

An example of a viscous Lissajous plot is presented in Fig. 4.17 to identify both stress amplitude (τ_a) and shear rate amplitude ($\dot{\gamma}_a$) values and illustrate the symmetry of the plot.

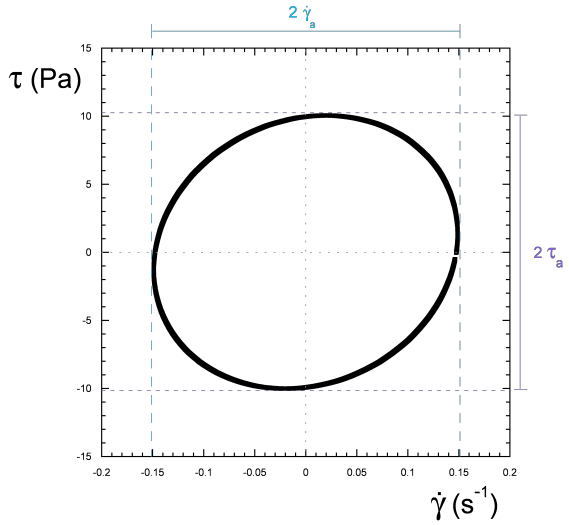

Figure 4.17: Example of viscous Lissajous plot highlighting τ_a and $\dot{\gamma}_a$.

As will be seen, the shape of the Lissajous curves is a strong function of the imposed values of stress amplitude and frequency.

Each figure presented next corresponds to a stress amplitude (Figs. 4.18, 4.19, 4.20 and 4.21). Since 13 frequencies were tested for each stress amplitude, the results were divided into different plots. Thus, each plot contains results for four different frequencies pertaining to a decade, e.g. 0.01 - 0.1 Hz (Figs. 4.x(a)), 0.1 - 1Hz (Figs. 4.x(b)), 1 - 10Hz (Figs. 4.x(c)), and 10 - 100Hz (Figs. 4.x(d)). Hence, in the plots (b), (c), and (d) for each τ_a, the inner cycle corresponds to the outer cycle of the previous plot. The difference in the width of the same curve plotted in two different scales may give an idea of how the shear rate amplitude varies significantly as the frequency is increased.

The first stress amplitude tested was equal to 10 Pa. Obviously, it pertains to the linear viscoelastic regime, as it is below the yield stress of the material (Sec. 4.3). Thus, the material remains fully structured throughout

PUC-Rio - Certificação Digital Nº 1121442/CA

the whole cycle, for all imposed frequencies, and it is expected that all viscous Lissajous curves present a circle shape (when properly scaled), once the response of the material is purely elastic. The results are shown in Fig. 4.18.

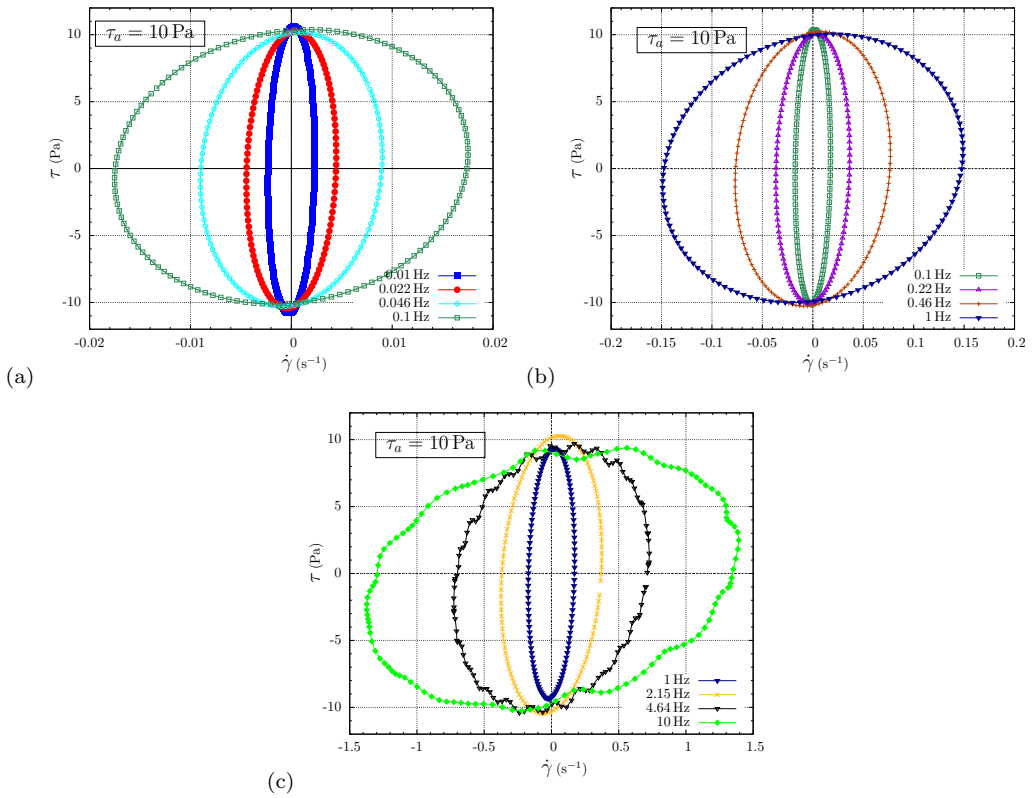

Figure 4.18: Viscous Lissajous-Bowditch curves for $\tau_a = 10$Pa.

In this case, the stress response is nearly orthogonal to the shear rate input: when the shear rate is at its maximum, the stress is zero. Contrariwise, when the shear rate is zero, the stress attains its maximum value. Below the yield stress, the material remains fully structured throughout the whole cycle, so that the orbits are always elliptical. Though, it is noticeable that for higher frequencies the curves present some oscillation within the cycle, probably due to measurement artifacts.

It is also possible to note that in this case, since no stress correction is needed, the stress amplitude of the Lissajous figures correspond exactly to the sought-for imposed stress amplitude value of 10 Pa. This is not the case for the other three stress amplitudes investigated, as can be seen next (Figs. 4.19, 4.20, and 4.21).

PUC-Rio - Certificação Digital Nº 1121442/CA

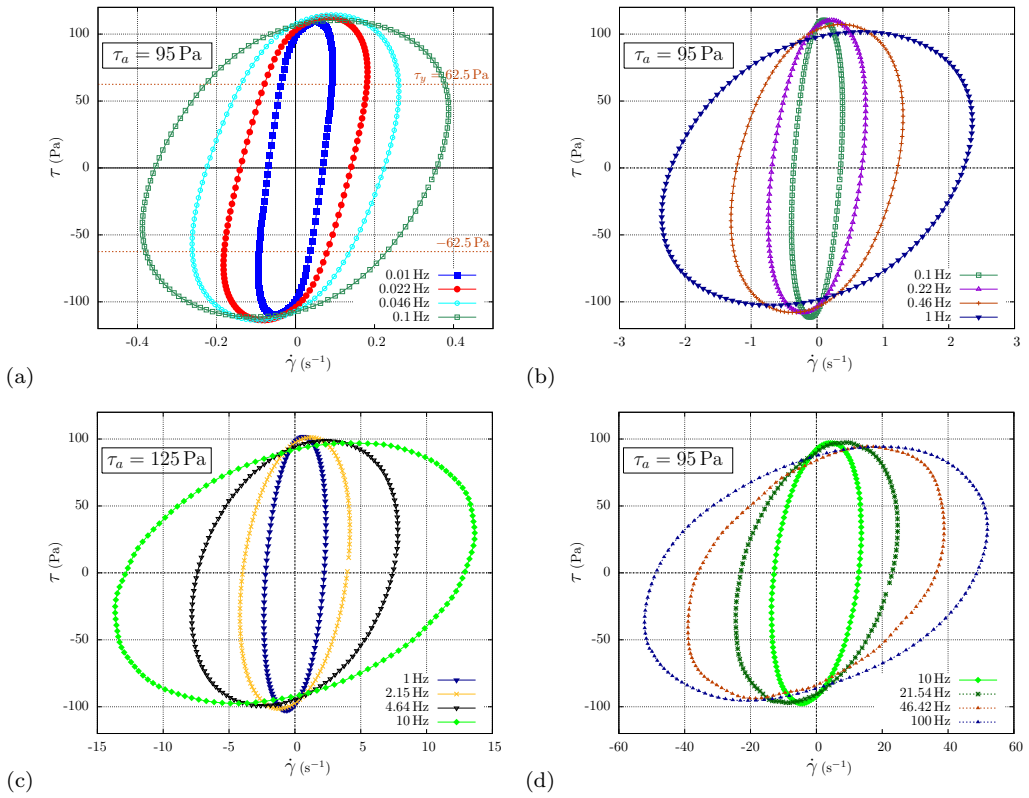

Figure 4.19: Viscous Lissajous-Bowditch curves for a corrected stress amplitude of $\tau_a = 95$Pa. The plotted stress is not corrected.

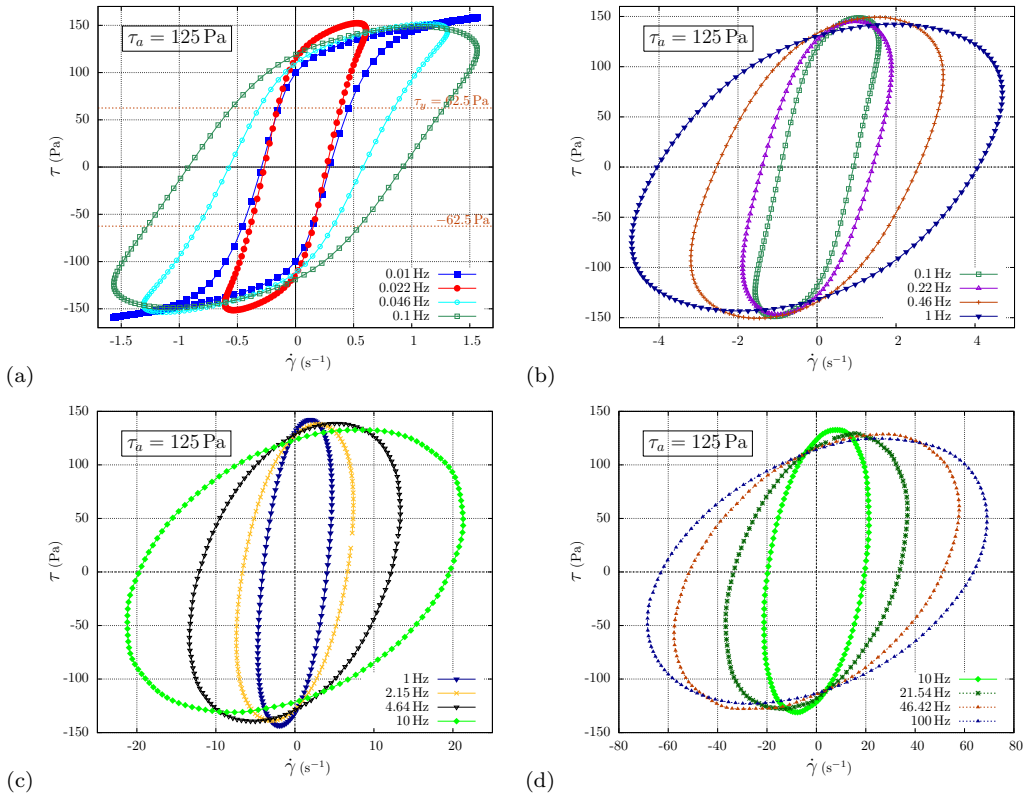

Figure 4.20: Viscous Lissajous-Bowditch curves for a corrected stress amplitude of $\tau_a = 125$Pa. The plotted stress is not corrected.

PUC-Rio - Certificação Digital Nº 1121442/CA

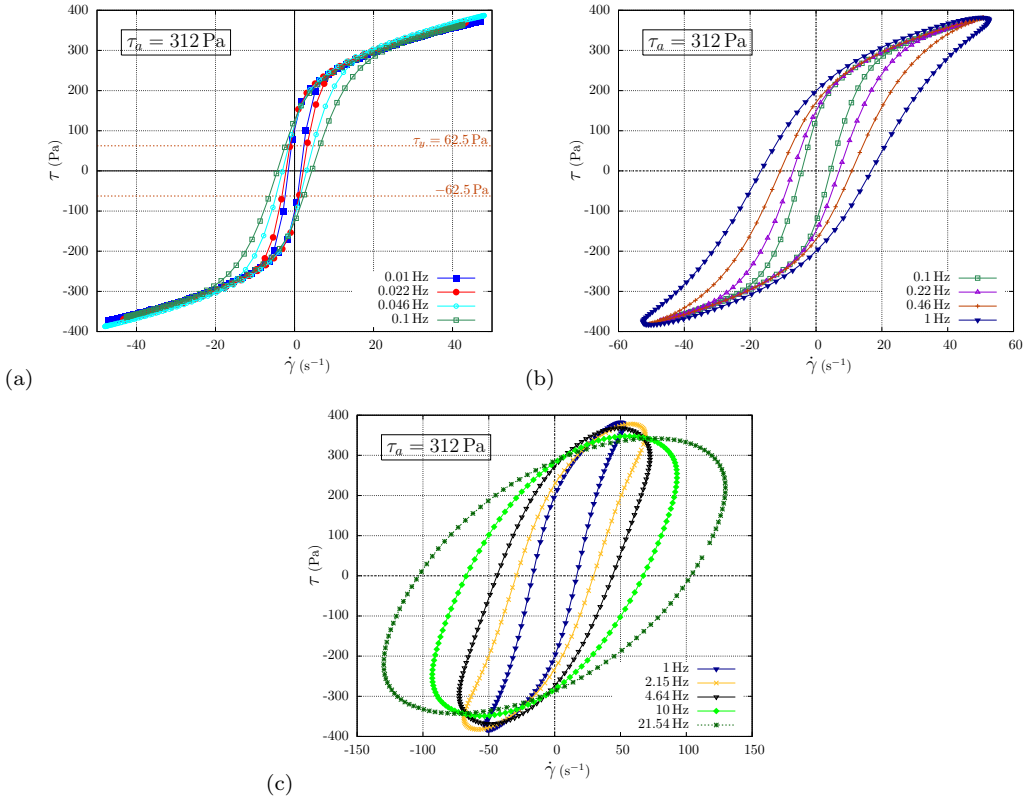

Figure 4.21: Viscous Lissajous-Bowditch curves for a corrected stress amplitude of $\tau_a = 312$Pa. The plotted stress is not corrected.

It is seen that the shape of the curves dramatically change as the stress amplitude and frequency are increased. Also, the magnitude of the shear rate amplitude increases significantly from the lowest to the highest applied frequency. The non-elliptical orbits occur due to intra-cycle changes of the structuring level. Overall, the degree of non-ellipticity increases with stress amplitude and with decrease in frequency. Fig. 4.21a exhibits the biggest departure from elliptical behavior, and can be explained by the fact that higher stress amplitudes lead to lower structuring levels. However, as the frequency is increased, the cycle period becomes much smaller than the time scale of microstructure buildup (t_{eq}). Therefore, the microstructural state remains unchanged along the cycle, and a quasi-linear viscoelastic regime is attained.

All 52 previous presented Lissajous curves were plotted together in the Pipkin diagram in Fig. 4.22. To enable a better comparison of the shapes of the curves, the results were normalized by dividing the instantaneous stress τ by the stress amplitude τ_a, and the instantaneous shear rate $\dot{\gamma}$ by the shear rate amplitude $\dot{\gamma}_a$.

PUC-Rio - Certificação Digital Nº 1121442/CA

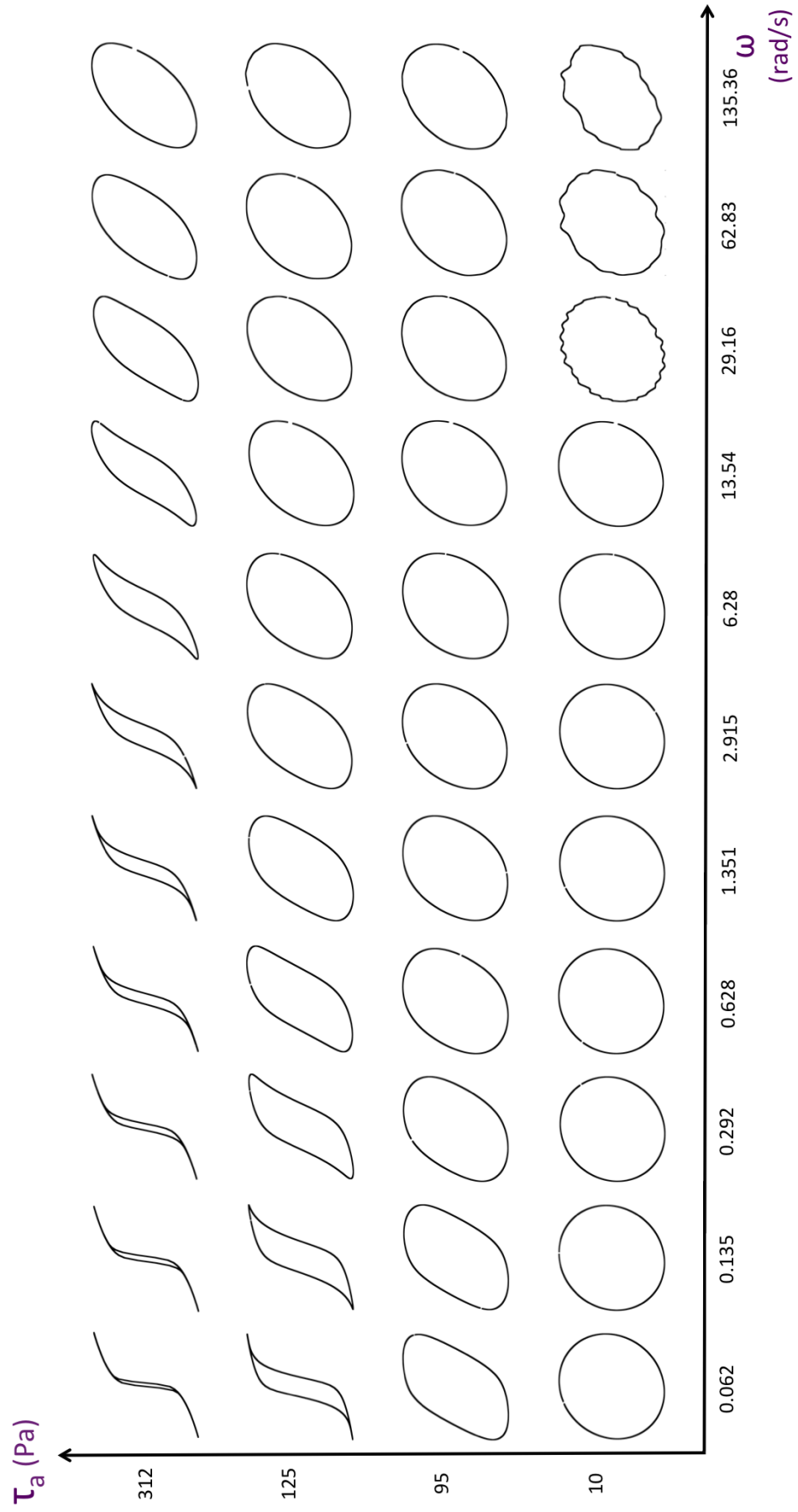

Figure 4.22: Summary of Lissajous curves on the Pipkin space.

PUC-Rio - Certificação Digital Nº 1121442/CA

For a given stress amplitude, it is seen that the area contained in the curves increase as the frequency is increased. Indeed, the area is usually related to the elasticity of the material, so that it is expected that the area increases with frequency (as previously explained, the elastic effects predominate for high *De*). Conversely, the smaller the area contained in the viscous Lissajous curve, the more the behavior of the material resembles the purely viscous behavior. The plots corresponding to τ_a= 312 Pa, from 0.062 to 2.915 rad/s, and to τ_a= 125 Pa for 0.062 rad/s exhibit a purely viscous behavior in its extremities, where the stress is approximately proportional to the shear rate. Indeed, when the shear rate is at its maximum, the shear stress also attains its maximum value, and in these cases the ratio $\tau_a/\dot{\gamma}_a$ is equal to η_v.

It is clear that for all stress amplitudes tested elliptical Lissajous curves were obtained at high enough frequencies. This fact is in agreement with the results observed from the input and output wave shapes, indicating that sinusoidal stress responses are always attainable.

Moreover, the shapes of the Lissajous curves obtained experimentally can be compared to the model predictions made by de Souza Mendes and Thompson [8]. A case corresponding to an apparent yield stress fluid ($\eta_0\dot{\gamma}_1/\tau_{yd} \neq \infty$) and no thixotropy ($t_{eq}\dot{\gamma}_1 = 0$) was chosen and is reproduced in Fig. 4.23. It presents results for three different dimensionless stress amplitudes and three dimensionless frequencies in a Pipkin space.

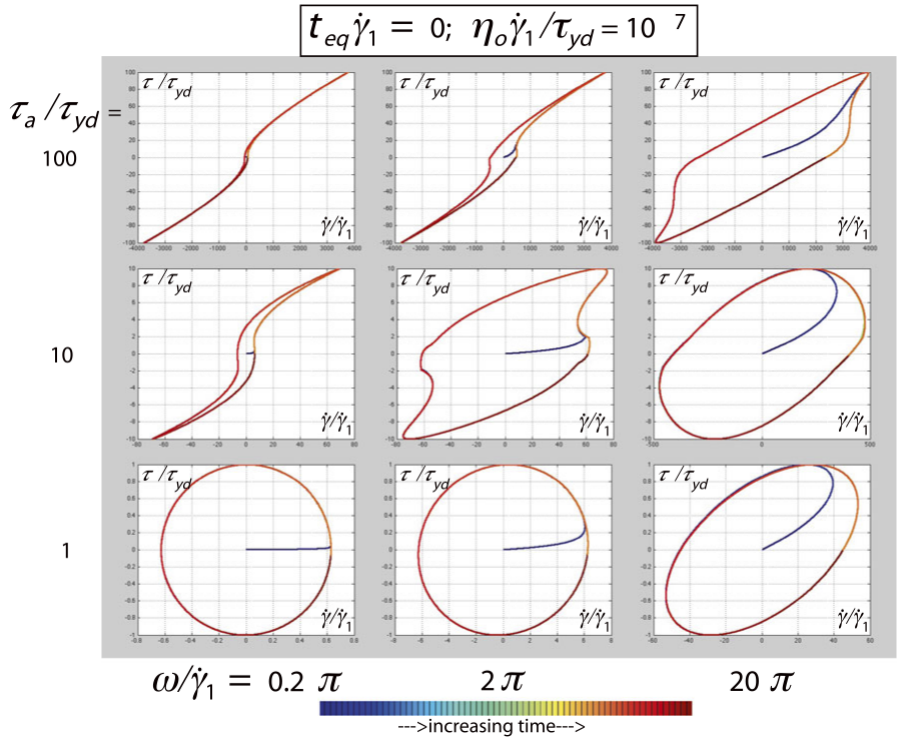

Figure 4.23: Model predictions of de Souza Mendes and Thompson [8].

It is possible to observe a qualitative concordance between the numerical and experimental results. For a stress amplitude below the yield stress (bottom row), the same trend is observed as in Fig. 4.22: the Lissajous figures are circles, but at high enough frequencies develop to a tilted ellipse. For the cases pertaining to higher stress amplitudes (middle and top rows), it is seen that the area contained in the cycles increases with frequency, once again showing that the elastic contribution is bigger at lower time scales. Also, as predicted by the theory, an elliptical Lissajous is obtained for 20π, indicating that a sinusoidal stress response is attainable at high enough frequencies.

4.7.3 Quasi-linear LAOS viscosity

Next, to quantitatively compare the experimental results with the Jeffrey's model predictions, the obtained data is plotted in terms of the QL-LAOS viscosity. The ratio $\tau_a/\dot{\gamma}_a$ was calculated for each Lissajous curve presented previously and fitted with Eq. 3. Figures 4.24, 4.26, 4.27 and 4.28 show the results for each stress amplitude in plots of $\tau_a/\dot{\gamma}_a$ as a function of the frequency ω, where the red dots correspond to experimental data and the blue curve to the theoretical predictions. Also, the material functions η_v, η_r, and G_s (and thus also θ_1 and θ_2) are indicated in each plot. Each curve corresponds to a given structuring level of the material, given by the applied stress amplitude.

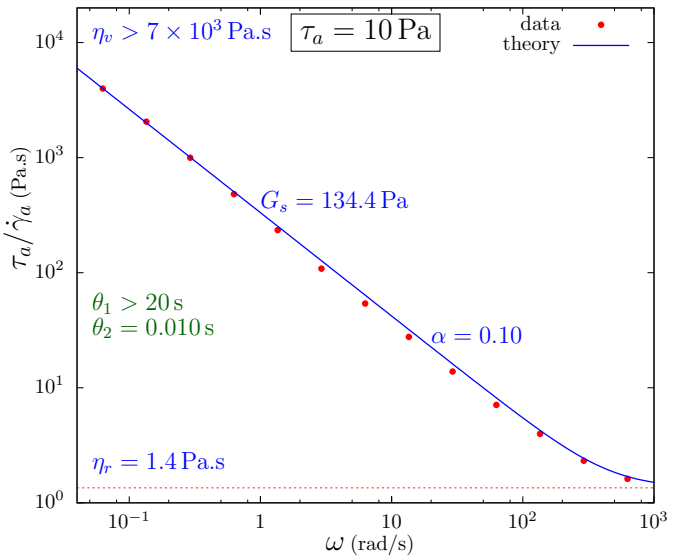

Figure 4.24: QL-LAOS viscosity for $\tau_a = 10$ Pa.

For this amplitude, the QL-LAOS viscosity is actually a "SAOS viscosity" corresponding to the linear viscoelastic regime. In this case, the ratio $\tau_a/\dot{\gamma}_a$ is equal to the modulus of the complex viscosity η^*. Indeed, this was verified

PUC-Rio - Certificação Digital Nº 1121442/CA

experimentally by performing a frequency sweep in the linear viscoelastic regime and plotting the results in terms of η^* vs. ω (Fig. 4.25).

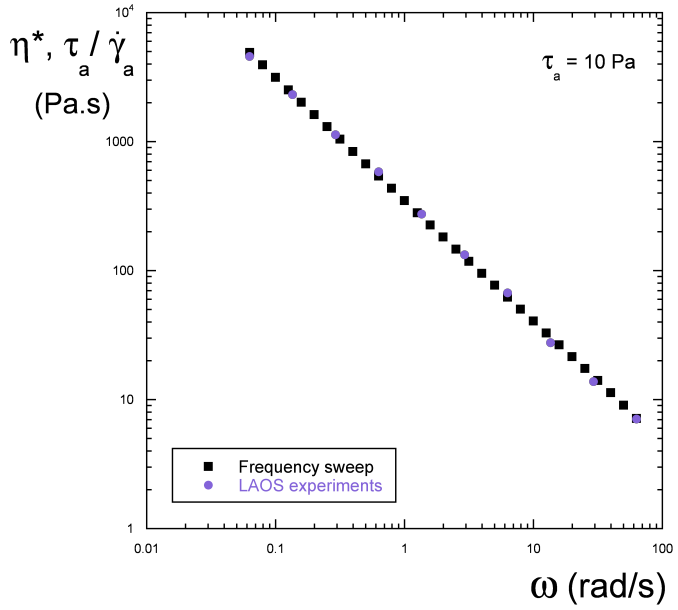

Figure 4.25: Comparison between complex viscosity η^* and QL-LAOS viscosities for $\tau_a = 10$ Pa.

The results of the QL-LAOS viscosity for the other three stress amplitudes investigated are presented next.

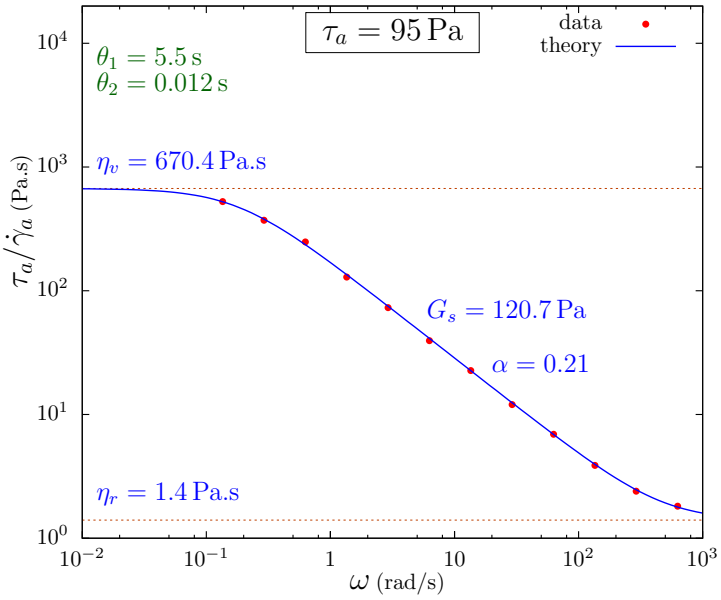

Figure 4.26: QL-LAOS viscosity for $\tau_a = 95$ Pa.

PUC-Rio - Certificação Digital Nº 1121442/CA

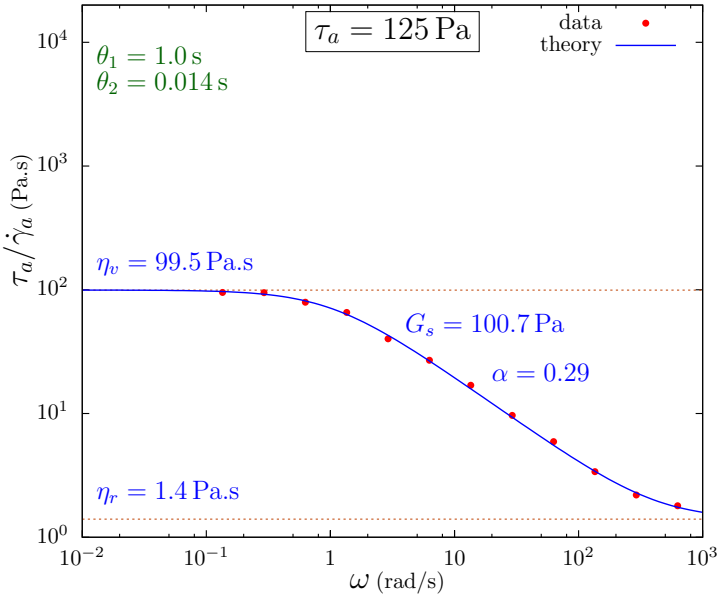

Figure 4.27: QL-LAOS viscosity for $\tau_a = 125$ Pa.

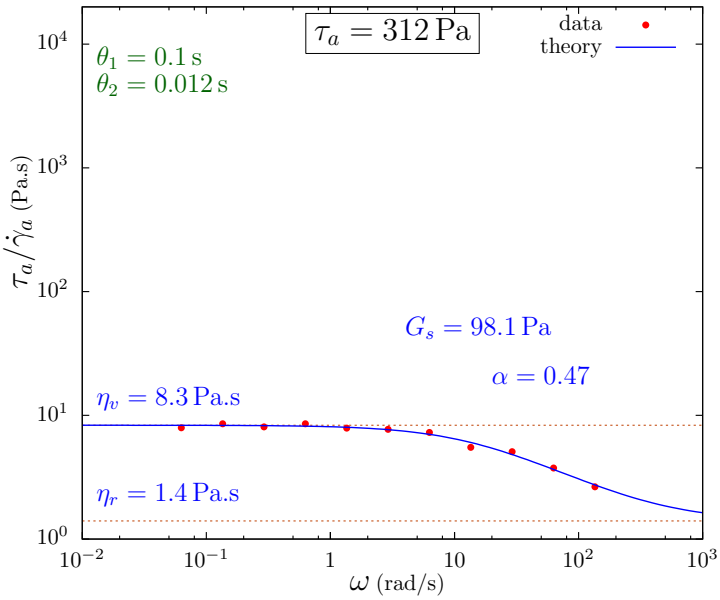

Figure 4.28: QL-LAOS viscosity for $\tau_a = 312$ Pa.

Firstly, it is evident that there is a remarkable agreement between experimental data and the theoretical predictions for all stress amplitudes. Curiously, even for the cases of structure changing motions, i.e. non-sinusoidal responses, the theory seems to correctly predict the response of the material. This fact indicates that the Jeffrey's framework seems to be very suitable to describe the mechanical behavior of an elasto-viscoplastic material.

PUC-Rio - Certificação Digital Nº 1121442/CA

The expected general behavior for the LAOS viscosity consists of a plateau corresponding to the total viscosity η_v at low frequencies, followed by a region of decrease in viscosity (where $\tau_a/\dot{\gamma}_a \approx \eta_s^{\alpha}(G_s/\omega)^{1-\alpha}$) at intermediate frequencies, and finally, at very large frequencies, a plateau corresponding to the retardation viscosity η_r. As previously stated, the points lying in the η_v plateau correspond to the Lissajous plots which exhibit a purely viscous behavior in its extremities. From the figures, it is possible to note that only Fig. 4.24 does not exhibit an η_v plateau in the range of frequencies studied.

The obtained values of the Jeffrey's model parameters are summarized in Tab. 4.3 for better comparison:

Table 4.3: Summary of the parameter values for each structuring level.

τ_a [Pa]	η_v [Pa.s]	η_r [Pa.s]	G_s [Pa]	α	$\theta_1[s]$	θ_2 [s]
10	7000	1.4	134.4	0.10	20	0.010
95	670.4	1.4	120.7	0.21	5.5	0.012
125	99.5	1.4	100.7	0.29	1.0	0.014
312	8.3	1.4	98.1	0.47	0.1	0.012

As can be seen, η_v decreases drastically as τ_a is increased, whereas η_r remains constant. Thus, once $\eta_s = \eta_v$ - η_r, the relaxation viscosity η_s also decreases significantly with increase of τ_a. The elastic modulus G_s decreases mildly. α increases with τ_a, i.e. as the structuring level is decreased. Indeed, this parameter was added to Eq. 3 (Chap. 3) in order to better adjust the experimental data. It can be interpreted as a measure of the departure from the Jeffreys-like behavior. With the combination of the before mentioned parameters through Eqs. 4 and 5, θ_1 and θ_2 can be obtained. While θ_1 decreases with increase in the stress amplitude, θ_2 remains approximately constant.

In addition, it is noted that the material functions η_v and η_r are independent on imposed frequency, whereas G_s weakly depends on frequency. The knowledge of these three material functions should be enough to fully describe the mechanical behavior of a material subjected to shear. This consists one major advantage to describe the mechanical behavior of a material, specially when comparing to the typical material functions suggested in the LAOS literature. Moreover, even in the linear viscoelastic regime, in which G' and G" greatly depend on imposed frequency (Fig. 4.11), the results suggest that the Jeffrey's material functions are more meaningful and robust.

PUC-Rio - Certificação Digital Nº 1121442/CA

5
Concluding Remarks

Large amplitude oscillatory shear flow (LAOS) is presently considered one of the most promising methodologies to investigate the behavior of complex materials. LAOS experiments allow probing the material under a wide range of conditions in the nonlinear viscoelastic regime while exploring the advantages of oscillatory motions, i.e. tunning amplitude and frequency independently. Since a wide range of industrial processes involves large deformations, understanding how complex materials behave under these conditions is fundamental for operation and design purposes.

A qualitative idea of the behavior of a material under LAOS can be given by Lissajous curves, where the degree of nonlinearity is given by the degree on "non-ellipticity" of the orbits. Although Lissajous curves may give a good insight into the material behavior, mathematically defined and physically meaningful quantities are necessary for proper description of the mechanical behavior of complex materials.

To this end, many research groups around the world have proposed different approaches for analyzing nonlinear data, among which may be mentioned the Fourier-transform rheology (FT-rheology) by Wilhem, the stress decomposition (SD) by Cho et al., the Chebyshev analysis by Ewoldt and coworkers, and the "sequence of physical processes" (SPP) by Rogers. Nonetheless, there is still a need for a more general, capable of accommodating all kinds of behaviors and physically meaningful model to analyze LAOS results.

In this work, a novel methodology for the rheological characterization and interpretation of the results under LAOS was tested under the guidelines proposed by de Souza Mendes and Thompson [8]. While all present LAOS analysis focus on non-sinusoidal stress responses, which imply major microstructural changes along the cycles, the proposed methodology relies on data obtained from sinusoidal responses, or the"constant-structure motions" which resembles the linear viscoelastic regime. This quasi-linear LAOS (QL-LAOS) methodology is a model-based framework, in which the structuring-level-dependent Jeffreys model is applied to rheometric oscillatory flows to obtain physically meaningful material functions.

PUC-Rio - Certificação Digital Nº 1121442/CA

An elasto-viscoplastic hair gel was chosen and different rheometric experiments were performed so as to characterize the mechanical behavior of the material at hand. Constant shear rate, flow curve, and constant stress tests, as well as oscillatory strain, stress and time sweeps were carried out. Thus, the material was probed under a wide range of conditions and results were correlated with its mechanical behavior. From the LAOS experiments, it was seen that the degree of "non-ellipticity" of the curves, which indicates the degree of nonlinearity of the response, depends on both applied stress amplitude and frequency. The nonlinear behavior is more pronounced for high stress amplitudes and low frequencies. In addition, the existence of a quasi-linear viscoelastic regime was verified whenever the frequency is high enough so that the period of a cycle is much lower than the timescale of microstructural changes, i.e. $t_{eq} \gg 1/\omega$.

Moreover, the QL-LAOS viscosity was defined as the ratio $\tau_a/\dot{\gamma}_a$. For each stress amplitude (or structuring level), a plot of the QL-LAOS viscosity vs. frequency can be obtained. From a curve fitting with Eq. 3 of Chap. 3, the model parameters η_v, η_r, G_s, and α can be calculated. The results showed a remarkable agreement between the theoretical predictions and experimental results, even for nonlinear responses. It was observed that the material functions G_s, η_v, and η_r present only weak (the first) or even no dependence at all (two latter) on the frequency. It is suggested that the knowledge of these three functions suffices to describe the mechanical behavior of a complex material. Therefore, the methodology employed here offers a major advantage to describe the mechanical behavior of a material over the typical material functions suggested in the LAOS literature.

Future steps include testing the commercial hair gel under different shear flows, such as stress step changes, so as to obtain the material functions and compare with the quasi-linear LAOS methodology. Also, another important step would be testing the quasi-linear LAOS methodology on different materials to see if a sinusoidal stress response is always attainable at high enough frequencies. Indeed, a shear-thinning polyacrylamide solution is presently being tested, with the advantage of using cone and plate geometry, so that no stress correction is needed. Moreover, instead of focusing only on steady state response, effects of thixotropy might be investigated using for instance a Laponite suspension.

PUC-Rio - Certificação Digital Nº 1121442/CA

Bibliography

[1] HYUN, K.; WILHELM, M.; KLEIN, C.; CHO, K. S.; NAM, J.; AHN, K.; LEE, S.; EWOLDT, R. ; MCKINLEY, G.. **A review of nonlinear oscillatory shear tests: Analysis and application of large amplitude oscillatory shear (laos)**. Progress in Polymer Science, 36:1697–1753, 2011. (document), 1.1, 2.2, 2.2, 2.2

[2] VAART, K.; DEPYPERE, F.; GRAEF, V.; SCHALL, P.; FALL, A.; BONN, D. ; DEWETTINCK, K.. **Dark chocolate's compositional effects revealed by oscillatory rheology**. Eur. Food. Res. Technol., 236:931–942, 2013. 1.1

[3] MELITO, H.; DAUBERT, C. ; FOEGEDING, E.. **Validation of a large amplitude oscillatory shear protocol**. Journal of Food Engineering, 113:124–135, 2012. 1.1

[4] MELITO, H.; DAUBERT, C. ; FOEGEDING, E.. **Relationships between nonlinear viscoelastic behavior and rheological, sensory and oral processing behavior of commercial cheese**. Journal of Texture Studies, 44(4):253–288, 2013. 1.1

[5] OZKAN, S.; GILLECE, T.; SENAK, I. ; MOORE, D.. **Characterization of yield stress and slip behaviour of skin/hair care gels using steady flow and laos measurements and their correlation with sensorial attributes**. International Journal of Cosmetic Science, 34:193–201, 2012. 1.1

[6] TAN, K.; CHENG, S.; JUGÉ, L. ; BILSTON, L.. **Characterising soft tissues under large amplitude oscillatory shear and combined loading**. Journal of Biomechanics, 46:1060–1066, 2013. 1.1

[7] LAMERS, E.; VAN KEMPEN, T.; BAAIJENS, F.; PETERS, G. ; OOMENS, C.. **Large amplitude oscillatory shear properties of human skin**. Journal of the Mechanical Behavior of Biomedical Materials, in press. 1.1

[8] DE SOUZA MENDES, P.; THOMPSON, R.. **A unified approach to model elasto-viscoplastic thixotropic yield-stress materials and**

PUC-Rio - Certificação Digital Nº 1121442/CA

apparent yield-stress fluids. Rheol Acta, 2013. (document), 1.2, 1.3, 2.2, 2.2, 2.14, 3.2, 4.7, 4.7.2, 4.23, 5, B.1

[9] BIRD, R.; ARMSTRONG, R. ; HASSAGER, O.. **Dynamics of polymeric liquids**, volumen 1. Wiley, 1987. 2.1

[10] FERRY, J.. **Viscoelastic properties of polymers**. Wiley, 1980. 2.1

[11] GIACOMIN, A.; DEALY, J.. **Rheological Measurement**, chapter Using large-amplitude oscillatory shear. Springer Netherlands, 1993. 2.1, 2.2

[12] MACOSKO, C.. **Rheology: Principles, measurements, and applications**. Wiley-VCH, 1994. (document), 2.1, 2.5, 3, B

[13] BARNES, H. A.. **Measuring the viscosity of large-particle (and flocculated) suspensions — a note on the necessary gap size of rotational viscometers**. J. Non-Newtonian Fluid Mech., 94:213–217, 2000. (document), 2.1, 2.3

[14] PIPKIN. **Lectures on viscoelastic theory**. 1972. 2.1

[15] PHILIPPOFF, W.. **Vibrational measurements with large-amplitudes**. Trans. Soc. Rheol., 10(1):317–334, 1966. 2.2

[16] TEE, T.; DEALY, J.. **Nonlinear viscoelasticity of polymer melts**. Trans. Soc. Rheol., 19(4):595–615, 1975. 2.2

[17] EWOLDT, R.; WINTER, P.; MAXEY, J. ; MCKINLEY, G.. **Large amplitude oscillatory shear of pseudoplastic and elastoviscoplastic materials**. Rheol Acta, 49:191–212, 2010. (document), 2.2, 2.8, 2.2, B

[18] WILHELM, M.. **New methods for the rheological characterization of materials**. Chemical Engineering and Processing, 50:486–488, 2011. (document), 2.2, 2.9, 2.2

[19] WILHELM, M.. **Fourier-transform rheology**. Macromol. Mater. Eng., 287(2):83–105, 2002. 2.2, 2.2

[20] HYUN, K.; WILHELM, M.. **Establishing a new mechanical nonlinear coefficient q from ft-rheology: First investigation of entangled linear and comb polymer model systems**. Macromolecules, 47:411–422, 2009. 2.2

[21] CHO, K. S.; HYUN, K.; AHN, K. ; LEE, S.. **A geometrical interpretation of large amplitude oscillatory shear response**. J. Rheol., 49(3):747–758, 2005. 2.2, 2.2

PUC-Rio - Certificação Digital Nº 1121442/CA

[22] EWOLDT, R.; HOSOI, A. ; MCKINLEY, G.. **New measures for characterizing nonlinear viscoelasticity in large amplitude oscillatory shear**. J. Rheol., 52(6):1427–1458, 2008. (document), 2.2, 2.10, 2.2, 2.11

[23] NG, T.; MCKINLEY, G. ; EWOLDT, R.. **Large amplitude oscillatory shear flow of gluten dough: A model power-law gel**. J. Rheol., 55(3):627–654, 2011. 2.2

[24] EWOLDT, R.; MCKINLEY, G.. **On secondary loops in laos via self-intersection of lissajous-bowditch curves**. Rheol Acta, 49:213–219, 2010. 2.2

[25] DIMITRIOU, C.; EWOLDT, R. ; MCKINLEY, G.. **Describing and prescribing the constitutive response of yield stress fluids using large amplitude oscillatory shear stress (laostress)**. J. Rheol., 57(1):27–70, 2013. 2.2

[26] ROGERS, S.; LETTINGA, M.. **A sequence of physical processes determined and quantified in large-amplitude oscillatory shear (laos): Application to theoretical nonlinear models**. Journal of Rheology, 2012. 2.2

[27] ROGERS, S.; ERWIN, B.; VLASSOPOULOS, D. ; CLOITRE, M.. **A sequence of physical processes determined and quantified in laos: Application to a yield stress fuid**. J. Rheol., 55(2):435–458, 2011. 2.2

[28] ROGERS, S.; ERWIN, B.; VLASSOPOULOS, D. ; CLOITRE, M.. **Oscillatory yielding of a colloidal star glass**. J. Rheol., 55(4):733–752, 2011. 2.2

[29] ROGERS, S.. **A sequence of physical processes determined and quantified in laos: An instantaneous local 2d/3d approach**. J. Rheol., 56(5):1129–1151, 2013. (document), 2.2, 2.12

[30] DE SOUZA MENDES, P.; THOMPSON, R.; ALICKE, A. ; LEITE, R.. **The linear large-amplitude viscoelastic regime and its significance in the rheological characterization of soft matter with laos**. J. Rheol., submitted, 2013. 2.2, 3.2

[31] THOMPSON, R.; DE SOUZA MENDES, P.. **Model-based framework rheology and its application to oscillatory shear flows**. J. Rheol., submitted. 2.2

PUC-Rio - Certificação Digital Nº 1121442/CA

[32] DE SOUZA MENDES, P.. **Thixotropic elasto-viscoplastic model for structured fluids**. Soft Matter, 7:2471–2483, 2011. 2.2

[33] COUSSOT, P.; NGUYEN, Q.; HUYNH, H. ; BONN, D.. **Avalanche behavior in yield stress fluids**. Physical Review Letters, 88(17):175501–1(4), 2002. 3.1

[34] COUSSOT, P.; NGUYEN, Q.; HUYNH, H. ; BONN, D.. **Viscosity bifurcation in thixotropic, yielding fluids**. J. Rheol., 46(3):573–589, 2002. 3.1

[35] HYUN, K.; KIM, S.; AHN, K. ; LEE, S.. **Large amplitude oscillatory shear as a way to classify the complex fluids**. J. Non-Newtonian Fluid Mech., 107:51–56, 2002. (document), 4.6, 4.10

[36] DEALY, J.; PETERSEN, J. ; TEE, T.. **A concentric cylinder rheometer for polymer melts**. Rheol Acta, 12:550–558, 1973. 4.7.2

[37] BARNES, H. A.. **A Handbook of Elementary Rheology**. University of Wales Institute of Non-Newtonian Fluids Mechanics, 2000. A.1

[38] BARNES, H. A.. **A review of the slip (wall depletion) of polymer solutions, emulsions and particle suspensions in viscometers: its cause, character, and cure**. J. Non-Newtonian Fluid Mech., 56:221–251, 1995. A.1, A.1

[39] YOSHIMURA, A.; PRUD'HOMME, R.. **Wall slip corrections for couette and parallel disk viscometers**. J. Rheol., 32(1):53–67, 1988. A.1

[40] RABINOWITSCH, B.. **über die viskosität und elastizität von solen**. Z. Phys. Chem., A145(1), 1929. B

[41] GIESEKUS, H.; LANGER, G.. **Determination of real flow curves of non-newtonian liquids and plastic materials using method of representative viscosity**. Rheol. Acta, 16(1):1–22, 1977. B

[42] SCHUMMER, P.; WORTHOFF, R.. **An elementary method for the evaluation of a flow curve**. Chem. Eng. Sc., 33:759–763, 1978. B

[43] CROSS, M.; KAYE, A.. **Simple procedures for obtaining viscosity/shear rate data from parallel disc viscometer**. Polymer, 28:435–440, 1987. B

PUC-Rio - Certificação Digital Nº 1121442/CA

[44] GEIGER, K.. **Weissenberg-rabinowitsch evaluation of flow curves measured with the parallel-disk rotational rheometer using a carreau-type flow formula**. Rheol. Acta, 27(2), 209-211 1988. B

[45] CARVALHO, M.; PADMANABHAN, M. ; MACOSKO, C.. **Single-point correction for parallel disks rheometry**. J. Rheol., 38(6):1925–1936, 1994. B

[46] SOSKEY, P.; WINTER, H.. **Large step shear strain experiments with parallel-disk rotational rheometers**. J. Rheol., 28(5):625–645, 1984. B

[47] MACSPORRAN, W.; SPIERS, R.. **The dynamic performance of the weissenberg rheogoniometer ii. large amplitude oscillatory shearing - fundamental response**. Rheol. Acta, 21:193–200, 1982. B

[48] MACSPORRAN, W.; SPIERS, R.. **The dynamic performance of the weissenberg rheogoniometer iii. large amplitude oscillatory shearing - harmonic analysis**. Rheol. Acta, 23:90–96, 1984. B

PUC-Rio - Certificação Digital Nº 1121442/CA

A
Geometry selection

As mentioned in Chapter 3, the cross-hatched parallel plates were used throughout the rheological characterization presented in this work. In this Appendix we briefly discuss the apparent wall slip artifact and show some results to corroborate our geometry choice.

In rheometry, the best geometry choice is usually one that maintains a homogeneous flow, i.e. where the shear rate is the same in the entire sample, as for example the cone and plate geometry. In the concentric cylinders (Couette), the shear rate is approximately constant if the gap is narrow ($R_i/R_o < 0.99$). The possibility of using the Couette geometry was discarded, since this kind of geometry is better suited for low viscosity systems. Also, oscillatory measurements in this geometry are not indicated. Still, this geometry might be used for high shear rates experiments, when the viscosity is much lower and wall slip is not a problem.

Regarding the cone and plate, the main disadvantage of this geometry is the fixed gap due to the cone angle. When using a multiphase material with particles or droplets in suspension, the small gaps, specially near the cone tip (where the truncation is of the order of dozen of microns), might induce measurement errors. Particularly in our case, this was not an issue. For our gel in hand, the main issue are the smooth walls. However, roughening the walls of the cone, e.g. by applying a grit sandpaper, and not affecting the small angle and/or truncation is a complicated task.

The parallel plates have the advantage of easily varying the gap and roughening surfaces, but the major disadvantage of variable shear rate across the radius and consequent need for stress correction of the results.

After this discussion, two geometries are left to use: the cone and plate with smooth walls or the parallel-plate geometry. If apparent wall slip is not an issue, the cone and plate is a better choice. Else, the parallel plate with roughened walls should be used. Therefore, we need to evaluate the effect of wall slip on our results.

PUC-Rio - Certificação Digital Nº 1121442/CA

A.1
Apparent wall slip

When a dispersion is in contact with a smooth wall, the original microstructure is locally disturbed and the disperse phase moves away from smooth walls. This effect is known as wall depletion. Thus, a very thin layer of continuous (usually low viscosity) phase is formed at the wall, with typical thickness of 0.1 - 10 μm. This narrow layer acts as a lubricant facilitating the flow of the adjacent bulk with original concentration [37, 38].

Apparent wall slip can be eliminated by altering the nature of the geometry walls, either chemically or physically. In the first case, the intention is to avoid repulsion effects. In the latter case, the idea is to physically "break" the low viscosity layer by roughening of the walls. Sandblasting or sticking grit sandpaper to the walls has been widely used. A common profiled parallel plate geometry offered by rheometer manufacturers is the cross hatched plate. It consists of 1x 1mm base pyramids, with heights equal to 1mm, covering the entire surface of the plates, as can be seen in Fig. A.1.

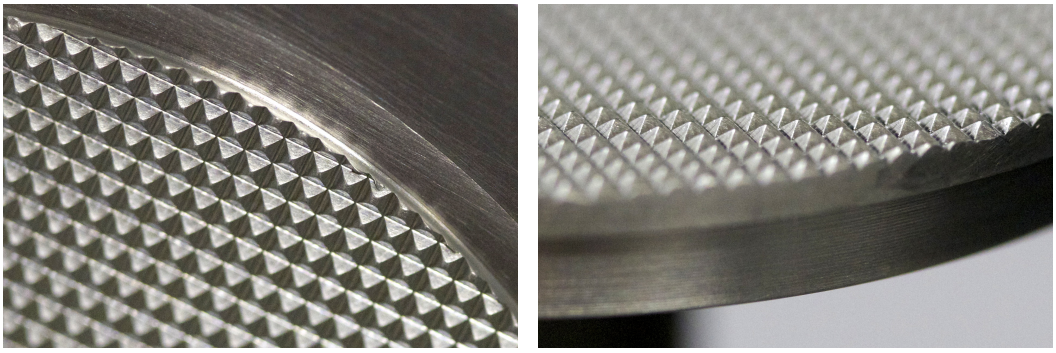

Figure A.1: Detail of the cross hatch profiling by *TA Instruments*.

The manifestation of apparent wall slip in the rheological results is usually characterized by lower apparent viscosity, sudden breaks in the curves at moderate shear rates, and "unexpected lower Newtonian plateaus, with "pseudo" yield stress at even lower stresses" [38]. Also, different geometries and gaps will generate different results. For smaller gaps, the effect of the continuous phase layer is more important, and hence lower stresses/viscosities are expected. Some authors show that slip-free results can be obtained by extrapolating the results for different gaps [38, 39].

As mentioned above, the effect of apparent wall slip needs to be evaluated so as to properly choose the geometry for the rheological characterization of the gel. The result of this investigation is presented in Figs. A.2(a) and A.2(b). The different geometries employed are:

PUC-Rio - Certificação Digital Nº 1121442/CA

1. Cone and plate, 60mm diameter, 1° angle, and truncation of 24μm ;
2. Smooth parallel plates, 60mm diameter, with gaps of 0.5 mm, 1.0 mm, 1.5 mm, and 2.0 mm ;
3. Cross hatched parallel plates (Fig. A.1), 60mm diameter, and 1.0 mm gap.

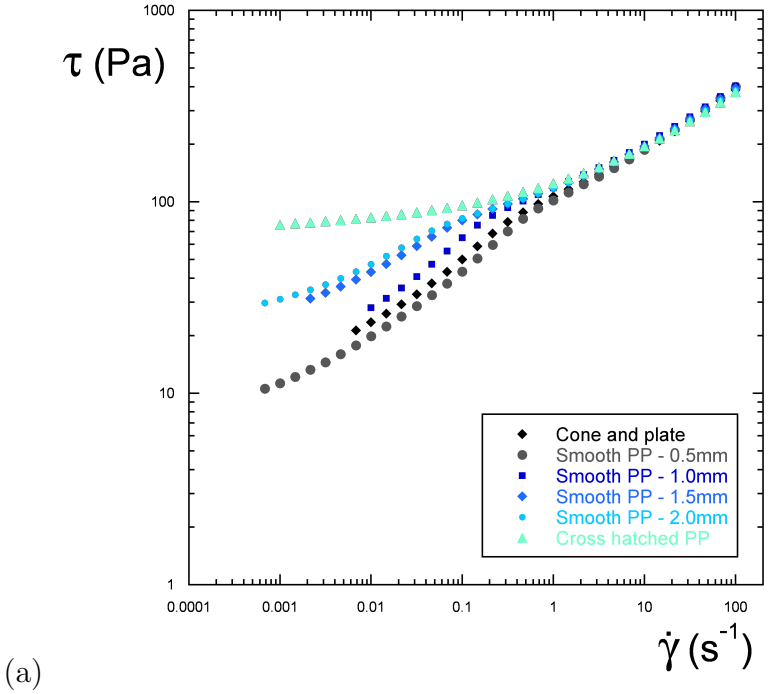

(a)

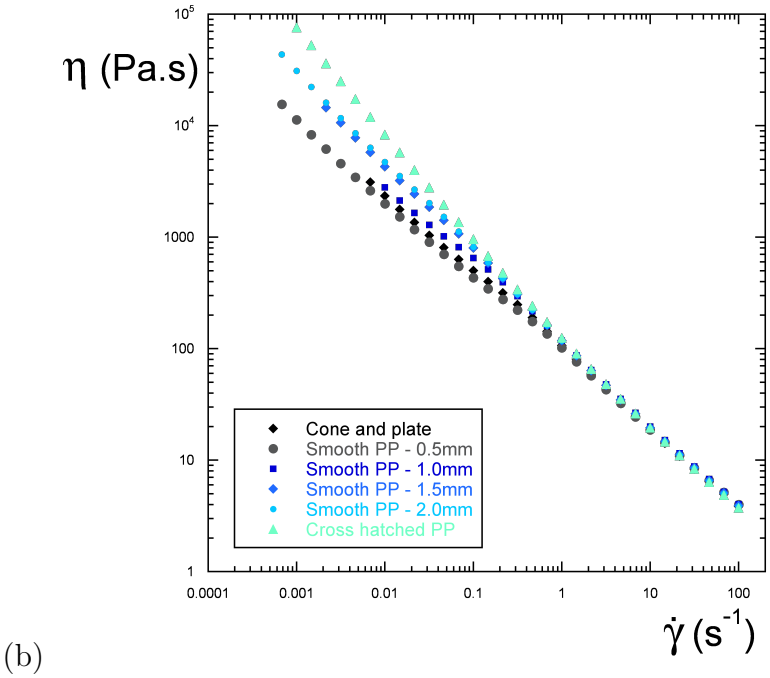

(b)

Figure A.2: Steady state flow curves for different geometries - (a) Stress vs. shear rate and (b) Viscosity vs. shear rate.

PUC-Rio - Certificação Digital Nº 1121442/CA

The curves for all geometries coincide for high shear rates ($> 3s^{-1}$). Actually, at the very high shear rate range, it is expected that the cross hatched parallel plates give rise to lower stresses, and hence lower viscosities, once secondary flows between the protrusions might occur. However, as can be observed, this effect is limited to the last two shear rate values and seems to have a minor impact on the results, at least for the range of shear rates applied to the sample.

Regarding the low shear rate range, it is clear that apparent wall slip occurs in all geometries, except for the cross hatched plates. Moreover, from the results of the four different smooth parallel plate gaps it is possible to note that increasing the gap indeed diminishes the effect of slip, but does not suffice to eliminate it. Thus, the obvious geometry choice for our material is to use the cross hatched parallel plates.

PUC-Rio - Certificação Digital Nº 1121442/CA

B
Parallel-plate correction

The parallel plate geometry is widely used in rheometry for a great variety of materials, such as polymer melts, suspensions, dispersions and emulsions. One of its advantages over the cone and plate or the concentric cylinder geometries is the easiness of varying the gap, which is crucial in the case of systems with particles or droplets. Moreover, the shear rate range is adjustable by varying the plate diameter or gap.

However, unlike the cone and plate or the narrow gap concentric cylinder geometries, the shear rate is not constant along the radius. Thus, to account for the non-homogeneous flow, the measured stress needs to be corrected. The Weissenberg-Rabinowitsch equation [40] accounts for the shear-rate dependence of non-Newtonian fluids, correcting the stress as follows:

$$\tau_R = \frac{T}{2\pi R^3}\left[3 + \frac{d\ln\left(T/2\pi R^3\right)}{d\ln\dot{\gamma}_R}\right] \tag{1}$$

where R is the radius of the plate, T the measured torque, and $\dot{\gamma}_R$ the shear rate at the rim. In the case of Newtonian fluids, the derivative of the logarithm of the torque with respect to the logarithm of the shear rate at the rim equals to one, and Eq. 1 reduces to

$$\tau_R = \frac{2T}{\pi R^3} \tag{2}$$

For non-Newtonian materials, the derivative needs to be calculated. It can be determined through differentiation of experimental data, if a sufficient amount of data is provided [12]. Nevertheless, commercial rheometers still use the Newtonian expression to calculate an apparent shear stress at the disk rim, which is used in further calculations, i.e. apparent viscosity. Stress corrections are available as a post-experiment step.

Another alternative to correct steady state flow data is to use the single-point method developed by Giesekus and Langer [41]. They generalized the concept of the representative viscosity to an exact method. The method is

PUC-Rio - Certificação Digital Nº 1121442/CA

applied to channel-, tube-, torsional-, and Couette flow, for both power-law and viscoplastic fluids, by considering that the apparent and the actual stress are equal at some position of the radius. It was found that this occurs at approximately r / R = 0.76. A similar and simpler study was performed by Schummer ad Worthoff [42].

Cross and Kaye [43] developed a similar method, where the idea is to approximate the derivative of the torque at a specific angular velocity by the torque value at some other speed. For shear-thinning fluids, the first order approximation leads to errors of less than 1%. Geiger [44] proposed a simplified form for the torque-shear rate relation based on the Carreau-type flow to expand the range of use of parallel disks for the characterization of polymer solutions and melts. Carvalho et. al [45] extended previous single-point methods to correct shear viscosity data and developed a new single point correction for the normal stress coefficient. Experimental results were compared to values obtained by numerical differentiation of raw data. They found that the single-point method yielded more accurate results than the apparent values calculated by regular rheometer software and faster than numerical differentiation, which is useful specially for process-line measurements.

Although it is clear that data pertaining to transient rheometric tests performed with the parallel plate geometry also need correction, only few studies were found. Soskey and Winter [46] obtained a correction similiar to the Rabinowitsch equation to apply to parallel-disk data in the large strain domain. Focus was given into obtaining the shear relaxation modulus for both linear and branched polymers. Corrected parallel plate results showed good agreement with the cone and plate geometry.

MacSporran and Spiers [47, 48] developed a parallel plate correction for large amplitude oscillatory flows in a Weissenberg rheogoniometer. However, none of the citing articles of this work have actually used this correction. The only work found to discuss this measurement artifact in oscillatory flows, specifically on the Lissajous curve results for yield materials, was performed by Ewoldt et. al [17]. By comparing plate-plate to cone-plate responses, little qualitative difference in the general shapes of the Lissajous curves could be observed. It was found that, in general, "the inhomogeneous strain field softens the nonlinear features of the response and leads to small overestimation of stresses for shear-thinning and yield stress materials".

The importance of correcting the stress response is evident, though. Thus, we also propose a different stress correction for oscillatory flows (Sec. B.1), as presented next and to be published in a near future.

PUC-Rio - Certificação Digital Nº 1121442/CA

B.1
Analysis for oscillatory flows

Considering a sinusoidal input for the angular velocity of amplitude Ω_a

$$\Omega(t) = \Omega_a \sin(\omega t) \tag{3}$$

and hence

$$\dot{\gamma}(r,t) = \frac{r\Omega(t)}{H} = \frac{r\Omega_a}{H}\sin(\omega t)\ . \tag{4}$$

The shear rate evaluated at the rim (r = R) is

$$\dot{\gamma}_R(t) \equiv \dot{\gamma}(R,t) = \frac{R\Omega(t)}{H} = \frac{R\Omega_a}{H}\sin(\omega t) \tag{5}$$

and hence

$$\dot{\gamma}(r,t) = \dot{\gamma}_a(r)\sin(\omega t) \tag{6}$$

$$\dot{\gamma}_R(t) = \dot{\gamma}_{R,a}\sin(\omega t)\ . \tag{7}$$

When the stress response is also sinusoidal, shifted by a phase angle ϕ

$$T(t) = T_a \sin(\omega t + \phi); \quad \tau(r,t) = \tau_a(r)\sin(\omega t + \phi)\ . \tag{8}$$

It is important to note that a sinusoidal response is not exclusive to the small strain region. If high enough frequencies are employed, a sinusoidal response can be "recovered", as observed by [8] .

The torque balance in the geometry gives

$$T(t) = \int_0^R r\tau(r,t)2\pi r dr = 2\pi\int_0^R r^2\tau(r,t)dr \tag{9}$$

Substituting (8) in (9)

$$T_a\sin(\omega t + \phi) = 2\pi\int_0^R r^2\tau_a(r)\sin(\omega t + \phi)dr \tag{10}$$

we obtain

$$T_a = 2\pi\int_0^R r^2\tau_a(r)dr\ . \tag{11}$$

PUC-Rio - Certificação Digital Nº 1121442/CA

Changing variables from r to $\dot{\gamma}_a$ using

$$\frac{\dot{\gamma}(r,t)}{\dot{\gamma}_R(t)} = \frac{\dot{\gamma}_a(r)}{\dot{\gamma}_{R,a}} = \frac{r}{R} \tag{12}$$

$$r = \frac{R}{\dot{\gamma}_{R,a}}\dot{\gamma}_a \quad and \quad dr = \frac{R}{\dot{\gamma}_{R,a}}d\dot{\gamma}_a \tag{13}$$

gives

$$T_a = 2\pi \int_0^{\dot{\gamma}_{R,a}} \left[\frac{R}{\dot{\gamma}_{R,a}}\dot{\gamma}_a\right]^2 \tau_a(\dot{\gamma}_a)\frac{R}{\dot{\gamma}_{R,a}}d\dot{\gamma}_a \tag{14}$$

$$T_a = 2\pi \left[\frac{R}{\dot{\gamma}_{R,a}}\right]^3 \int_0^{\dot{\gamma}_{R,a}} \dot{\gamma}_a^2\tau_a(\dot{\gamma}_a)d\dot{\gamma}_a \tag{15}$$

$$\frac{\dot{\gamma}_{R,a}^3 T_a}{2\pi R^3} = \int_0^{\dot{\gamma}_{R,a}} \dot{\gamma}_a^2\tau_a(\dot{\gamma}_a)d\dot{\gamma}_a \ . \tag{16}$$

By differentiating using Leibnitz's rule we obtain

$$\frac{d}{d\dot{\gamma}_{R,a}}\left[\frac{\dot{\gamma}_{R,a}^3 T_a}{2\pi R^3}\right] = \dot{\gamma}_{R,a}^2\tau_{R,a} \tag{17}$$

where $\tau_{R,a} \equiv \tau_a(\dot{\gamma}_{R,a})$. Rearranging for $\tau_{R,a}$

$$\tau_{R,a} = \frac{T_a}{2\pi R^3}\left[3 + \frac{d\ln\left(T_a/2\pi R^3\right)}{d\ln\dot{\gamma}_{R,a}}\right] \tag{18}$$

where the derivative $\frac{d\ln\left(T_a/2\pi R^3\right)}{d\ln\dot{\gamma}_{R,a}}$ is a function of the amplitude $\dot{\gamma}_{R,a}$ and needs to be evaluated at a constant frequency and varying $\dot{\gamma}_{R,a}$ around the value of interest.

It is worth noting that the same analysis is valid for the reverse case, i.e. a stress input and strain rate output, as long as both are sinusoidal.

To illustrate the correction, a 1.5% polyacrylamide solution was used to perform strain sweep tests with two different geometries, namely a cone and plate and smooth parallel plates with 1mm gap. Since apparent wall slip does not occur for this material, smooth walls can be used without any concerns. Instead of presenting the results in Fig. B.1 in terms of G' and G", a plot of the stress vs. strain was used. The vertical axis is displayed in linear scale to highlight the differences between the curves.

PUC-Rio - Certificação Digital Nº 1121442/CA

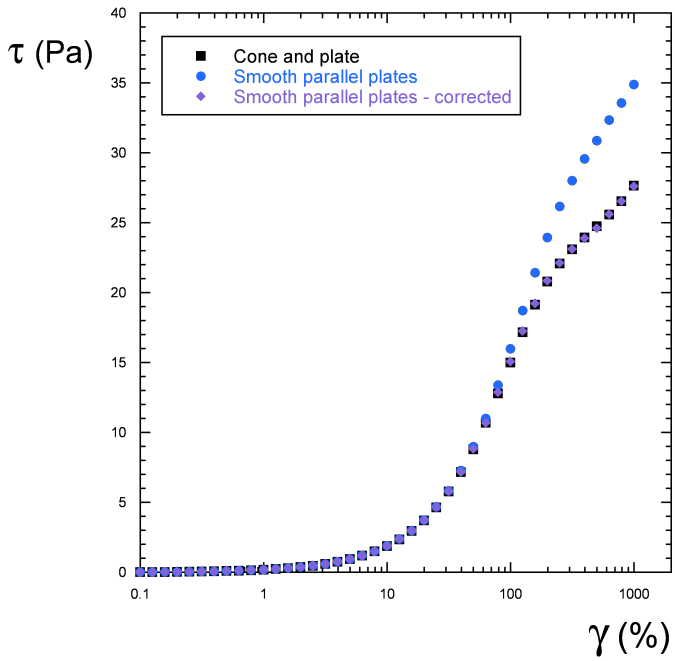

Figure B.1: Strain sweep for a 1.5 % polyacrylamide solution, with different geometries.

Firstly, it is possible to note that all curves coincide in the small strain region, which pertains to the linear viscoelastic regime. Indeed, in this region, the derivative is approximately equal to 1, already indicating that no correction is needed. However, when comparing the results for the cone and plate (black curve) and the parallel plate (blue curve), it becomes evident that the differences increase with strain amplitude and are not negligible. In fact, it was verified that errors induced by the non-homogeneity can be as great as 25%. Nonetheless, the curve corresponding to the corrected curve coincides with the cone and plate resuls, showing that the developed stress correction is able to successfully correct the results for the parallel plate geometry.

PUC-Rio - Certificação Digital Nº 1121442/CA

C
Details on the LAOS experiments

As previously discussed, in regular oscillatory experiments the recorded data corresponds to the amplitudes of the input and output waves. For instance in a strain sweep, each data point in a G' / G" vs. strain plot corresponds to the amplitude of the input strain wave.

However, in LAOS experiments there is a need to collect the "raw data". This means that, instead of saving only the amplitude information, the software also needs to collect intra-cycle data. In order to do this, some adjustments must be done when setting up the rheometric experiment. Fig. C.1 shows the print screen of a time sweep procedure used in this investigation:

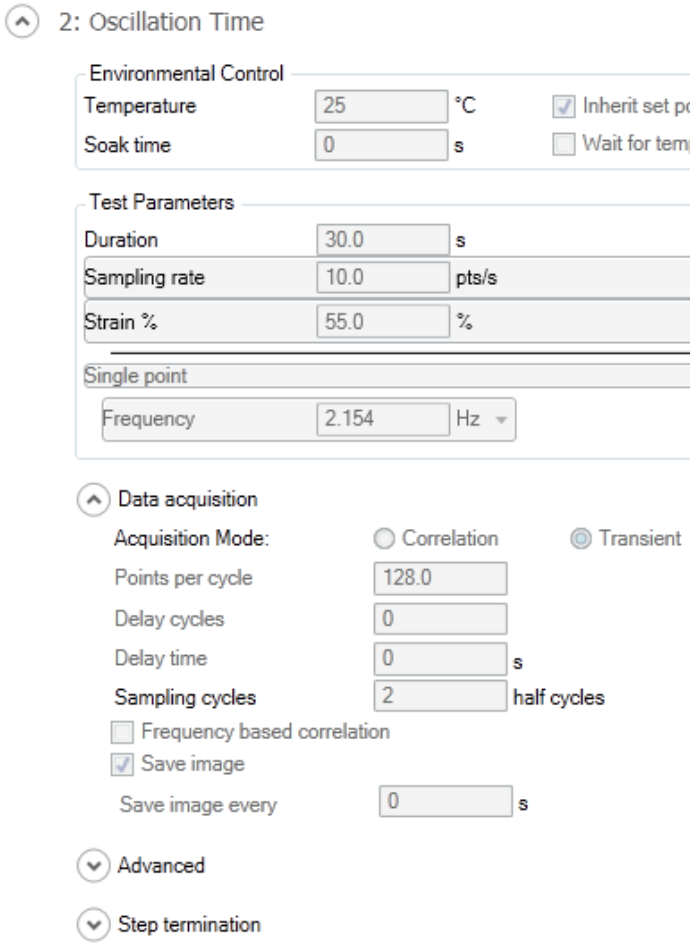

Figure C.1: Oscillation time sweep set up.

PUC-Rio - Certificação Digital Nº 1121442/CA

As can be seen, the main test parameters are the duration (s), sampling rate (pts/s), strain amplitude (%), and frequency (Hz) are set. The difference to regular time sweep tests is the data acquisition. Instead of using the "correlation acquisition mode", the "transient" mode must be selected. Also, in order not to miss any time effects, the "frequency based correlation" must be unchecked. Both delay cycles and delay time must be set to 0s, as they indicate the number of cycles and the time, respectively, to apply the sinusoidal deformation before beginning the data collection. Moreover, we chose to use one sampling cycle (2 half cycles) with 128 points per cycle.

According to the manufacturer, a step of conditioning the transducer is indicated when collecting raw data. This enables achieving better performance of the motor and higher accuracy of the torque transducer. Fig. C.2 shows the conditioning transducer set-up.

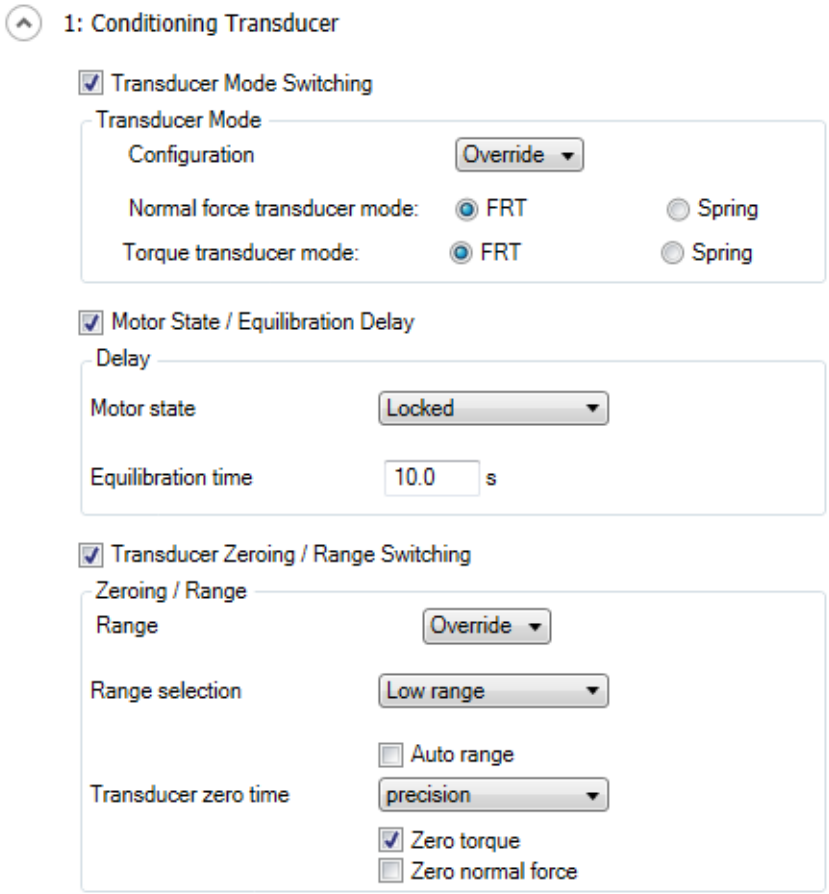

Figure C.2: Conditioning transducer set up.

The transducer mode switching is set to FRT (force rebalance transducer) for both normal force and torque transducer modes, which imply a stiff mode, recommended in the case of moderate to high viscosity systems. In addition, the motor state is set to "locked", preventing the motor from drifting during the sample equilibrium, and consequently introducing a residual torque to the

PUC-Rio - Certificação Digital Nº 1121442/CA

sample at the beginning of the oscillation time step. The "equilibration" time indicates the time for the material to relax. Once we wait for the material to relax before starting the rheometric experiment, a time of 10.0 s seems to be sufficient for this equilibrium delay.

Regarding the range selection for the transducer, the appropriate range depends on the material used. The manufacturer recommends the low range for 0.05 to 5000 μNm, the med range for 0.4 to 20.000 μNm, and high range for 4 to 200.000 μNm. Thus, for our elasto-viscoplastic material, the low range was selected for the lowest stress amplitude, and the medium range for the rest of the tests. It is necessary to emphasize that choosing the appropriate range is important to avoid the loss of torque sensitivity. Moreover, the transducer zero time is recommended to be set to standard for regular experiments and to fast for high frequency experiments. Also, it is important to check the "zero torque" box for the torque to be zeroed prior to starting the experiment.

PUC-Rio - Certificação Digital Nº 1121442/CA